Chapter 11 Generalized Conforming Membrane and Shell Elements

Zhi-Fei Long
School of Mechanics & Civil Engineering, China University of Mining & Technology, Beijing, 100083, China

Song Cen
Department of Engineering Mechanics, School of Aerospace, Tsinghua University, Beijing, 100084, China

Abstract Besides the various plate problems discussed in the previous chapters, the idea of the generalized conforming element has already been successfully generalized to many other areas. As the final chapter of Part Ⅱ, this chapter mainly introduces some research achievements on the applications of the generalized conforming element method for isoparametric membrane element (Sect. 11.2), membrane element with drilling freedoms (Sects. 11.3 and 11.4), flat-shell element (Sect. 11.5), curved shell element (Sects. 11.6 and 11.7) and shell element for geometrically nonlinear analysis (Sects. 11.8 and 11.9). Thus, the universal significance of the generalized conforming theory can be clearly illustrated.

Keywords finite element, generalized conforming, membrane element, shell element.

11.1 Introduction

The generalized conforming element method was originally proposed for solving the difficulty of C^1-continuity required by thin plate elements. It opens a new way between the conforming and non-conforming elements: on the one hand, the shortcomings that sometimes the conforming elements are over-stiff and even difficult to be constructed are overcome; on the other hand, the major weakness that the non-conforming elements may not be convergent is also eliminated. As described in Chap. 5 to Chap. 7, first it obtains success in the construction of thin plate elements, and various high-performance thin plate element models of different types are then successfully constructed.

At the same time, the idea of the generalized conforming element has also been successfully generalized to many other areas: besides the applications of thick plate in Chap. 8, laminated composite plate in Chap. 9 and piezoelectric laminated composite plate in Chap. 10, generalized conforming isoparametric membrane elements are proposed in reference [1], generalized conforming membrane elements with drilling freedoms are proposed in references [2,3], generalized conforming flat-shell elements are proposed in references [4−9], generalized conforming curved shallow shell elements are proposed in references [10,11], and generalized conforming plate and shell elements for geometrically nonlinear analysis are also proposed in [9−12].

This chapter will mainly introduce some research achievements on the applications of the generalized conforming element method for isoparametric membrane element, membrane element with drilling freedoms, flat-shell element, curved shell element and shell element for geometrically nonlinear analysis. Thus, the universal significance of the generalized conforming theory can be exhibited.

11.2 Generalized Conforming Isoparametric Membrane Element

This section will introduce the construction mode of the generalized conforming isoparametric element GC-Q6[1].

For the plane 4-node isoparametric element Q4 (Fig. 11.1), its nodal DOFs are defined as:

$$\boldsymbol{q}^e = [u_1 \quad v_1 \quad u_2 \quad v_2 \quad u_3 \quad v_3 \quad u_4 \quad v_4]^{\mathrm{T}} \tag{11-1}$$

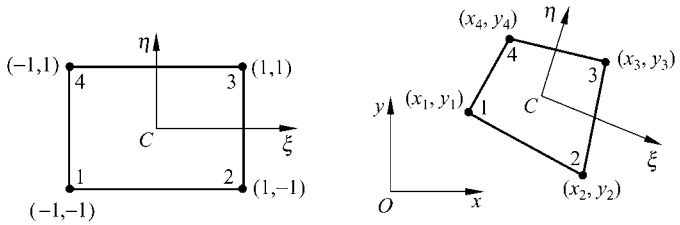

Figure 11.1 4-node quadrilateral plane isoparametric element

The interpolation functions for displacements u and v are given by

$$u = \sum_{i=1}^{4} N_i u_i, \quad v = \sum_{i=1}^{4} N_i v_i \tag{11-2}$$

where u_i and v_i ($i = 1,2,3,4$) are the nodal displacements; N_i the shape functions

which are bilinear functions of the natural coordinates ξ, η

$$N_i = \frac{1}{4}(1+\xi_i\xi)(1+\eta_i\eta) \quad (i=1,2,3,4) \tag{11-3}$$

Element Q4 is very popular. However, for bending problems it gives results with low accuracy.

In order to improve the bending behavior of the element Q4, Wilson et al.[13] propose a non-conforming element in which the displacements are split into compatible and incompatible parts:

$$\boldsymbol{u} = \boldsymbol{u}_q + \boldsymbol{u}_\lambda \tag{11-4}$$

where $\boldsymbol{u}_q = [u \quad v]^{\mathrm{T}}$ are the compatible displacements and given by Eqs. (11-2) and (11-3); and $\boldsymbol{u}_\lambda$ are the incompatible displacements given by

$$\boldsymbol{u}_\lambda = \begin{Bmatrix} u_\lambda \\ v_\lambda \end{Bmatrix} = \begin{bmatrix} 1-\xi^2 & 1-\eta^2 & 0 & 0 \\ 0 & 0 & 1-\xi^2 & 1-\eta^2 \end{bmatrix} \begin{Bmatrix} \lambda_1 \\ \lambda_2 \\ \lambda_3 \\ \lambda_4 \end{Bmatrix} \tag{11-5}$$

where λ_i $(i=1,2,3,4)$ are 4 internal displacement parameters. This element is denoted as Q6. Some excellent numerical results are obtained by the element Q6, however, it cannot pass the patch test for irregular mesh.

In this section, according to the basic idea of the generalized conforming element, the generalized conforming isoparametric element GC-Q6 is obtained based on the generalized conforming conditions under constant and linear stress fields. Here, the generalized conforming conditions under constant stresses are used to ensure convergence, and the generalized conforming conditions under linear stresses are used to improve computational accuracy.

11.2.1 Generalized Conforming Conditions under Constant and Linear Stress Fields

For the conforming element, the element displacement fields $\boldsymbol{u}$ must satisfy the conforming conditions along the element boundary ∂A^e

$$\boldsymbol{u} - \tilde{\boldsymbol{u}} = \boldsymbol{0} \quad (\text{on } \partial A^e) \tag{11-6}$$

where $\tilde{\boldsymbol{u}}$ denote the boundary displacement of the element.

For the generalized conforming element, the conforming condition (11-6) are relaxed and replaced by the following generalized conforming conditions in the limit of mesh refinement (the stresses and strains of each element tends to be constant):

$$\oint_{\partial A^e} \boldsymbol{T}_{\mathrm{c}}^{\mathrm{T}}(\boldsymbol{u}-\tilde{\boldsymbol{u}})\,\mathrm{d}s = 0 \tag{11-7}$$

where $\boldsymbol{T}_{\mathrm{c}}$ denotes the boundary tractions of the constant stress field.

In reference [14], during the derivation of the generalized conforming element, the following conforming conditions of the average displacement along each element side S_i are used:

$$\int_{S_i} (\boldsymbol{u}-\tilde{\boldsymbol{u}})\,\mathrm{d}s = \boldsymbol{0} \tag{11-8}$$

Obviously, the condition (11-8) are the strong forms of the condition (11-7).

In reference [1], a new kind of generalized conforming element is established by using another strong form of the condition (11-7), i.e.,

$$\oint_{\partial A^e} \boldsymbol{T}^{\mathrm{T}}(\boldsymbol{u}-\tilde{\boldsymbol{u}})\,\mathrm{d}s = 0 \tag{11-9}$$

where $\boldsymbol{T}$ denotes the boundary tractions under both the constant and linear stress fields. Substituting Eq. (11-4) into Eq. (11-9), and applying the following condition satisfied by the conforming displacement $\boldsymbol{u_q}$:

$$\boldsymbol{u_q}-\tilde{\boldsymbol{u}} = \boldsymbol{0} \quad (\text{on } \partial A^e) \tag{11-10}$$

we have

$$\oint_{\partial A^e} \boldsymbol{T}^{\mathrm{T}}\boldsymbol{u}_\lambda\,\mathrm{d}s = 0 \tag{11-11}$$

Considering the following linear stress state:

$$\sigma_x = \beta_1 + \beta_4\eta, \quad \sigma_y = \beta_2 + \beta_5\xi, \quad \tau_{xy} = \beta_3 \tag{11-12}$$

we obtain

$$T_x = l\beta_1 + m\beta_3 + l\eta\beta_4, \quad T_y = m\beta_2 + l\beta_3 + m\xi\beta_5 \tag{11-13}$$

where l and m are the directional cosines of the outward normal to the boundary.

Substitution of Eq. (11-13) into Eq. (11-11) yields

$$\oint_{\partial A^e} [\beta_1 l u_\lambda + \beta_2 m v_\lambda + \beta_3(m u_\lambda + l v_\lambda) + \beta_4 l\eta u_\lambda + \beta_5 m\xi v_\lambda]\,\mathrm{d}s = 0 \tag{11-14}$$

Since the 5 parameters β_i are independent to each other, 5 conditions can be obtained as follows:

$$\left.\begin{aligned} &\oint_{\partial A^e} l u_\lambda\,\mathrm{d}s = 0\ , \quad \oint_{\partial A^e} m v_\lambda\,\mathrm{d}s = 0 \\ &\oint_{\partial A^e} (m u_\lambda + l v_\lambda)\,\mathrm{d}s = 0 \\ &\oint_{\partial A^e} l\eta u_\lambda\,\mathrm{d}s = 0\ , \quad \oint_{\partial A^e} m\xi v_\lambda\,\mathrm{d}s = 0 \end{aligned}\right\} \tag{11-15}$$

The conditions given by Eq. (11-15) are the generalized conforming conditions under constant and linear stress fields.

11.2.2 Determination of the Generalized Conforming Displacements u_λ

Firstly, the generalized conforming displacements u_λ and v_λ are expressed in a complete quadratic polynomial form:

$$\left.\begin{aligned} u_\lambda &= \lambda_1 + \lambda_2\xi + \lambda_3\eta + \lambda_4\xi^2 + \lambda_5\xi\eta + \lambda_6\eta^2 \\ v_\lambda &= \lambda_1' + \lambda_2'\xi + \lambda_3'\eta + \lambda_4'\xi^2 + \lambda_5'\xi\eta + \lambda_6'\eta^2 \end{aligned}\right\} \tag{11-16}$$

From this equation, the displacements u_C, v_C and rotation ω_C at the centroid C ($\xi = 0,\ \eta = 0$) of the element can be obtained as follows:

$$u_C = \lambda_1\ ,\ v_C = \lambda_1'\ ,\ \omega_C = \frac{1}{2\,|\boldsymbol{J}|_C}\left(a_3\lambda_2 - a_1\lambda_3 + b_3\lambda_2' - b_1\lambda_3'\right) \tag{11-17}$$

where the following notations are used:

$$\left.\begin{aligned} a_1 &= \frac{1}{4}\left(-x_1 + x_2 + x_3 - x_4\right)\ ,\ a_2 = \frac{1}{4}\left(x_1 - x_2 + x_3 - x_4\right) \\ a_3 &= \frac{1}{4}\left(-x_1 - x_2 + x_3 + x_4\right) \\ b_1 &= \frac{1}{4}\left(-y_1 + y_2 + y_3 - y_4\right)\ ,\ b_2 = \frac{1}{4}\left(y_1 - y_2 + y_3 - y_4\right) \\ b_3 &= \frac{1}{4}\left(-y_1 - y_2 + y_3 + y_4\right) \\ |\boldsymbol{J}|_C &= a_1b_3 - a_3b_1 \neq 0 \end{aligned}\right\} \tag{11-18}$$

Secondly, substitution of Eq. (11-16) into the generalized conforming condition (11-15) yields

$$\left.\begin{aligned} &3b_3\lambda_2 - 3b_1\lambda_3 + 2b_2(\lambda_4 - \lambda_6) = 0 \\ &3a_3\lambda_2' - 3a_1\lambda_3' + 2a_2(\lambda_4' - \lambda_6') = 0 \\ &[3a_3\lambda_2 - 3a_1\lambda_3 + 2a_2(\lambda_4 - \lambda_6)] + [3b_3\lambda_2' - 3b_1\lambda_3' + 2b_2(\lambda_4' - \lambda_6')] = 0 \\ &3b_1\lambda_1 + 2b_2\lambda_3 + b_1\lambda_4 - b_3\lambda_5 + 3b_1\lambda_6 = 0 \\ &3a_3\lambda_1' + 2a_2\lambda_2' + 3a_3\lambda_4' - a_1\lambda_5' + a_3\lambda_6' = 0 \end{aligned}\right\} \tag{11-19}$$

From Eqs. (11-19) and (11-17), 8 parameters λ_1, λ_2, λ_3, λ_5, λ_1', λ_2', λ_3' and λ_5' can be expressed in terms of another 4 independent parameters λ_4, λ_6, λ_4', λ_6'

and three centroid displacements u_C, v_C, ω_C.

Finally, if we let

$$u_C = -\lambda_4 - \lambda_6, \quad v_C = -\lambda_4' - \lambda_6', \quad \omega_C = 0 \tag{11-20}$$

then from Eq. (11-16) we obtain

$$\begin{Bmatrix} u_\lambda \\ v_\lambda \end{Bmatrix} = \begin{bmatrix} \xi^2 - 1 + F_1 & \eta^2 - 1 + F_2 & F_3 & -F_3 \\ F_3' & -F_3' & \xi^2 - 1 + F_1' & \eta^2 - 1 + F_2' \end{bmatrix} \begin{Bmatrix} \lambda_4 \\ \lambda_6 \\ \lambda_4' \\ \lambda_6' \end{Bmatrix} \tag{11-21}$$

where

$$\left.\begin{aligned}
F_1 &= \frac{1}{3|\boldsymbol{J}|_C}\left\{-(2a_1b_2 - a_2b_1)\xi - (2a_3b_2 - a_2b_3)\eta \right.\\
&\quad \left. + \left[(3a_1b_1 + 2a_2b_2) - \frac{a_3}{b_3}(3b_1^2 + 4b_2^2) - \frac{b_1}{b_3}|\boldsymbol{J}|_C\right]\xi\eta\right\}\\
F_1' &= \frac{1}{3|\boldsymbol{J}|_C}\left\{(2a_2b_1 - a_1b_2)\xi + (2a_2b_3 - a_3b_2)\eta \right.\\
&\quad \left. + \left[(9a_3b_3 - 2a_2b_2) + \frac{b_1}{a_1}(4a_2^2 - 9a_3^2) - \frac{a_3}{a_1}|\boldsymbol{J}|_C\right]\xi\eta\right\}\\
F_2 &= -F_1 - \frac{2b_1}{b_3}\xi\eta\ , \quad F_2' = -F_1' - \frac{2a_3}{a_1}\xi\eta\\
F_3 &= \frac{-1}{3|\boldsymbol{J}|_C}[b_1b_2\xi + b_2b_3\eta + 2b_2^2\xi\eta]\\
F_3' &= \frac{1}{3|\boldsymbol{J}|_C}[a_1a_2\xi + a_2a_3\eta + 2a_2^2\xi\eta]
\end{aligned}\right\} \tag{11-22}$$

Equation (11-21), involving 4 internal displacement parameters λ_4, λ_6, λ_4' and λ_6', represents the required generalized conforming displacement mode which satisfies the condition (11-15). If the element is a parallelogram, Eq. (11-21) degenerates to Eq. (11-5).

11.2.3 Stiffness Matrix of the Element GC-Q6

As soon as the generalized conforming displacement mode (11-21) is determined, the stiffness matrix may be derived by the conventional procedure.

Substituting Eqs. (11-2) and (11-21) into Eq. (11-4), the element displacement may be written as

$$\boldsymbol{u} = \boldsymbol{u}_q + \boldsymbol{u}_\lambda = \boldsymbol{N}\boldsymbol{q}^e + \boldsymbol{N}_\lambda \boldsymbol{\lambda} \tag{11-23}$$

Element strain may be expressed as

$$\boldsymbol{\varepsilon} = \boldsymbol{B}\boldsymbol{q}^e + \boldsymbol{B}_\lambda \boldsymbol{\lambda} \tag{11-24}$$

And, the element strain energy is

$$U = \frac{h}{2}\iint_{A^e} \boldsymbol{\varepsilon}^{\mathrm{T}} \boldsymbol{D}\boldsymbol{\varepsilon}\mathrm{d}A = \frac{1}{2}\boldsymbol{q}^{e\mathrm{T}}\boldsymbol{K}_{qq}\boldsymbol{q}^e + \frac{1}{2}\boldsymbol{\lambda}^{\mathrm{T}}\boldsymbol{K}_{\lambda\lambda}\boldsymbol{\lambda} + \boldsymbol{\lambda}^{\mathrm{T}}\boldsymbol{K}_{\lambda q}\boldsymbol{q}^e \tag{11-25}$$

in which h is the thickness of the element;

$$\left.\begin{aligned} \boldsymbol{K}_{qq} &= h\int_{-1}^{1}\int_{-1}^{1} \boldsymbol{B}^{\mathrm{T}}\boldsymbol{D}\boldsymbol{B}\ |\boldsymbol{J}|\ \mathrm{d}\xi\mathrm{d}\eta \\ \boldsymbol{K}_{\lambda\lambda} &= h\int_{-1}^{1}\int_{-1}^{1} \boldsymbol{B}_\lambda{}^{\mathrm{T}}\boldsymbol{D}\boldsymbol{B}_\lambda\ |\boldsymbol{J}|\ \mathrm{d}\xi\mathrm{d}\eta \\ \boldsymbol{K}_{\lambda q} &= h\int_{-1}^{1}\int_{-1}^{1} \boldsymbol{B}_\lambda{}^{\mathrm{T}}\boldsymbol{D}\boldsymbol{B}\ |\boldsymbol{J}|\ \mathrm{d}\xi\mathrm{d}\eta \end{aligned}\right\} \tag{11-26}$$

where $|\boldsymbol{J}|$ is the determinant of the Jacobian matrix; $\boldsymbol{D}$ is the matrix of the elasticity coefficients, for the plane stress problem, we have

$$\boldsymbol{D} = \frac{E}{1-\mu^2}\begin{bmatrix} 1 & \mu & 0 \\ \mu & 1 & 0 \\ 0 & 0 & \dfrac{1-\mu}{2} \end{bmatrix} \tag{11-27}$$

in which E and μ are the Young's modulus and Poisson's ratio, respectively. For the plane strain problem, the E and μ in the above equation should be replaced by $E/(1-\mu^2)$ and $\mu/(1-\mu)$, respectively.

From $\partial U/\partial\boldsymbol{\lambda} = \boldsymbol{0}$, we obtain

$$\boldsymbol{\lambda} = -\boldsymbol{K}_{\lambda\lambda}{}^{-1}\boldsymbol{K}_{\lambda q}\boldsymbol{q}^e \tag{11-28}$$

and finally the element stiffness matrix can be written as

$$\boldsymbol{K}^e = \boldsymbol{K}_{qq} - \boldsymbol{K}_{\lambda q}{}^{\mathrm{T}}\boldsymbol{K}_{\lambda\lambda}{}^{-1}\boldsymbol{K}_{\lambda q} \tag{11-29}$$

11.2.4 Numerical Examples

Example 11.1 Analysis of a rectangular plate using irregular mesh (Fig. 11.2).

Two load cases are considered: Uniform tension under load 1 (an experiment problem for patch test) and pure bending under load 2. Owing to the symmetry of the plate, only $1/4$ of the plate is modelled. Irregular mesh as shown in Fig. 11.2 is used. Computational results are given in Table 11.1. For comparison, the results by the other 6 element models and exact results are also given. From Table 11.1, it can be seen that, except the element Q6, the other models can all pass the patch test.

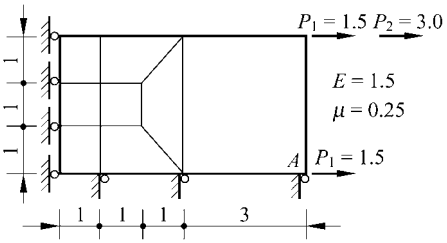

Figure 11.2 A 1/4 rectangular plate subjected to uniform tension and pure bending loads

Table 11.1 Comparison of results for Example 11.1 (7 elements)

Element type	Load 1 (uniform tension)		Load 2 (bending)
	u_A	Patch test	v_A
Q4 (isoparametric)	6.00	pass	– 17.00
Q6[13]	6.70	fail	– 19.66
QM6[15]	6.00	pass	– 17.61
QP6[16]	6.00	pass	– 17.61
NQ6[17]	6.00	pass	– 17.61
QC6[18]	6.00	pass	– 17.61
GC-Q6 (presented)	6.00	pass	– 17.62
Analytical solution	6.00		– 18.00

Example 11.2 Analysis of a cantilever beam using irregular mesh (Fig. 11.3).

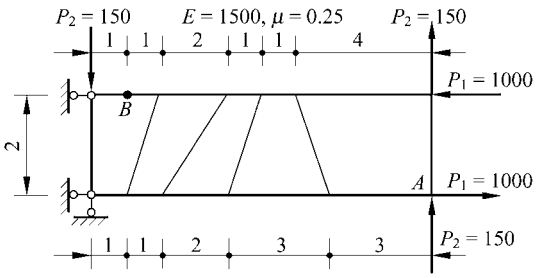

Figure 11.3 A cantilever beam subjected to pure bending and transverse bending loads

Two load cases are considered: pure bending under load 1 and transverse bending under load 2.

From Table 11.2, it can be seen that the accuracy of the isoparametric element Q4 is the worst, but the other 4 elements can provide good accuracy, especially the element QC-Q6 which gives the best answers.

Table 11.2 Comparison of results for Example 11.2 (5 elements)

Element type	Load 1 (pure bending)		Load 2 (transverse bending)	
	v_A	σ_{xB}	v_A	σ_{xB}
Q4 (isoparametric)	45.7	– 1761	50.7	– 2448
Q6[13]	98.4	– 2428	100.4	– 3354
QC6[18]	96.1	– 2439	98.1	– 3339
NQ6[17]	96.1	– 2439	98.0	– 3294
GC-Q6 (presented)	95.0	– 3036①	96.1	– 4182①
Analytical solution	100	– 3000	102.6	– 4050

① Stress at point B is computed by extrapolation from the stresses at the 2 × 2 Gauss quadrature points.

Example 11.3 Cook's skew beam problem: analysis of a tapered and swept panel with unit load uniformly distributed along the right edge (Fig. 11.4, mesh by real line).

This example has been discussed in reference [30]. From Table 11.3, it can be seen that the presented element GC-Q6 gives more accurate results than the element HL for coarser meshes.

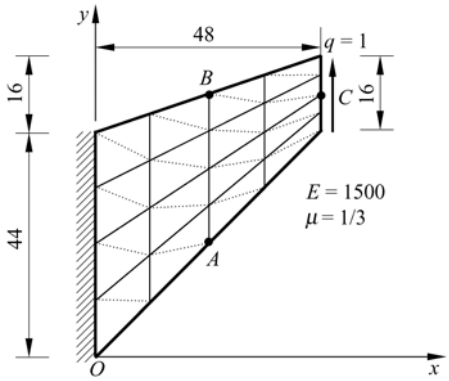

Figure 11.4 Cook's skew beam problem, mesh 4 × 4

Table 11.3 Comparison of results for Cook's skew beam problem (5 elements)

Element	v_C (the vertical displacement at point C)			$\sigma_{A\max}$ (the maximum stress at point A)			$\sigma_{B\min}$ (the minimum stress at point B)		
	2×2	4×4	8×8	2×2	4×4	8×8	2×2	4×4	8×8
Q4	11.80	18.29	22.08	0.1217	0.1873	0.2242	–0.0960	–0.1524	–0.1869
Q6[13]	22.94	23.48		0.2029	0.2258		–0.1734	–0.1915	
QM6[15]	21.05	23.02		0.1928	0.2243		–0.1580	–0.1856	
HL[19]	18.17	22.03	23.39	0.1582	0.1980	0.2205	–0.1335	–0.1770	–0.1931
GC-Q6①	27.61	24.31	23.99	0.2538	0.2349	0.2318	–0.1688	–0.1930	–0.1965
Reference②	23.96			0.2362			–0.2023		

① Nodal stresses are computed by extrapolation from the stresses at 2×2 Gauss quadrature points and nodal stresses of neighboring element are averaged.

② Results by the element GT9M8[3] using 64×64 mesh.

11.3 Membrane Elements with Drilling Freedoms—Definition of the Drilling Freedom and the Corresponding Rectangular and Quadrilateral Elements

The introduction of drilling freedom at each node in a plane stress element can improve the order of the element displacement fields, so it can enhance the element performance without increasing the number of the element nodes. And, such drilling freedoms in membrane elements possess special significance for the finite element analysis of shells. The membrane elements with drilling freedoms can be combined with plate bending elements to form flat-shell elements, which contain 3 translational freedoms and 3 rotational freedoms at each node. Thus, when a flat-shell element is used for the analysis of shell structures, the problem that the global stiffness matrix may be singular can be naturally solved. And, the troubles caused by some other treatments[20,21] for this problem can also be avoided.

11.3.1 Notes on the Definition of Nodal Drilling Freedom θ_z in a Membrane Element

Following are 3 definitions of the drilling freedom θ_z at the node in a membrane element, and comparisons of their advantages and disadvantages are also given.

(1) Definition in the early time—the nodal drilling freedom θ_z in a membrane element is defined as the nodal rigid rotation

In the early definition of the nodal drilling freedom in a membrane element, the rotation of two adjacent sides of the element is assumed to be equal. So, during the whole deformation process of the element under this definition, the angle

between two adjacent sides which meet at the same corner node will indeed keep invariant. The introduction of this improper constraint will make the deformation state of the element quite different from the real situation. And, the triangular membrane element established by this method in [22] cannot be convergent to correct solutions.

(2) The second definition—the nodal drilling freedom θ_z in a membrane element is defined as the nodal rotation ω according to the concept of continuum mechanics

From the displacements u and v of the membrane element, its rotation can be derived by the concept of continuum mechanics as follows:

$$\omega = \frac{1}{2}\left(\frac{\partial v}{\partial x} - \frac{\partial u}{\partial y}\right) \tag{11-30}$$

In many recent literatures, this concept of rotation ω was adopted to define the nodal drilling freedom θ_z of the membrane element as

$$\theta_z = \omega = \frac{1}{2}\left(\frac{\partial v}{\partial x} - \frac{\partial u}{\partial y}\right) \tag{11-31}$$

Now, the properties of the rotation ω are listed as follows.

Property 1 When the axes of the Cartesian coordinate system rotate, ω is an invariant.

Assume that the Cartesian coordinate system xOy will change to another Cartesian coordinate system $x'Oy'$ after it rotates an arbitrary angle. Then, the corresponding rotations of these two coordinate systems are

$$\omega_{xy} = \frac{1}{2}\left(\frac{\partial v}{\partial x} - \frac{\partial u}{\partial y}\right), \quad \omega_{x'y'} = \frac{1}{2}\left(\frac{\partial v'}{\partial x'} - \frac{\partial u'}{\partial y'}\right) \tag{11-32}$$

By using the coordinate transformation (8-22), it can be proved that

$$\omega_{xy} = \omega_{x'y'} \tag{11-33}$$

i.e., ω is an invariant.

That ω is an invariant is just one of the important reasons why it has been selected as the definition of the nodal drilling freedom θ_z.

Property 2 The rotation of the x-axis is $\theta_x = \dfrac{\partial v}{\partial x}$, and the rotation of the y-axis is $\theta_y = -\dfrac{\partial u}{\partial y}$. Then, the shear strain γ_{xy} and rotation ω can be expressed in terms of θ_x and θ_y as

$$\gamma_{xy} = \theta_x - \theta_y, \quad \omega = \frac{1}{2}(\theta_x + \theta_y) \tag{11-34}$$

i.e., the shear strain γ_{xy} is the difference value of θ_x and θ_y, and the rotation ω is the average value of θ_x and θ_y.

Property 3 θ_x and θ_y can be expressed in terms of ω and γ_{xy} as follows:

$$\theta_x = \omega + \frac{1}{2}\gamma_{xy}, \quad \theta_y = \omega - \frac{1}{2}\gamma_{xy} \tag{11-35}$$

Similarly, we have

$$\theta_{x'} = \omega + \frac{1}{2}\gamma_{x'y'}, \quad \theta_{y'} = \omega - \frac{1}{2}\gamma_{x'y'} \tag{11-36}$$

Property 4 Under the general strain state in which the strain circle does not degenerate to be a point, when the coordinate axes $x'Oy'$ rotate, $\gamma_{x'y'}$ is a variant, so $\theta_{x'}$ and $\theta_{y'}$ are also variants.

Since $\theta_{x'}$ and $\theta_{y'}$ are variants, it is impossible that they are identically equal to the invariant ω. Only for the special case in which the x'-axis and the y'-axis are the strain principal axes, and then $\gamma_{x'y'} = 0$, ω will be equal to θ_x and θ_y. Thus, we can obtain:

$$(\theta)_{\text{principal axis}} = \omega, \quad (\theta)_{\text{non principal axis}} \neq \omega \tag{11-37}$$

Property 5 Under the special strain state in which the strain circle degenerates to be a point (isotropic spherical stress-strain state), axes along arbitrary directions are all strain principal axes. Therefore, the rotation θ of a line segment in the arbitrary direction will be identically equal to ω, it is an invariant, i.e.,

$$(\theta)_{\text{line segment in arbitrary direction}} = \omega \quad \text{(Under isotropic spherical stress state)} \tag{11-38}$$

From the above properties of rotation ω, it can be seen that the second definition described in this section is inappropriate, either. Its main shortcoming is: in general cases, the nodal rotation ω and the rotation θ of the element side are two different geometric quantities, and there is no definitive relation between them. For instance, from Property 2, it can be seen that ω is the average value of the rotation $\theta_{x'}$ of the element side and the rotation $\theta_{y'}$ of the side normal, and has no definitive relation with the rotation $\theta_{x'}$ of the element side; and from property 4, it can be seen that, if the element side is not the strain principal axis, the rotation θ of the element side will not be equal to ω.

In order to explain the reason why the second definition is inappropriate, three other examples are given as follows:

Example 1 At common nodes, the values of ω in adjacent elements are generally not equal to each other, thereby, ω is not suitable for being taken as the nodal freedom.

In Fig. 11.5, e and e' represent two adjacent elements, and point 1 is the common

node. Let the common side 12 be the x'-axis, then the rotation at the common node 1 of elements e and e' are

$$\omega^e = \theta^e_{x'} - \frac{1}{2}\gamma^e_{x'y'}, \quad \omega^{e'} = \theta^{e'}_{x'} - \frac{1}{2}\gamma^{e'}_{x'y'} \tag{11-39}$$

where $\theta^e_{x'}$ and $\theta^{e'}_{x'}$ are the rotations along the common side of the two elements at node 1, and should be equal; and $\gamma^e_{x'y'}$ and $\gamma^{e'}_{x'y'}$ are the shear strains of the two elements at node 1, but they are generally not equal. Hence, at common node 1, ω^e and $\omega^{e'}$ are generally not equal, either. So, ω is not suitable for being taken as the nodal freedom.

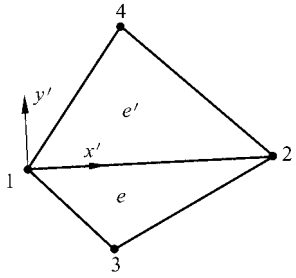

Figure 11.5 Two adjacent elements

Example 2 Assume that the two elements e and e' in Fig. 11.6 are both triangular element CST (Constant Strain Triangle), their strains are constants, and displacements are linear, so the rotations ω^e and $\omega^{e'}$ are also both constants (expressed by constants C_1 and C_2, respectively), i.e.,

$$\omega^e_1 = \omega^e_2 = \omega^e_3 = C_1, \quad \omega^{e'}_1 = \omega^{e'}_2 = \omega^{e'}_4 = C_2 \tag{11-40}$$

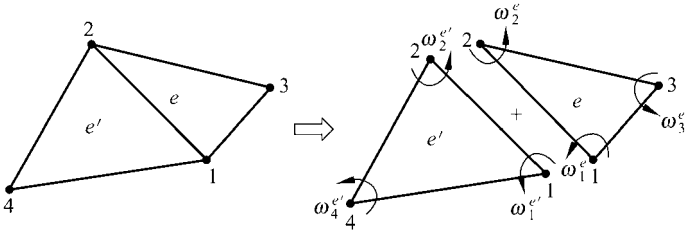

Figure 11.6 Two adjacent CST elements

Since constants C_1 and C_2 are generally not equal, it can also be concluded that ω^e and $\omega^{e'}$ at the common nodes 1 and 2 are generally not equal. So, ω is not suitable for being taken as the nodal freedom.

By the way, for the CST elements, stress σ, strain ε and rotation ω within each element are all constants, but generally different in adjacent elements, and

discontinuity phenomena will happen at two sides of the common side. Thereby, the quantities related to the derivatives of the displacements, such as σ, ε, ω, and so on, are not suitable for being selected as the nodal freedoms.

Example 3 Along a fixed edge where the displacements are specified as zero, the boundary conditions of the translational displacements u and v can be expressed as follows:

$$u = 0, \quad v = 0 \quad \text{(at the nodes on the fixed edge)} \tag{11-41}$$

But, the rotation ω on the fixed edge generally cannot be expressed by

$$\omega = 0 \quad \text{(at the nodes on the fixed edge)} \tag{11-42}$$

Therefore, ω is not suitable for being selected as the nodal freedom.

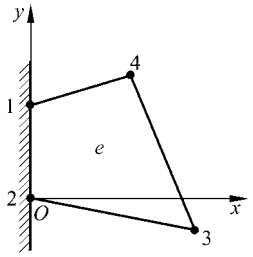

Figure 11.7 The boundary conditions on fixed edge

In Fig. 11.7, side $\overline{12}$ is a fixed edge. The boundary conditions of the element e at nodes 1 and 2 are

$$u_1 = u_2 = 0, \quad v_1 = v_2 = 0 \tag{11-43}$$

And, the following conditions can also be obtained:

$$\left(\frac{\partial u}{\partial y}\right)_1 = \left(\frac{\partial u}{\partial y}\right)_2 = 0 \tag{11-44}$$

Then, the rotation at node 1 can be derived from the above conditions:

$$\omega_1 = \frac{1}{2}\left(\frac{\partial v}{\partial x} - \frac{\partial u}{\partial y}\right)_1 = \frac{1}{2}\left(\frac{\partial v}{\partial x}\right)_1 \tag{11-45}$$

Since the term $\left(\frac{\partial v}{\partial x}\right)_1$ at the right side of the above equation is generally nonzero, so the following boundary condition

$$\omega = 0 \tag{11-46}$$

generally cannot come into existence. Therefore, ω is not suitable for being selected as the nodal freedom.

While the second definition possesses the above disadvantages, references [2, 3] proposed the third definition for the nodal drilling freedom θ_z of the membrane element.

(3) The third definition—the nodal drilling freedom θ_z in the membrane element is defined as the additional rigid rotation at the element node.

In this definition, the displacement fields within the domain of an element are assumed to include two parts:

$$\boldsymbol{u} = \boldsymbol{u}^0 + \boldsymbol{u}_\theta \tag{11-47}$$

where $\boldsymbol{u}^0 = [u^0 \ v^0]^{\mathrm{T}}$ are the displacement fields determined by the nodal translational displacements; $\boldsymbol{u}_\theta = [u_\theta \ v_\theta]^{\mathrm{T}}$ are the additional displacement fields only determined by the vertex rigid rotations. According to Eq. (11-47), the deformation process of the element under external load can be expressed by Fig. 11.8. The element deformation caused by the nodal translational displacements is shown in Fig. 11.8(a), and the element deformation caused by the vertex rigid rotations is shown in Fig. 11.8(b). It should be emphatically pointed out that the above two deformation states are independent of each other.

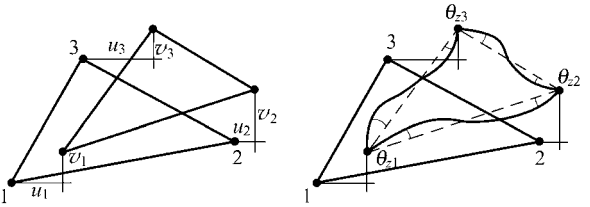

Figure 11.8 The deformation process of a plane membrane element

The characteristics of the nodal drilling freedom defined in Fig. 11.8 are as follows:

(1) The change of the angle between two adjacent sides along with the element deformation is allowed (see Fig. 11.8(a)), which overcomes the shortcomings caused by the improper constraint introduced by the early definition.

(2) The rotation θ of the element side has definite relation with the nodal drilling freedomθ_z. In fact, the rotation θ of element side is composed of two parts θ' and θ'', in which θ' is given by Fig. 11.8(a), and θ'' is just θ_z.

Just because of these two characteristics, the irrationalities in the former two definitions are avoided.

11.3.2 The Rectangular Membrane Element with Drilling Freedoms GR12

A rectangular membrane element with 12 DOFs is shown in Fig. 11.9, and the freedoms at each node are:

$$\boldsymbol{q}_i = \begin{bmatrix} u_i & v_i & \theta_i \end{bmatrix}^{\mathrm{T}} \quad (i = 1, 2, 3, 4) \tag{11-48}$$

where u_i and v_i are the translational freedoms; and θ_i is just the additional in-plane rigid rotational freedom which is defined previously.

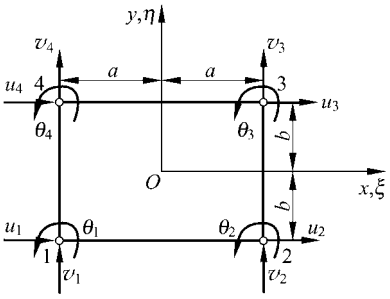

Figure 11.9 Rectangular membrane element

Assume that the element displacement mode is given by Eq. (11-47), which includes two parts $\boldsymbol{u}^0$ and $\boldsymbol{u}_\theta$. $\boldsymbol{u}^0$ are the bilinear compatible displacement fields expressed by the translational freedoms as

$$\boldsymbol{u}^0 = \begin{Bmatrix} u^0 \\ v^0 \end{Bmatrix} = \sum_{i=1}^{4} N_i^0 \begin{Bmatrix} u_i \\ v_i \end{Bmatrix} \tag{11-49}$$

where

$$N_i^0 = \frac{1}{4}(1 + \xi_i \xi)(1 + \eta_i \eta) \tag{11-50}$$

And, $\boldsymbol{u}_\theta = [u_\theta \quad v_\theta]^{\mathrm{T}}$ in Eq. (11-47) are only the additional displacement fields caused by the additional vertex rigid rotations θ_i $(i = 1, 2, 3, 4)$, as shown in Fig. 11.10. Here, θ_i is only related to the additional displacement fields $\boldsymbol{u}_\theta$ and independent of $\boldsymbol{u}^0$. The rotational freedom defined as above can describe the deformation behavior of the element boundary more clearly.
The additional displacement fields $\boldsymbol{u}_\theta$ can be assumed as

$$\left.\begin{aligned} u_\theta &= (1-\xi^2)(\alpha_1 + \alpha_2 \eta) + (1-\eta^2)(\alpha_3 + \alpha_4 \xi) \\ v_\theta &= (1-\eta^2)(\beta_1 + \beta_2 \xi) + (1-\xi^2)(\beta_3 + \beta_4 \eta) \end{aligned}\right\} \tag{11-51}$$

The values of the displacement fields expressed by the above equation at the element corner nodes are all zero.

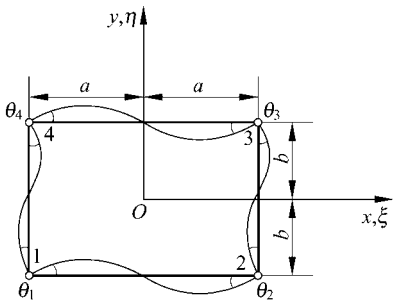

Figure 11.10 Additional displacement field

The element boundary displacements $\overline{\boldsymbol{u}}_\theta$ caused by the additional vertex rigid rotations can be written as:

$$\left.\begin{aligned}
\overline{\boldsymbol{u}}_{\theta 12} &= \begin{Bmatrix}\overline{u}_{\theta 12}\\ \overline{v}_{\theta 12}\end{Bmatrix} = \frac{a}{4}(1-\xi^2)\left[\theta_1(1-\xi)-\theta_2(1+\xi)\right]\begin{Bmatrix}0\\1\end{Bmatrix}\\
\overline{\boldsymbol{u}}_{\theta 43} &= \begin{Bmatrix}\overline{u}_{\theta 43}\\ \overline{v}_{\theta 43}\end{Bmatrix} = \frac{a}{4}(1-\xi^2)\left[\theta_4(1-\xi)-\theta_3(1+\xi)\right]\begin{Bmatrix}0\\1\end{Bmatrix}\\
\overline{\boldsymbol{u}}_{\theta 23} &= \begin{Bmatrix}\overline{u}_{\theta 23}\\ \overline{v}_{\theta 23}\end{Bmatrix} = -\frac{b}{4}(1-\eta^2)\left[\theta_2(1-\eta)-\theta_3(1+\eta)\right]\begin{Bmatrix}1\\0\end{Bmatrix}\\
\overline{\boldsymbol{u}}_{\theta 14} &= \begin{Bmatrix}\overline{u}_{\theta 14}\\ \overline{v}_{\theta 14}\end{Bmatrix} = -\frac{b}{4}(1-\eta^2)\left[\theta_1(1-\eta)-\theta_4(1+\eta)\right]\begin{Bmatrix}1\\0\end{Bmatrix}
\end{aligned}\right\} \tag{11-52}$$

From the generalized conforming condition (11-8), which can be written as

$$\int_{S_k}(\boldsymbol{u}_\theta - \overline{\boldsymbol{u}}_\theta)\mathrm{d}s = \boldsymbol{0} \quad (k=1,\,2,\,3,\,4) \tag{11-53}$$

the unknown coefficients α_i and β_i ($i=1,\,2,\,3,\,4$) in Eq. (11-51) can be solved. Then, substituting them back into Eq. (11-51), we have

$$\boldsymbol{u}_\theta = \begin{Bmatrix}u_\theta\\ v_\theta\end{Bmatrix} = \sum_{i=1}^{4}\begin{Bmatrix}N_{u\theta i}\\ N_{v\theta i}\end{Bmatrix}\theta_i \tag{11-54}$$

where

$$\left.\begin{aligned}
N_{u\theta i} &= \frac{b}{8}(1-\eta^2)(1+\xi_i\xi)\eta_i\\
N_{v\theta i} &= -\frac{a}{8}(1-\xi^2)(1+\eta_i\eta)\xi_i
\end{aligned}\right\} \tag{11-55}$$

Substitution of Eqs. (11-49) and (11-54) into Eq. (11-47) yields the displacement fields expressed in terms of the shape functions:

$$\boldsymbol{u} = \boldsymbol{u}^0 + \boldsymbol{u}_\theta = \boldsymbol{N}\boldsymbol{q}^e = \sum_{i=1}^{4} \boldsymbol{N}_i \boldsymbol{q}_i \tag{11-56}$$

where

$$\boldsymbol{q}^e = [\boldsymbol{q}_1^{\mathrm{T}} \quad \boldsymbol{q}_2^{\mathrm{T}} \quad \boldsymbol{q}_3^{\mathrm{T}} \quad \boldsymbol{q}_4^{\mathrm{T}}]^{\mathrm{T}} \tag{11-57}$$

$$\boldsymbol{N} = \begin{bmatrix} \boldsymbol{N}_1 & \boldsymbol{N}_2 & \boldsymbol{N}_3 & \boldsymbol{N}_4 \end{bmatrix} \tag{11-58}$$

$$\boldsymbol{N}_i = \begin{bmatrix} N_i^0 & 0 & N_{u\theta i} \\ 0 & N_i^0 & N_{v\theta i} \end{bmatrix} \tag{11-59}$$

and N_i^0, $N_{u\theta i}$ and $N_{v\theta i}$ are given by Eqs. (11-50) and (11-55), respectively.

Though the displacement fields expressed by Eq. (11-56) are not exactly compatible on the element boundary, they have already satisfied the generalized conforming conditions in Eq. (11-53). Therefore, the finite element formulations can be established by the potential energy principle. This element is denoted as GR12. According to the conventional procedure, the element stiffness matrix $\boldsymbol{K}^e$ can be obtained:

$$\boldsymbol{K}^e = \begin{bmatrix} \boldsymbol{K}_{11} & \boldsymbol{K}_{12} & \boldsymbol{K}_{13} & \boldsymbol{K}_{14} \\ \boldsymbol{K}_{21} & \boldsymbol{K}_{22} & \boldsymbol{K}_{23} & \boldsymbol{K}_{24} \\ \boldsymbol{K}_{31} & \boldsymbol{K}_{32} & \boldsymbol{K}_{33} & \boldsymbol{K}_{34} \\ \boldsymbol{K}_{41} & \boldsymbol{K}_{42} & \boldsymbol{K}_{43} & \boldsymbol{K}_{44} \end{bmatrix} \tag{11-60}$$

where

$$\boldsymbol{K}_{ij} = \frac{habE}{24(1-\mu^2)} \begin{bmatrix} \overline{k}_{11} & \overline{k}_{12} & \overline{k}_{13} \\ \overline{k}_{21} & \overline{k}_{22} & \overline{k}_{23} \\ \overline{k}_{31} & \overline{k}_{32} & \overline{k}_{33} \end{bmatrix} \tag{11-61}$$

with

$$\overline{k}_{11} = \frac{2}{a^2}\xi_i\xi_j\left(3+\eta_i\eta_j\right) + \frac{1-\mu}{b^2}\eta_i\eta_j\left(3+\xi_i\xi_j\right)$$

$$\overline{k}_{12} = \frac{6\mu}{ab}\xi_i\eta_j + \frac{3(1-\mu)}{ab}\eta_i\xi_j$$

$$\overline{k}_{13} = \frac{2b}{a^2}\xi_i\xi_j\eta_j - \frac{1}{b}\xi_i\xi_j\left[2\mu\eta_j - (1-\mu)\eta_i\right]$$

$$\overline{k}_{21} = \frac{6\mu}{ab}\eta_i\xi_j + \frac{3(1-\mu)}{ab}\xi_i\eta_j$$

$$\bar{k}_{22}=\frac{2}{b^2}\eta_i\eta_j\left(3+\xi_i\xi_j\right)+\frac{1-\mu}{a^2}\xi_i\xi_j\left(3+\eta_i\eta_j\right)$$

$$\bar{k}_{23}=-\frac{2a}{b^2}\eta_i\eta_j\xi_j+\frac{1}{a}\eta_i\eta_j\left[2\mu\xi_j-(1-\mu)\xi_i\right]$$

$$\bar{k}_{31}=\frac{2b}{a^2}\eta_i\xi_i\xi_j-\frac{1}{b}\xi_i\xi_j\left[2\mu\eta_i-(1-\mu)\eta_j\right]$$

$$\bar{k}_{32}=-\frac{2a}{b^2}\xi_i\eta_i\eta_j+\frac{1}{a}\eta_i\eta_j\left[2\mu\xi_i-(1-\mu)\xi_j\right]$$

$$\bar{k}_{33}=\frac{4}{5}\left(\frac{a^2}{b^2}+\frac{b^2}{a^2}-\frac{5}{3}\mu\right)\xi_i\xi_j\eta_i\eta_j+(1-\mu)\left(\xi_i\xi_j+\eta_i\eta_j\right)$$

11.3.3 The Rectangular Membrane Element with Drilling Freedoms GR12M—with Internal Freedoms

Consider the following bubble displacement fields:

$$\boldsymbol{u}_\lambda=\begin{Bmatrix}u_\lambda\\v_\lambda\end{Bmatrix}=\boldsymbol{N}_\lambda\boldsymbol{\lambda}=\begin{bmatrix}N_\lambda & 0\\0 & N_\lambda\end{bmatrix}\begin{Bmatrix}\lambda_1\\\lambda_2\end{Bmatrix} \tag{11-62}$$

where

$$N_\lambda=(1-\xi^2)(1-\eta^2) \tag{11-63}$$

λ_1 and λ_2 are arbitrary parameters.

By the superposition of Eqs. (11-62) and (11-47), the displacement fields with three parts can be obtained

$$\boldsymbol{u}=\boldsymbol{u}^0+\boldsymbol{u}_\theta+\boldsymbol{u}_\lambda \tag{11-64}$$

This is the displacement mode of the element GR12M. Substitution of Eqs. (11-56) and (11-62) into the above equation yields

$$\boldsymbol{u}=\boldsymbol{N}\boldsymbol{q}^e+\boldsymbol{N}_\lambda\boldsymbol{\lambda} \tag{11-65}$$

The corresponding strain fields can be expressed as

$$\boldsymbol{\varepsilon}=\boldsymbol{B}\boldsymbol{q}^e+\boldsymbol{B}_\lambda\boldsymbol{\lambda} \tag{11-66}$$

in which $\boldsymbol{B}$ and $\boldsymbol{B}_\lambda$ are the strain matrices corresponding to Eqs. (11-56) and (11-62), respectively.

According to Eq. (11-66), the strain energy of element GR12M can be written as

$$U = \frac{h}{2}\iint_{A^e} \boldsymbol{\varepsilon}^{\mathrm{T}} \boldsymbol{D}\boldsymbol{\varepsilon}\mathrm{d}A = \frac{1}{2}\boldsymbol{q}^{e\mathrm{T}}\boldsymbol{K}_{qq}\boldsymbol{q}^{e} + \boldsymbol{\lambda}^{\mathrm{T}}\boldsymbol{K}_{\lambda q}\boldsymbol{q}^{e} + \frac{1}{2}\boldsymbol{\lambda}^{\mathrm{T}}\boldsymbol{K}_{\lambda\lambda}\boldsymbol{\lambda} \tag{11-67}$$

in which

$$\boldsymbol{K}_{qq} = abh\int_{-1}^{1}\int_{-1}^{1} \boldsymbol{B}^{\mathrm{T}}\boldsymbol{D}\boldsymbol{B}\mathrm{d}\xi\mathrm{d}\eta \tag{11-68a}$$

$$\boldsymbol{K}_{\lambda q} = abh\int_{-1}^{1}\int_{-1}^{1} \boldsymbol{B}_{\lambda}{}^{\mathrm{T}}\boldsymbol{D}\boldsymbol{B}\mathrm{d}\xi\mathrm{d}\eta \tag{11-68b}$$

$$\boldsymbol{K}_{\lambda\lambda} = abh\int_{-1}^{1}\int_{-1}^{1} \boldsymbol{B}_{\lambda}{}^{\mathrm{T}}\boldsymbol{D}\boldsymbol{B}_{\lambda}\mathrm{d}\xi\mathrm{d}\eta \tag{11-68c}$$

From the stationary condition

$$\frac{\partial U}{\partial \boldsymbol{\lambda}} = \boldsymbol{0} \tag{11-69}$$

the arbitrary parameters $\boldsymbol{\lambda}$ can be expressed in terms of the external DOFs as

$$\boldsymbol{\lambda} = -\boldsymbol{K}_{\lambda\lambda}^{-1}\boldsymbol{K}_{\lambda q}\boldsymbol{q}^{e} \tag{11-70}$$

Substitution of the above equation into Eq. (11-65) yields

$$\boldsymbol{u} = \boldsymbol{N}^{*}\boldsymbol{q}^{e} \tag{11-71}$$

where

$$\boldsymbol{N}^{*} = \boldsymbol{N} - \boldsymbol{N}_{\lambda}\boldsymbol{K}_{\lambda\lambda}^{-1}\boldsymbol{K}_{\lambda q} \tag{11-72}$$

The above equation includes the shape functions of the element GR12M, in which $\boldsymbol{K}_{\lambda q}$ and $\boldsymbol{K}_{\lambda\lambda}^{-1}$ are evaluated from Eqs. (11-68b) and (11-68c), respectively,

$$\boldsymbol{K}_{\lambda q} = [\boldsymbol{K}_1' \quad \boldsymbol{K}_2' \quad \boldsymbol{K}_3' \quad \boldsymbol{K}_4'] \tag{11-73}$$

where

$$\boldsymbol{K}_i' = -\frac{2Eh}{9(1-\mu^2)}\begin{bmatrix} 0 & (1+\mu)\xi_i\eta_i & -a(1-\mu)\eta_i \\ (1+\mu)\xi_i\eta_i & 0 & b(1-\mu)\xi_i \end{bmatrix} \quad (i = 1, 2, 3, 4) \tag{11-74}$$

$$\boldsymbol{K}_{\lambda\lambda}{}^{-1} = \frac{45(1-\mu^2)ab}{128E}\begin{bmatrix} \dfrac{1}{b^2 + \dfrac{1-\mu}{2}a^2} & 0 \\ 0 & \dfrac{1}{a^2 + \dfrac{1-\mu}{2}b^2} \end{bmatrix} \tag{11-75}$$

According to the element shape function (11-72), the element stiffness matrix can be written as

$$\boldsymbol{K}^e = \boldsymbol{K}_{qq} - \boldsymbol{K}_{\lambda q}^{\mathrm{T}} \boldsymbol{K}_{\lambda\lambda}^{-1} \boldsymbol{K}_{\lambda q} \tag{11-76}$$

here $\boldsymbol{K}_{qq}$ is the same as the element stiffness matrix of the element GR12.

The stress vector of the element GR12 is $\boldsymbol{\sigma} = \boldsymbol{S}\boldsymbol{q}^e$, in which the stress matrix $\boldsymbol{S}$ is

$$\boldsymbol{S} = [\boldsymbol{S}_1 \quad \boldsymbol{S}_2 \quad \boldsymbol{S}_3 \quad \boldsymbol{S}_4] \tag{11-77}$$

in which

$$\boldsymbol{S}_i = \frac{E}{8ab(1-\mu^2)} \begin{bmatrix} s_{11} & s_{12} & s_{13} \\ s_{21} & s_{22} & s_{23} \\ s_{31} & s_{32} & s_{33} \end{bmatrix} \quad (i = 1,2,3,4) \tag{11-78}$$

with

$$\begin{aligned}
s_{11} &= 2b\xi_i(1+\eta_i\eta), \quad s_{12} = 2a\mu\eta_i(1+\xi_i\xi) \\
s_{13} &= [b^2(1-\eta^2) - \mu a^2(1-\xi^2)]\xi_i\eta_i \\
s_{21} &= 2b\mu\xi_i(1+\eta_i\eta), \quad s_{22} = 2a\eta_i(1+\xi_i\xi) \\
s_{23} &= [\mu b^2(1-\eta^2) - a^2(1-\xi^2)]\xi_i\eta_i \\
s_{31} &= a(1-\mu)\eta_i(1+\xi_i\xi) \\
s_{32} &= b(1-\mu)\xi_i(1+\eta_i\eta) \\
s_{33} &= ab(1-\mu)(\xi_i\xi - \eta_i\eta)
\end{aligned}$$

And the stress vector of the element GR12M can be written as

$$\boldsymbol{\sigma} = \boldsymbol{D}(\boldsymbol{\varepsilon} - \boldsymbol{\varepsilon}') = (\boldsymbol{S} - \boldsymbol{S}')\boldsymbol{q}^e = \sum_{i=1}^{4} (\boldsymbol{S}_i - \boldsymbol{S}_i')\boldsymbol{q}_i \tag{11-79}$$

in which $\boldsymbol{S}_i$ is given by Eq. (11-78), and $\boldsymbol{S}_i'$ is

$$\boldsymbol{S}_i' = \boldsymbol{D}\boldsymbol{B}_\lambda \boldsymbol{K}_{\lambda\lambda}^{-1} \boldsymbol{K}_i' = \boldsymbol{S}_\lambda \boldsymbol{K}_{\lambda\lambda}^{-1} \boldsymbol{K}_i' \quad (i = 1,2,3,4) \tag{11-80}$$

where

$$\boldsymbol{S}_\lambda = -\frac{2E}{ab(1-\mu^2)} \begin{bmatrix} b(1-\eta^2)\xi & a\mu(1-\xi^2)\eta \\ b\mu(1-\eta^2)\xi & a(1-\xi^2)\eta \\ \dfrac{a(1-\mu)}{2}(1-\xi^2)\eta & \dfrac{b(1-\mu)}{2}(1-\eta^2)\xi \end{bmatrix} \tag{11-81}$$

$\boldsymbol{K}_i'$ and $\boldsymbol{K}_{\lambda\lambda}^{-1}$ are given by Eqs. (11-74) and (11-75), respectively.

11.3.4 Quadrilateral Membrane Elements with Drilling Freedoms GQ12 and GQ12M

The rectangular elements GR12 and GR12M can be generalized to quadrilateral elements, the details can be found in reference [2].

11.4 Membrane Elements with Drilling Freedoms —Triangular Elements

On the basis of the constant strain triangular element, if we use the additional rigid rotational freedom proposed previously, the additional displacement fields caused only by the vertex rigid rotations can be introduced into the constant-strain displacement fields, and then, the triangular membrane element with drilling freedoms, GT9, can be derived. On the basis of the element GT9, by adding the generalized bubble displacement field, the new triangular membrane elements with higher accuracy, GT9M and GT9M8, can be obtained. These three elements can pass the patch test with arbitrary shape, so they are convergent models.

11.4.1 Triangular Membrane Element with Drilling Freedoms GT9

A triangular membrane element is shown in Fig. 11.11. At each node, there are two translational freedoms and one in-plane rotational freedom. The element nodal displacement vector is

$$\boldsymbol{q}^e = [\boldsymbol{q}_1^{\mathrm{T}} \quad \boldsymbol{q}_2^{\mathrm{T}} \quad \boldsymbol{q}_3^{\mathrm{T}}]^{\mathrm{T}} \tag{11-82}$$

where

$$\boldsymbol{q}_i = [u_i \quad v_i \quad \theta_i]^{\mathrm{T}} \quad (i = 1,2,3) \tag{11-83}$$

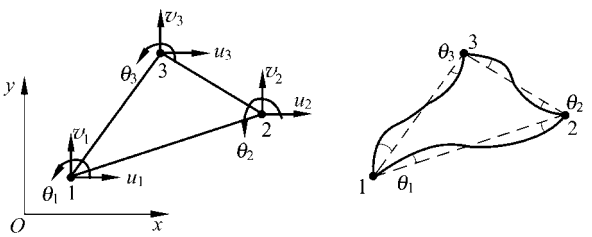

Figure 11.11 A triangular membrane element and its additional displacement field

in which u_i and v_i are the translational displacements at the corner node; θ_i is the additional rigid rotation at the corner node. As described in Sect. 11.3.1, θ_i used here is different from the rotation defined in continuum mechanics.

The basic displacement fields are assumed to be composed of two parts:

$$\boldsymbol{u}_{\mathrm{b}} = \boldsymbol{u}^0 + \boldsymbol{u}_\theta \tag{11-84}$$

where $\boldsymbol{u}^0 = [u^0 \; v^0]^{\mathrm{T}}$ are the linear displacement fields, which are determined by the translational freedoms at the corner nodes uniquely. These are compatible displacement fields, and can be expressed in terms of the triangular area coordinates as

$$\boldsymbol{u}^0 = \begin{Bmatrix} u^0 \\ v^0 \end{Bmatrix} = \sum_{i=1}^{3} \begin{bmatrix} L_i & 0 \\ 0 & L_i \end{bmatrix} \begin{Bmatrix} u_i \\ v_i \end{Bmatrix} \tag{11-85}$$

And, $\boldsymbol{u}_\theta = [u_\theta \;\; v_\theta \;]^{\mathrm{T}}$ are the additional displacement fields only caused by the in-plane vertex rigid rotational freedoms. It can be assumed to be the pure quadric polynomial in terms of the area coordinates

$$\boldsymbol{u}_\theta = \begin{Bmatrix} u_\theta \\ v_\theta \end{Bmatrix} = L_2 L_3 \begin{Bmatrix} \alpha_1 \\ \beta_1 \end{Bmatrix} + L_3 L_1 \begin{Bmatrix} \alpha_2 \\ \beta_2 \end{Bmatrix} + L_1 L_2 \begin{Bmatrix} \alpha_3 \\ \beta_3 \end{Bmatrix} \tag{11-86}$$

The value of $\boldsymbol{u}_\theta$ in the above equation at the corner node i is zero.

Along the sides of triangular element, the normal displacements due to the vertex rigid rotations can be written as the cubic interpolation formulas

$$\left.\begin{aligned} \overline{u}_{n\theta 23} &= -d_1 L_2 L_3 \left(\theta_2 L_2 - \theta_3 L_3\right) \\ \overline{u}_{n\theta 31} &= -d_2 L_3 L_1 \left(\theta_3 L_3 - \theta_1 L_1\right) \\ \overline{u}_{n\theta 12} &= -d_3 L_1 L_2 \left(\theta_1 L_1 - \theta_2 L_2\right) \end{aligned}\right\} \tag{11-87}$$

in which $d_i \, (i = 1, 2, 3)$ are the lengths of the triangular element sides. And, the vertex rotations will not produce the tangent displacements along the element sides, i.e.,

$$\overline{u}_{s\theta 23} = \overline{u}_{s\theta 12} = \overline{u}_{s\theta 31} = 0 \tag{11-88}$$

The direction cosines of the normal on the element side (L_i=0) are

$$n_{xi} = -\frac{b_i}{d_i}, \quad n_{yi} = -\frac{c_i}{d_i} \quad (i = 1, 2, 3) \tag{11-89}$$

where b_i and c_i are given by Eq. (6-13). The projections of the normal displacements in Eq. (11-87) on x-axes and y-axes are

$$\left.\begin{aligned}
\left\{\begin{matrix}\overline{u}_\theta\\ \overline{v}_\theta\end{matrix}\right\}_{L_1=0} &= \left\{\begin{matrix}b_1\\ c_1\end{matrix}\right\} L_2L_3\left(\theta_2L_2-\theta_3L_3\right)\\
\left\{\begin{matrix}\overline{u}_\theta\\ \overline{v}_\theta\end{matrix}\right\}_{L_2=0} &= \left\{\begin{matrix}b_2\\ c_2\end{matrix}\right\} L_3L_1\left(\theta_3L_3-\theta_1L_1\right)\\
\left\{\begin{matrix}\overline{u}_\theta\\ \overline{v}_\theta\end{matrix}\right\}_{L_3=0} &= \left\{\begin{matrix}b_3\\ c_3\end{matrix}\right\} L_1L_2\left(\theta_1L_1-\theta_2L_2\right)
\end{aligned}\right\} \tag{11-90}$$

Between the element boundary displacements (11-90) and the element additional displacement fields (11-86), we introduce the following generalized conforming conditions

$$\int_{L_i=0}\left(\left\{\begin{matrix}u_\theta\\ v_\theta\end{matrix}\right\}-\left\{\begin{matrix}\overline{u}_\theta\\ \overline{v}_\theta\end{matrix}\right\}\right)\mathrm{d}s=0 \qquad (i=1,2,3) \tag{11-91}$$

from which 6 unknown coefficients α_i and $\beta_i\,(i=1,2,3)$ in Eq. (11-86) can be solved. So, the additional displacement fields expressed only by θ_i can be obtained

$$\boldsymbol{u}_\theta=\left\{\begin{matrix}u_\theta\\ v_\theta\end{matrix}\right\}=\sum_{i=1}^{3}\left\{\begin{matrix}N_{u\theta i}\\ N_{v\theta i}\end{matrix}\right\}\theta_i \tag{11-92}$$

where

$$\left.\begin{aligned}
N_{u\theta i}&=\frac{1}{2}L_i\left(b_mL_j-b_jL_m\right)\\
N_{v\theta i}&=\frac{1}{2}L_i\left(c_mL_j-c_jL_m\right)
\end{aligned}\right\} \quad (i,j,m=\overleftrightarrow{1,2,3}) \tag{11-93}$$

The displacement mode of the triangular membrane element GT9 is given by Eq. (11-84). From Eqs. (11-85) and (11-92), it can be expressed in terms of the shape functions

$$\boldsymbol{u}_{\mathrm{b}}=\boldsymbol{u}^0+\boldsymbol{u}_\theta=\boldsymbol{N}\boldsymbol{q}^e=\sum_{i=1}^{3}\boldsymbol{N}_i\boldsymbol{q}_i \tag{11-94}$$

in which

$$\boldsymbol{N}=[\boldsymbol{N}_1 \quad \boldsymbol{N}_2 \quad \boldsymbol{N}_3] \tag{11-95}$$

$$\boldsymbol{N}_i=\begin{bmatrix}L_i & 0 & N_{u\theta i}\\ 0 & L_i & N_{v\theta i}\end{bmatrix} \quad (i=1,2,3) \tag{11-96}$$

where $N_{u\theta i}$ and $N_{v\theta i}$ are given by Eq. (11-93).

Since the displacement fields (11-94) satisfy the generalized conforming conditions (11-8), therefore, the element stiffness matrix $\boldsymbol{K}^e$ can be derived by the conventional procedure:

$$\boldsymbol{K}^e = \begin{bmatrix} \boldsymbol{K}_{11} & \boldsymbol{K}_{12} & \boldsymbol{K}_{13} \\ \boldsymbol{K}_{21} & \boldsymbol{K}_{22} & \boldsymbol{K}_{23} \\ \boldsymbol{K}_{31} & \boldsymbol{K}_{32} & \boldsymbol{K}_{33} \end{bmatrix} \tag{11-97}$$

where the sub-matrices are

$$\boldsymbol{K}_{ij} = h \iint_{A^e} \boldsymbol{B}_i^{\mathrm{T}} \boldsymbol{D} \boldsymbol{B}_j \mathrm{d}A \quad (i, j = 1,2,3) \tag{11-98}$$

in which

$$\boldsymbol{B}_i = \frac{1}{4A} \begin{bmatrix} 2b_i & 0 & b_i\left(b_m L_j - b_j L_m\right) \\ 0 & 2c_i & c_i\left(c_m L_j - c_j L_m\right) \\ 2c_i & 2b_i & \left(c_i b_m + b_i c_m\right) L_j - \left(c_i b_j + b_i c_j\right) L_m \end{bmatrix} \quad (i, j, m = \overrightarrow{1,2,3}) \tag{11-99}$$

11.4.2 Triangular Membrane Element with Drilling Freedoms GT9M—with an Internal Freedom

The displacement functions with one arbitrary internal parameter λ can be assumed as

$$\boldsymbol{u}_\lambda = \begin{Bmatrix} u_\lambda \\ v_\lambda \end{Bmatrix} = \boldsymbol{N}_\lambda \lambda = \begin{Bmatrix} N_{u\lambda} \\ N_{v\lambda} \end{Bmatrix} \lambda \tag{11-100}$$

where

$$\boldsymbol{N}_\lambda = [N_{u\lambda} \quad N_{v\lambda}]^{\mathrm{T}} \tag{11-101}$$

$$N_{u\lambda} = \sum_{i=1}^{3} b_i F_i \ , \qquad N_{v\lambda} = \sum_{i=1}^{3} c_i F_i \tag{11-102}$$

and

$$F_i = L_j L_m \left(L_j - L_m\right) \tag{11-103}$$

It can be easily verified that Eq. (11-100) satisfies the following equation:

$$\int_{L_i = 0} \boldsymbol{u}_\lambda \mathrm{d}s = \boldsymbol{0} \quad (i = 1,2,3) \tag{11-104}$$

and is equal to zero at 3 corner nodes. Hence, the displacement functions given by Eq. (11-100) are the generalized bubble displacements whose average values along the element sides are zero.

The displacement fields of the element GT9M are composed of 3 parts:

$$\boldsymbol{u} = \boldsymbol{u}^0 + \boldsymbol{u}_\theta + \boldsymbol{u}_\lambda \tag{11-105}$$

From Eqs. (11-94) and (11-100), the above equation can be expressed as

$$\boldsymbol{u} = \boldsymbol{N}\boldsymbol{q}^e + \boldsymbol{N}_\lambda \lambda \tag{11-106}$$

in which $\boldsymbol{N}$ and $\boldsymbol{N}_\lambda$ are given by Eqs. (11-95) and (11-101), respectively. The strain fields corresponding to Eq. (11-106) are

$$\boldsymbol{\varepsilon} = \boldsymbol{B}\boldsymbol{q}^e + \boldsymbol{B}_\lambda \lambda \tag{11-107}$$

where $\boldsymbol{B}$ is the strain matrix corresponding to Eq. (11-94); $\boldsymbol{B}_\lambda$ is the strain vector corresponding to Eq. (11-100). From Eq. (11-107), the strain energy of the element GT9M can be written as

$$U = \frac{h}{2}\iint_{A^e} \boldsymbol{\varepsilon}^{\mathrm{T}} \boldsymbol{D}\boldsymbol{\varepsilon}\mathrm{d}A = \frac{1}{2}\boldsymbol{q}^{e\mathrm{T}}\boldsymbol{K}_{qq}\boldsymbol{q}^e + \lambda \boldsymbol{K}_{\lambda q}\boldsymbol{q}^e + \frac{1}{2}\lambda^2 k_{\lambda\lambda} \tag{11-108}$$

where

$$\boldsymbol{K}_{qq} = h\iint_{A^e} \boldsymbol{B}^{\mathrm{T}}\boldsymbol{D}\boldsymbol{B}\mathrm{d}A \tag{11-109a}$$

$$\boldsymbol{K}_{\lambda q} = h\iint_{A^e} \boldsymbol{B}_\lambda{}^{\mathrm{T}}\boldsymbol{D}\boldsymbol{B}\mathrm{d}A \tag{11-109b}$$

$$k_{\lambda\lambda} = h\iint_{A^e} \boldsymbol{B}_\lambda{}^{\mathrm{T}}\boldsymbol{D}\boldsymbol{B}_\lambda\mathrm{d}A \tag{11-109c}$$

with

$$\boldsymbol{B} = [\boldsymbol{B}_1 \quad \boldsymbol{B}_2 \quad \boldsymbol{B}_3] \tag{11-110}$$

in which $\boldsymbol{B}_i$ ($i = 1,2,3$) are given by Eq. (11-99); and

$$\boldsymbol{B}_\lambda = \frac{1}{A}\sum_{i=1}^{3}\begin{Bmatrix} b_m^2 - b_j^2 \\ c_m^2 - c_j^2 \\ 2\left(b_m c_m - b_j c_j\right) \end{Bmatrix} L_m L_j \qquad (i, j, m = \overrightarrow{1,2,3}) \tag{11-111}$$

From the stationary condition

$$\frac{\partial U}{\partial \lambda} = 0 \tag{11-112}$$

the arbitrary parameter λ in Eq. (11-106) can be expressed in terms of $\boldsymbol{q}^e$

$$\lambda = -\frac{1}{k_{\lambda\lambda}} \boldsymbol{K}_{\lambda q} \boldsymbol{q}^e \tag{11-113}$$

Substituting the above equation into Eq. (11-106), the displacement fields of the element GT9M expressed only in terms of external freedoms $\boldsymbol{q}^e$ can be obtained

$$\boldsymbol{u} = \boldsymbol{N}^* \boldsymbol{q}^e \tag{11-114}$$

where

$$\boldsymbol{N}^* = \boldsymbol{N} - \frac{1}{k_{\lambda\lambda}} \boldsymbol{N}_\lambda \boldsymbol{K}_{\lambda q} \tag{11-115}$$

The stiffness matrix of the element GT9M is

$$\boldsymbol{K}^e = \boldsymbol{K}_{qq} - \frac{1}{k_{\lambda\lambda}} \boldsymbol{K}_{\lambda q}^{\mathrm{T}} \boldsymbol{K}_{\lambda q} \tag{11-116}$$

in which $\boldsymbol{K}_{qq}$ is the same as $\boldsymbol{K}^e$ in Eq. (11-97).

11.4.3 Triangular Membrane Element with Drilling Freedoms GT9M8—with 8 Internal Freedoms

The element GT9M derived above contains one internal freedom, and the corresponding generalized bubble displacement is cubic. Now, we will develop a new element GT9M8 with 8 internal freedoms, and the corresponding generalized bubble displacement is still cubic.

Assume that the element displacement fields are composed of two parts:

$$\boldsymbol{u} = \boldsymbol{u}_{\mathrm{b}} + \boldsymbol{u}_\lambda \tag{11-117}$$

where $\boldsymbol{u}_{\mathrm{b}}$ are the basic displacement functions given by Eq. (11-94); $\boldsymbol{u}_\lambda$ are the additional displacement fields expressed by internal freedoms, here they are assumed to be complete cubic polynomials in the area coordinates

$$\begin{aligned}\boldsymbol{u}_\lambda = \begin{Bmatrix} u_\lambda \\ v_\lambda \end{Bmatrix} &= L_1 \begin{Bmatrix} \alpha_1 \\ \beta_1 \end{Bmatrix} + L_2 \begin{Bmatrix} \alpha_2 \\ \beta_2 \end{Bmatrix} + L_3 \begin{Bmatrix} \alpha_3 \\ \beta_3 \end{Bmatrix} + L_2 L_3 \begin{Bmatrix} \alpha_4 \\ \beta_4 \end{Bmatrix} + L_3 L_1 \begin{Bmatrix} \alpha_5 \\ \beta_5 \end{Bmatrix} \\ &+ L_1 L_2 \begin{Bmatrix} \alpha_6 \\ \beta_6 \end{Bmatrix} + L_2^2 L_3 \begin{Bmatrix} \lambda_1 \\ \lambda_2 \end{Bmatrix} + L_3^2 L_1 \begin{Bmatrix} \lambda_3 \\ \lambda_4 \end{Bmatrix} + L_1^2 L_2 \begin{Bmatrix} \lambda_5 \\ \lambda_6 \end{Bmatrix} + L_1 L_2 L_3 \begin{Bmatrix} \lambda_7 \\ \lambda_8 \end{Bmatrix}\end{aligned} \tag{11-118}$$

where α_i and β_i ($i=1, 2, \cdots, 6$), λ_i ($i=1, 2, \cdots, 8$) are the arbitrary parameters. Substitution of Eq. (11-118) into the generalized conforming conditions corresponding to zero average side displacements and zero vertex displacement conditions:

$$\int_{L_i=0} \boldsymbol{u}_\lambda \mathrm{d}s = \boldsymbol{0}, \quad \boldsymbol{u}_\lambda\big|_{L_i=1} = \boldsymbol{0} \qquad (i=1, 2, 3) \tag{11-119}$$

yields the additional displacement functions expressed by 8 arbitrary parameters λ_i ($i=1, 2, \cdots, 8$):

$$\boldsymbol{u}_\lambda = \begin{Bmatrix} u_\lambda \\ v_\lambda \end{Bmatrix} = \sum_{i=1}^{3} L_j L_m \left(L_j - \frac{1}{2} \right) \begin{Bmatrix} \lambda_{2i-1} \\ \lambda_{2i} \end{Bmatrix} + L_1 L_2 L_3 \begin{Bmatrix} \lambda_7 \\ \lambda_8 \end{Bmatrix} \tag{11-120}$$

The above formulas are the generalized bubble functions which satisfy the generalized conforming conditions. And $\lambda_1, \lambda_2, \cdots, \lambda_8$ are 8 internal freedoms.

By the way, the internal displacement field that is exactly compatible with zero boundary displacement is called bubble displacement, and that is generalized conforming to zero boundary displacement is called generalized bubble displacement. Equation (11-120) contains 8 internal freedoms, in which λ_7 and λ_8 are corresponding to the bubble displacements, while $\lambda_1, \lambda_2, \cdots, \lambda_6$ are corresponding to the generalized bubble displacements.

The additional displacements (11-120) expressed by internal freedoms can be written as the following matrix form:

$$\boldsymbol{u}_\lambda = \boldsymbol{N}_\lambda \boldsymbol{\lambda} \tag{11-121}$$

in which

$$\boldsymbol{N}_\lambda = \begin{bmatrix} F_1 & 0 & F_2 & 0 & F_3 & 0 & F_4 & 0 \\ 0 & F_1 & 0 & F_2 & 0 & F_3 & 0 & F_4 \end{bmatrix} \tag{11-122}$$

where

$$F_i = L_j L_m \left(L_j - \frac{1}{2} \right) \quad (i=1,2,3), \quad F_4 = L_1 L_2 L_3 \tag{11-123}$$

And, $\boldsymbol{\lambda}$ in Eq. (11-121) is the internal freedom vector:

$$\boldsymbol{\lambda} = [\lambda_1 \quad \lambda_2 \quad \lambda_3 \quad \lambda_4 \quad \lambda_5 \quad \lambda_6 \quad \lambda_7 \quad \lambda_8]^{\mathrm{T}} \tag{11-124}$$

From Eqs. (11-117), (11-94) and (11-121), the displacement fields of the element GT9M8 can be expressed in terms of the shape functions

$$\boldsymbol{u} = \boldsymbol{N}\boldsymbol{q}^e + \boldsymbol{N}_\lambda \boldsymbol{\lambda} \tag{11-125}$$

where $\boldsymbol{N}$ and $\boldsymbol{N}_\lambda$ are given by Eqs. (11-95) and (11-122), respectively.

From the element displacement given by Eq. (11-125), and according to the procedure similar to those in Sects. 11.3.2 and 11.3.3, the internal freedoms $\boldsymbol{\lambda}$ can be expressed in terms of $\boldsymbol{q}^e$ by condensation

$$\boldsymbol{\lambda} = -\boldsymbol{K}_{\lambda\lambda}^{-1}\boldsymbol{K}_{\lambda q}\boldsymbol{q}^e \tag{11-126}$$

where

$$\boldsymbol{K}_{\lambda q} = h\iint_{A^e}\boldsymbol{B}_\lambda^{\mathrm{T}}\boldsymbol{D}\boldsymbol{B}\mathrm{d}A \tag{11-127a}$$

$$\boldsymbol{K}_{\lambda\lambda} = h\iint_{A^e}\boldsymbol{B}_\lambda^{\mathrm{T}}\boldsymbol{D}\boldsymbol{B}_\lambda\mathrm{d}A \tag{11-127b}$$

in which $\boldsymbol{B}$ in Eq. (11-127a) is given by Eq. (11-110); and $\boldsymbol{B}_\lambda$ in Eq. (11-127) is

$$\boldsymbol{B}_\lambda = \begin{bmatrix} F_{1x} & 0 & F_{2x} & 0 & F_{3x} & 0 & F_{4x} & 0 \\ 0 & F_{1y} & 0 & F_{2y} & 0 & F_{3y} & 0 & F_{4y} \\ F_{1y} & F_{1x} & F_{2y} & F_{2x} & F_{3y} & F_{3x} & F_{4y} & F_{4x} \end{bmatrix} \tag{11-128}$$

$$\left.\begin{aligned} F_{ix} &= \frac{1}{2A}\left[b_j L_m\left(2L_j - \frac{1}{2}\right) + b_m L_j\left(L_j - \frac{1}{2}\right)\right] \\ F_{iy} &= \frac{1}{2A}\left[c_j L_m\left(2L_j - \frac{1}{2}\right) + c_m L_j\left(L_j - \frac{1}{2}\right)\right] \\ F_{4x} &= \frac{1}{2A}\left(b_1 L_2 L_3 + b_2 L_3 L_1 + b_3 L_1 L_2\right) \\ F_{4y} &= \frac{1}{2A}\left(c_1 L_2 L_3 + c_2 L_3 L_1 + c_3 L_1 L_2\right) \end{aligned}\right\} \quad (i,j,m = \overrightarrow{1,2,3}) \tag{11-129}$$

Thus, Eq. (11-125) can be expressed in terms of external freedoms as

$$\boldsymbol{u} = \boldsymbol{N}^*\boldsymbol{q}^e \tag{11-130}$$

where

$$\boldsymbol{N}^* = \boldsymbol{N} - \boldsymbol{N}_\lambda\boldsymbol{K}_{\lambda\lambda}^{-1}\boldsymbol{K}_{\lambda q} \tag{11-131}$$

According to the displacement field (11-130) expressed by the shape functions, the element stiffness matrix can be obtained

$$\boldsymbol{K}^e = \boldsymbol{K}_{qq} - \boldsymbol{K}_{\lambda q}^{\mathrm{T}}\boldsymbol{K}_{\lambda\lambda}^{-1}\boldsymbol{K}_{\lambda q} \tag{11-132}$$

where $\boldsymbol{K}_{qq}$ is evaluated by Eq. (11-97).

Example 11.4 Pure in-plane bending of a square plate.

A square plate of side length L is shown in Fig. 11.12. It is subjected to a linear

varying normal stress on the left and right sides:

$$\sigma_x\Big|_{x=\pm(L/2)} = 2\left(\frac{y}{L}\right)\sigma_0$$

In view of the symmetry of the problem, only 1/4 of the plate is considered and meshed. Numerical results of the displacement and stress at corner point C are listed in Table 11.4. For comparison, the other results obtained by Allman[23] and the bilinear rectangular element R4 are also given.

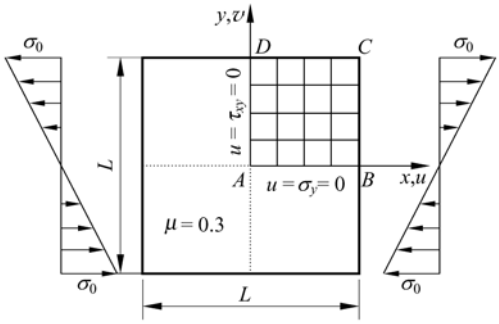

Figure 11.12 Pure in-plane bending of a square plate (Mesh 4 × 4)

From Table 11.4, it can be seen that the presented two rectangular elements GR12 and GR12M can provide more accurate results for displacement and stress.

Table 11.4 The displacement and stress at point C of a square plate under pure in-plane bending

Mesh (1/4 plate)	(1 × 1)			(2 × 2)		
Element	$\frac{Eu_C}{\sigma_0 L}$	$\frac{Ev_C}{\sigma_0 L}$	$\frac{\sigma_{xC}}{\sigma_0}$	$\frac{Eu_C}{\sigma_0 L}$	$\frac{Ev_C}{\sigma_0 L}$	$\frac{\sigma_{xC}}{\sigma_0}$
R4	0.4461	– 0.2900	0.9363	0.4797	– 0.3120	0.9770
Allman[23]	0.4738	– 0.3070	0.9784	0.4910	– 0.3191	0.9912
GR12	0.4823	– 0.3108	1.0220	0.4941	– 0.3206	1.0129
GR12M	0.4961	– 0.3218	1.0055	0.4987	– 0.3241	1.0029
Mesh (1/4 plate)	(4 × 4)			(8 × 8)		
Element	$\frac{Eu_C}{\sigma_0 L}$	$\frac{Ev_C}{\sigma_0 L}$	$\frac{\sigma_{xC}}{\sigma_0}$	$\frac{Eu_C}{\sigma_0 L}$	$\frac{Ev_C}{\sigma_0 L}$	$\frac{\sigma_{xC}}{\sigma_0}$
R4	0.4931	– 0.3206	0.9894	0.4978	– 0.3236	0.9947
Allman[23]	0.4971	– 0.3231	0.9956	0.4991	– 0.3244	0.9978
GR12	0.4982	– 0.3237	1.0066	0.4994	– 0.3246	1.0033
GR12M	0.4996	– 0.3247	1.0015	0.4999	– 0.3249	1.0007

Note: Exact solutions are given by [23] $\frac{Eu_C}{\sigma_0 L} = 0.5000$, $\frac{Ev_C}{\sigma_0 L} = -0.3250$, $\frac{\sigma_{xC}}{\sigma_0} = 1.0000$.

Example 11.5 Cantilever beam under a tip shear load.

As shown in Fig. 11.13, a cantilever beam is subjected to a tip parabolic shear load

$$\tau_{xy}\Big|_{x=L} = \frac{3W}{2Hh}\left[1-4\left(\frac{y}{H}\right)^2\right]$$

where L, H and h are the length, height and thickness of the beam, respectively. 3 finite element meshes plotted in the figure are used. Numerical results for the deflection at the mid-side point C of the beam tip and stress of point A are listed in Table 11.5, where the coordinates of the point A is (12, 6).

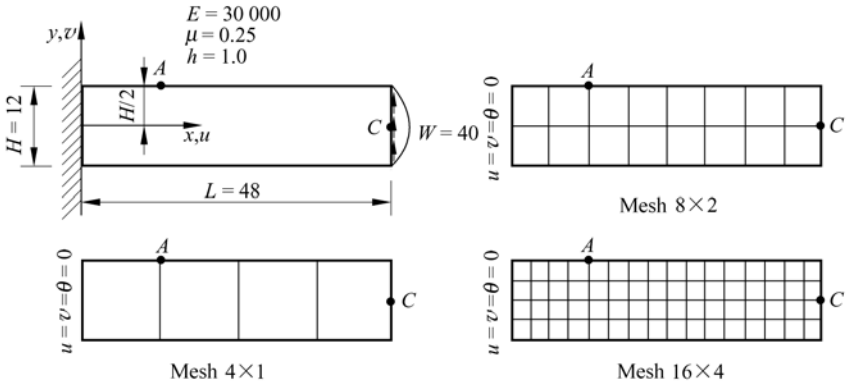

Figure 11.13 A cantilever beam under tip shear load

It can be seen from the results that, the performance of the bilinear element R4 is obviously lower than those of the other elements. And, the precisions of the presented two elements GR12 and GR12M are both better than that of similar element proposed by Allman.

Table 11.5 Deflection and stress at selected points of a cantilever

Element	(4 × 1) mesh		(8 × 2) mesh		(16 × 4) mesh	
	v_C	σ_{xA}	v_C	σ_{xA}	v_C	σ_{xA}
R4	0.2424	– 43.64	0.3162	– 55.70	0.3447	– 59.28
Allman[23]	0.3026	– 52.70	0.3394	– 58.40	0.3512	– 59.70
GR12	0.3283	– 60.00	0.3475	– 61.31	0.3535	– 60.76
GR12M	0.3446	– 60.00	0.3527	– 60.65	0.3550	– 60.20
Comparison solutions[23]	$v_C = 0.3558$			$\sigma_{xA} = -60.0$ ($x = 12$, $y = 6$)		

Example 11.6 Cantilever beam under a tip shear load (3-node triangular element).

This problem is the same as the Example 11.5. Numerical results for deflection at the mid-side point at the beam tip by using different meshes are listed in Table 11.6. Two different meshes are shown in Fig. 11.14(a) and (b), respectively. Mesh Ⅰ is for the three presented elements GT9, GT9M and GT9M8. And mesh Ⅱ, in which each rectangle is divided into four half-thickness overlaid triangles, is for the elements in reference [24], so the computing work will be twice as much as that for mesh Ⅰ.

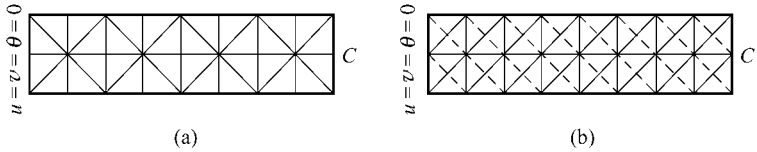

Figure 11.14 Meshes for Example 11.6
(a) Mesh Ⅰ 8 × 2; (b) Mesh Ⅱ 8 × 2

Table 11.6 The tip deflection of cantilever beam under tip shear load

Element	$100v_C$/0.356 01				
	8 × 2	16 × 4	32 × 8	64 × 16	
	Mesh Ⅰ				
T3(CST)	46.73	81.14	94.69	99.01	
GT9	94.41	98.74	99.76	99.98	
GT9M	95.60	99.10	99.86	99.85	
GT9M8	103.15	100.59	100.10	100.02	
	Mesh Ⅱ				
EFFAND[24]	101.68	100.30	100.03	100.00	
FF[24]	99.15	99.71	99.87	99.96	
	2 × 2	4 × 4	8 × 8	16 × 16	32 × 32
	Mesh Ⅰ				
T3(CST)	18.39	45.06	76.02	92.53	98.18
GT9	60.47	85.64	95.72	98.79	98.87
GT9M	61.65	86.24	95.91	98.84	99.88
GT9M8	92.13	97.37	99.08	99.67	99.89
	Mesh Ⅱ				
EFFAND[24]	92.24	96.99	98.70	99.48	98.81
FF[24]	89.26	96.37	98.66	99.50	99.83

Numerical results in Table 11.6 show that, the computational precision by the three presented elements GT9, GT9M and GT9M8 using mesh Ⅰ is close to that of the elements in reference [24] using mesh Ⅱ. And, in the 2×2 and 4×4 slim triangular meshes, the element GT9M8 exhibits much higher precision.

Example 11.7 Cook's skew beam problem (3-node triangular element).

This problem is the same as Example 11.3. The mesh division can be referred to Fig. 11.4, and the results are listed in Table 11.7. It can be seen that the generalized conforming elements proposed in this chapter possess better performance than those of the other elements.

Table 11.7 Comparison of results for Cook's skew beam problem (triangular elements)

Element	v_C (the vertical displacement at point C)			$\sigma_{A\max}$ (the maximum stress at point A)			$\sigma_{B\min}$ (the minimum stress at point B)		
	2×2	4×4	8×8	2×2	4×4	8×8	2×2	4×4	8×8
T3(CST)	11.99	18.28	22.02	0.0760	0.1498	0.1999	–0.0360	–0.1002	–0.1567
EFFAND[24]	20.56	22.45	23.43						
FF [25]	20.36	22.42	23.41	0.1700	0.2129	0.2309	–0.1804	–0.1706	–0.1902
GT9	20.08	22.71	23.61	0.1610	0.2073	0.2266	–0.1467	–0.1721	–0.1900
GT9M	20.36	22.80	23.63	0.1650	0.2093	0.2274	–0.1519	–0.1734	–0.1905
GT9M8	21.75	23.21	23.74	0.1827	0.2171	0.2304	–0.1981	–0.1777	–0.1924
reference①	23.96			0.2362			–0.2023		

① Results by the element GT9M8 using 64 × 64 mesh.

11.5 Flat-Shell Elements—Triangular Thick/Thin Shell Element GMST18

The flat-shell element, which is composed of plate bending element and plane membrane element[20], is the simplest shell element model, and widely used in the linear and nonlinear problems. Reviews on the general formulations and characteristics of the flat-shell element can be found in reference [26]. The appearance of the new generalized conforming membrane element with drilling freedoms and the new generalized conforming thin plate element makes it possible to construct high performance flat-shell elements.

Sects. 11.3 and 11.4 have introduced the concept of drilling freedom (the additional in-plane rigid vertex rotational freedom), and given the formulations of the new generalized conforming rectangular membrane element GR12 and triangular membrane elements GT9 and GT9M8 with drilling freedoms. Furthermore, in reference [27], the generalized conforming rectangular thin plate element GPL-R12 and triangular thin plate element GPL-T9 (this element has been

introduced in Sect. 6.3 of this book) are constructed. Then, in references [4–8], by starting with the generalized conforming theory and the degenerated potential energy principle, the above plane membrane and plate bending elements are used to formulate several generalized conforming flat-shell elements for the analysis of cylindrical and arbitrary shells:

(1) Generalized conforming rectangular flat-shell element GCR24[5]: developed by the combination of the generalized conforming rectangular membrane element GR12 and the rectangular thin plate element GPL-R12;

(2) Generalized conforming triangular flat-shell element GST18[4]: developed by the combination of the generalized conforming triangular membrane element GT9 and the triangular thin plate element GPL-T9, and one-point reduced integration scheme is used for GT9;

(3) Generalized conforming triangular flat-shell element GST18M[8]: developed by the combination of the generalized conforming triangular membrane element GT9M8 and the triangular thin plate element GPL-T9.

Furthermore, reference [9] developed a generalized conforming triangular thick/thin flat-shell element GMST18. Firstly, the formulation of the generalized conforming triangular membrane element GT9 is employed as the membrane component of the shell element. Both one-point reduced integration scheme and a corresponding stabilization matrix proposed by Fish et al.[27] are adopted for avoiding membrane locking and hourglass phenomenon. Secondly, the bending component of the element comes from a new generalized conforming thick/thin plate element TSL-T9, which is derived based on the rational shear interpolation proposed in Chap. 8 and the SemiLoof conforming scheme in Sect. 6.6. In this section, as an example, the element GMST18 will be used to describe the construction procedure of the generalized conforming flat-shell element.

11.5.1 Two Component Parts of the Flat-Shell Element

As shown in Fig. 11.15, the flat-shell element in the local coordinate system *Oxyz* is assembled by plane membrane and plate bending element.

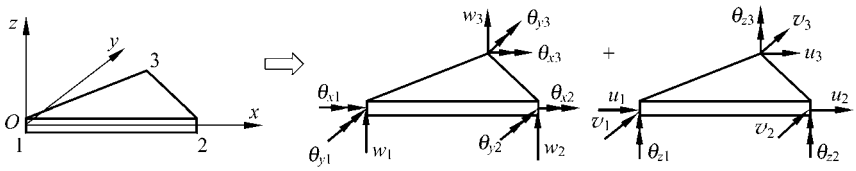

Figure 11.15 Flat-shell element in the local coordinate system O*xyz*

(a) Flat-shell element; (b) Plate bending element; (c) Membrane element

The element nodal displacement vector $\boldsymbol{q}^e$ in local coordinate system Oxyz is composed of the vertex freedoms:

$$\boldsymbol{q}^e = \begin{Bmatrix} \boldsymbol{q}_1^e \\ \boldsymbol{q}_2^e \\ \boldsymbol{q}_3^e \end{Bmatrix}, \quad \boldsymbol{q}_i^e = [u_i \quad v_i \quad w_i \quad \theta_{xi} \quad \theta_{yi} \quad \theta_{zi}]^{\mathrm{T}} \quad (i = 1, 2, 3) \tag{11-133}$$

Let $\boldsymbol{q}_{\mathrm{m}}^e$ be the nodal displacement vector related to the membrane element, $\boldsymbol{q}_{\mathrm{p}}^e$ be the nodal displacement vector related to the plate element, then we have

$$\boldsymbol{q}_{\mathrm{m}}^e = \begin{Bmatrix} \boldsymbol{q}_{\mathrm{m1}}^e \\ \boldsymbol{q}_{\mathrm{m2}}^e \\ \boldsymbol{q}_{\mathrm{m3}}^e \end{Bmatrix}, \quad \boldsymbol{q}_{\mathrm{m}i}^e = \begin{Bmatrix} u_i \\ v_i \\ \theta_{zi} \end{Bmatrix}, \quad \boldsymbol{q}_{\mathrm{p}}^e = \begin{Bmatrix} \boldsymbol{q}_{\mathrm{p1}}^e \\ \boldsymbol{q}_{\mathrm{p2}}^e \\ \boldsymbol{q}_{\mathrm{p3}}^e \end{Bmatrix}, \quad \boldsymbol{q}_{\mathrm{p}i}^e = \begin{Bmatrix} w_i \\ \theta_{xi} \\ \theta_{yi} \end{Bmatrix} \quad (i = 1, 2, 3) \tag{11-134}$$

11.5.2 Membrane Part—Triangular Membrane Element GT9

The plane membrane element GT9 introduced in Sect. 11.4.1 is a triangular generalized conforming membrane element with additional rigid rotational freedoms, its element stiffness matrix $\boldsymbol{K}_{\mathrm{m}}^e$ is given by Eq. (11-97) to Eq. (11-99). In order to avoid membrane locking in the calculation of shells, one-point reduced integration is often employed for computing $\boldsymbol{K}_{\mathrm{m}}^e$. But unfortunately, extra zero energy modes of the element will appear, and for some special cases, such as the twisted cantilever beam problem, the hourglass phenomenon may occur. Reference [28] suggested a method of adding a stabilization matrix to overcome this shortcoming. According to their approach, the stabilization matrix of the element GT9 is given as follows:

$$\boldsymbol{K}_{\mathrm{m\,stab}}^e = \bar{\omega} \left[\begin{array}{ccc:ccc:ccc} 0 & 0 & 0 & 0 & 0 & 0 & 0 & 0 & 0 \\ 0 & 0 & 0 & 0 & 0 & 0 & 0 & 0 & 0 \\ 0 & 0 & 2 & 0 & 0 & -1 & 0 & 0 & -1 \\ \hdashline 0 & 0 & 0 & 0 & 0 & 0 & 0 & 0 & 0 \\ 0 & 0 & 0 & 0 & 0 & 0 & 0 & 0 & 0 \\ 0 & 0 & -1 & 0 & 0 & 2 & 0 & 0 & -1 \\ \hdashline 0 & 0 & 0 & 0 & 0 & 0 & 0 & 0 & 0 \\ 0 & 0 & 0 & 0 & 0 & 0 & 0 & 0 & 0 \\ 0 & 0 & -1 & 0 & 0 & -1 & 0 & 0 & 2 \end{array}\right] \tag{11-135}$$

in which

$$\bar{\omega} = \frac{1}{3}\chi\left[\boldsymbol{K}_{\mathrm{m}}^{1}(3,3)^{e} + \boldsymbol{K}_{\mathrm{m}}^{1}(6,6)^{e} + \boldsymbol{K}_{\mathrm{m}}^{1}(9,9)^{e}\right] \tag{11-136}$$

where $\boldsymbol{K}_{\mathrm{m}}^{1e}$ denotes the element stiffness matrix of GT9 using one-point integration; χ is a perturbation factor. From numerical experiments, it is found that, when χ is not less than 10^{-6}, the rank and eigenvalues of the new shell element are correct. So, $\chi = 10^{-6}$ is adopted. Thus, the element stiffness matrix of GT9 in the local coordinate system can be modified as

$$\boldsymbol{K}_{\mathrm{m}}^{e} = \boldsymbol{K}_{\mathrm{m}}^{1e} + \boldsymbol{K}_{\mathrm{m\,stab}}^{e} \tag{11-137}$$

11.5.3 Plate Bending Part—Triangular Thick/Thin Plate Element TSL-T9

The triangular plate bending element TSL-T9 in the local coordinate system *Oxyz* is shown in Fig. 11.16. The element nodal displacement vector is composed of deflection w and normal slopes ψ_x and ψ_y of the mid-surface

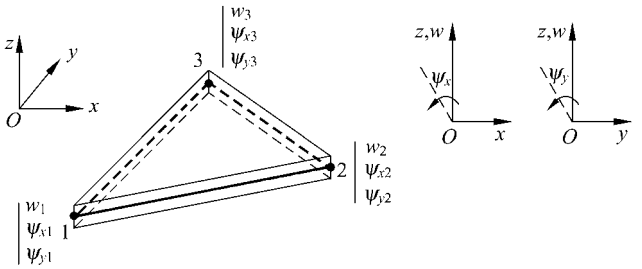

Figure 11.16 Triangular plate bending element TSL-T9

$$\bar{\boldsymbol{q}}^{e} = [w_1 \quad \psi_{x1} \quad \psi_{y1} \quad w_2 \quad \psi_{x2} \quad \psi_{y2} \quad w_3 \quad \psi_{x3} \quad \psi_{y3}]^{\mathrm{T}} \tag{11-138}$$

Note that, since the definitions of the rotations (ψ_x, ψ_y and θ_x, θ_y) are different, there exists the following relation between $\bar{\boldsymbol{q}}^{e}$ and $\boldsymbol{q}_{\mathrm{p}}^{e}$ in Eq. (11-134):

$$\bar{\boldsymbol{q}}^{e} = \boldsymbol{L}\boldsymbol{q}_{\mathrm{p}}^{e}, \quad \boldsymbol{L} = \begin{bmatrix} \boldsymbol{I} & \boldsymbol{0} & \boldsymbol{0} \\ \boldsymbol{0} & \boldsymbol{I} & \boldsymbol{0} \\ \boldsymbol{0} & \boldsymbol{0} & \boldsymbol{I} \end{bmatrix}, \quad \boldsymbol{I} = \begin{bmatrix} 1 & 0 & 0 \\ 0 & 0 & -1 \\ 0 & 1 & 0 \end{bmatrix}, \quad \boldsymbol{0} = \begin{bmatrix} 0 & 0 & 0 \\ 0 & 0 & 0 \\ 0 & 0 & 0 \end{bmatrix} \tag{11-139}$$

The construction procedure of the element shear strain fields is the same as that described in Sect. 8.5.3, then the final element shear strain field is

$$\boldsymbol{\gamma} = \boldsymbol{B}_{\mathrm{s}}\boldsymbol{q}_{\mathrm{p}}^{e} = \boldsymbol{H}\boldsymbol{\Delta}'\tilde{\boldsymbol{G}}\boldsymbol{L}\boldsymbol{q}_{\mathrm{p}}^{e} \tag{11-140}$$

where $\boldsymbol{B}_{\mathrm{s}}$ is the element shear strain matrix; $\boldsymbol{H}$, $\boldsymbol{\Delta}'$ and $\tilde{\boldsymbol{G}}$ are given by Eqs. (8-137), (8-139) and (8-127), respectively.

The element deflection field is assumed to be the same as that of the thin plate element LSL-T9 introduced in Sect. 6.6, i.e.,

$$w = \boldsymbol{F}_{\lambda}\boldsymbol{\lambda} \tag{11-141}$$

where

$$\boldsymbol{\lambda} = [\lambda_1 \quad \lambda_2 \quad \lambda_3 \quad \lambda_4 \quad \lambda_5 \quad \lambda_6 \quad \lambda_7 \quad \lambda_8 \quad \lambda_9 \quad \lambda_{10} \quad \lambda_{11} \quad \lambda_{12}]^{\mathrm{T}} \tag{11-142}$$

$$\begin{aligned}\boldsymbol{F}_{\lambda} = [&L_1 \quad L_2 \quad L_3 \quad L_2L_3 \quad L_3L_1 \quad L_1L_2 \quad L_2L_3(L_2 - L_3) \quad L_3L_1(L_3 - L_1) \\ &L_1L_2(L_1 - L_2) \quad L_1^2L_2L_3 \quad L_2^2L_3L_1 \quad L_3^2L_1L_2]\end{aligned} \tag{11-143}$$

According to the Mindlin plate theory, the element rotation fields are

$$\boldsymbol{\psi} = \begin{Bmatrix}\psi_x \\ \psi_y\end{Bmatrix} = \begin{Bmatrix}\dfrac{\partial w}{\partial x} - \gamma_{xz} \\ \dfrac{\partial w}{\partial y} - \gamma_{yz}\end{Bmatrix} = \begin{bmatrix}\boldsymbol{F}_{\lambda,x} \\ \boldsymbol{F}_{\lambda,y}\end{bmatrix}\boldsymbol{\lambda} - \boldsymbol{B}_{\mathrm{s}}\boldsymbol{q}_{\mathrm{p}}^{e}. \tag{11-144}$$

where $\boldsymbol{F}_{\lambda,x}$ and $\boldsymbol{F}_{\lambda,y}$ denote the derivative matrices of $\boldsymbol{F}_{\lambda}$ with respect to x and y, respectively.

Along the element sides, deflection $\tilde{w}$ is interpolated according to the thick beam theory, and the normal slope $\tilde{\psi}_n$ is assumed to be linearly distributed, as shown in Eq. (8-146).

The following 12 SemiLoof point conforming conditions (refer to Fig. 6.16)

$$(w - \tilde{w})_i = 0 \quad (i = 1,2,3) \tag{11-145}$$

$$(w - \tilde{w})_j = 0 \quad (j = 4,5,6) \tag{11-146}$$

$$(\psi_n - \tilde{\psi}_n)_k = 0 \quad (k = A_1, B_1, A_2, B_2, A_3, B_3) \tag{11-147}$$

are introduced. Equations (11-145) and (11-146) are the point conforming conditions about deflections at the corner nodes (nodes 1, 2, 3) and mid-side points (points 4, 5, 6), respectively; Eq. (11-147) denotes the point conforming conditions about the normal slopes at the Gauss points on the element side (points A_1, B_1, A_2, B_2, A_3, B_3).

Then, $\lambda_1, \lambda_2, \cdots, \lambda_{12}$ can be obtained, in which the last 3 coefficients are equal to each other, i.e., $\lambda_{10} = \lambda_{11} = \lambda_{12}$. Therefore, Eq. (11-141) can be rewritten as

$$w = \boldsymbol{F}_{\lambda}'\boldsymbol{\lambda}' \tag{11-148}$$

where

$$\boldsymbol{\lambda}' = [\lambda_1 \quad \lambda_2 \quad \lambda_3 \quad \lambda_4 \quad \lambda_5 \quad \lambda_6 \quad \lambda_7 \quad \lambda_8 \quad \lambda_9 \quad \lambda_{10}]^{\mathrm{T}} \tag{11-149}$$

$$\boldsymbol{F}'_{\lambda} = [L_1 \quad L_2 \quad L_3 \quad L_2L_3 \quad L_3L_1 \quad L_1L_2 \quad L_2L_3(L_2-L_3) \quad L_3L_1(L_3-L_1) \quad L_1L_2(L_1-L_2) \quad L_1L_2L_3] \tag{11-150}$$

$\boldsymbol{\lambda}'$ can be expressed in terms of the element nodal displacement vector

$$\boldsymbol{\lambda}' = \boldsymbol{C}\overline{\boldsymbol{q}}^{e} \tag{11-151}$$

where

$$\boldsymbol{C} = [\boldsymbol{C}_1 \quad \boldsymbol{C}_2 \quad \boldsymbol{C}_3] \tag{11-152}$$

$$\boldsymbol{C}_1 = \begin{bmatrix}
1 & 0 & 0 \\
0 & 0 & 0 \\
0 & 0 & 0 \\
0 & 0 & 0 \\
0 & -\frac{1}{2}c_2 & \frac{1}{2}b_2 \\
0 & \frac{1}{2}c_3 & -\frac{1}{2}b_3 \\
\frac{1}{2}(r_2+r_3)-\left(\frac{1}{3}+r_2\right)\delta_2 & \frac{1}{12}(c_1-3r_2c_2+3r_3c_3) & -\frac{1}{12}(b_1-3r_2b_2+3r_3b_3) \\
+\left(\frac{1}{3}-r_3\right)\delta_3 & +\frac{1}{6}(1+3r_2)c_2\delta_2 & -\frac{1}{6}(1+3r_2)b_2\delta_2 \\
 & +\frac{1}{6}(1-3r_3)c_3\delta_3 & -\frac{1}{6}(1-3r_3)b_3\delta_3 \\
-\frac{1}{2}(3+r_3)+\frac{8}{3}\delta_2 & -\frac{1}{12}(3r_3c_3+c_3-8c_2) & \frac{1}{12}(3r_3b_3+b_3-8b_2)+\frac{4}{3}b_2\delta_2 \\
+\left(\frac{1}{3}+r_3\right)\delta_3 & -\frac{4}{3}c_2\delta_2+\frac{1}{6}(1+3r_3)c_3\delta_3 & -\frac{1}{6}(1+3r_3)b_3\delta_3 \\
\frac{1}{2}(3-r_2)-\left(\frac{1}{3}-r_2\right)\delta_2 & \frac{1}{12}(3r_2c_2-c_2+8c_3) & -\frac{1}{12}(3r_2b_2-b_2+8b_3) \\
-\frac{8}{3}\delta_3 & +\frac{1}{6}(1-3r_2)c_2\delta_2-\frac{4}{3}c_3\delta_3 & -\frac{1}{6}(1-3r_2)b_2\delta_2+\frac{4}{3}b_3\delta_3 \\
(r_3-r_2)+2(r_2\delta_2-r_3\delta_3) & \frac{1}{2}(r_2c_2+r_3c_3) & -\frac{1}{2}(r_2b_2+r_3b_3) \\
 & -r_2c_2\delta_2-r_3c_3\delta_3 & +r_2b_2\delta_2+r_3b_3\delta_3
\end{bmatrix} \tag{11-153a}$$

$$
\boldsymbol{C}_2=\begin{bmatrix}
0 & 0 & 0 \\
1 & 0 & 0 \\
0 & 0 & 0 \\
0 & \frac{1}{2}c_1 & -\frac{1}{2}b_1 \\
0 & 0 & 0 \\
0 & -\frac{1}{2}c_3 & \frac{1}{2}b_3 \\
\frac{1}{2}(3-r_3)-\left(\frac{1}{3}-r_3\right)\delta_3 & \frac{1}{12}(3r_3c_3-c_3+8c_1) & -\frac{1}{12}(3r_3b_3-b_3+8b_1) \\
-\frac{8}{3}\delta_1 & +\frac{1}{6}(1-3r_3)c_3\delta_3-\frac{4}{3}c_1\delta_1 & -\frac{1}{6}(1-3r_3)b_3\delta_3+\frac{4}{3}b_1\delta_1 \\
\frac{1}{2}(r_3+r_1)-\left(\frac{1}{3}+r_3\right)\delta_3 & \frac{1}{12}(c_2-3r_3c_3+3r_1c_1) & -\frac{1}{12}(b_2-3r_3b_3+3r_1b_1) \\
+\left(\frac{1}{3}-r_1\right)\delta_1 & +\frac{1}{6}(1+3r_3)c_3\delta_3 & -\frac{1}{6}(1+3r_3)b_3\delta_3 \\
 & +\frac{1}{6}(1-3r_1)c_1\delta_1 & -\frac{1}{6}(1-3r_1)b_1\delta_1 \\
-\frac{1}{2}(3+r_1)+\frac{8}{3}\delta_3 & -\frac{1}{2}(3r_1c_1+c_1-8c_3)-\frac{4}{3}c_3\delta_3 & \frac{1}{12}(3r_1b_1+b_1-8b_3)+\frac{4}{3}b_3\delta_3 \\
+\left(\frac{1}{3}+r_1\right)\delta_1 & +\frac{1}{6}(1+3r_1)c_1\delta_1 & -\frac{1}{6}(1+3r_1)b_1\delta_1 \\
(r_1-r_3)+2(r_3\delta_3-r_1\delta_1) & \frac{1}{2}(r_3c_3+r_1c_1) & -\frac{1}{2}(r_3b_3+r_1b_1) \\
 & -r_3c_3\delta_3-r_1c_1\delta_1 & +r_3b_3\delta_3+r_1b_1\delta_1
\end{bmatrix}
$$

(11-153b)

$$
\boldsymbol{C}_3=\begin{bmatrix}
0 & 0 & 0 \\
0 & 0 & 0 \\
1 & 0 & 0 \\
0 & -\frac{1}{2}c_1 & \frac{1}{2}b_1 \\
0 & \frac{1}{2}c_2 & -\frac{1}{2}b_2 \\
0 & 0 & 0 \\
-\frac{1}{2}(3+r_2)+\frac{8}{3}\delta_1 & -\frac{1}{12}(3r_2c_2+c_2-8c_1)-\frac{4}{3}c_1\delta_1 & \frac{1}{12}(3r_2b_2+b_2-8b_1)+\frac{4}{3}b_1\delta_1 \\
+\left(\frac{1}{3}+r_2\right)\delta_2 & +\frac{1}{6}(1+3r_2)c_2\delta_2 & -\frac{1}{6}(1+3r_2)b_2\delta_2 \\
\frac{1}{2}(3-r_1)-\left(\frac{1}{3}-r_1\right)\delta_1 & \frac{1}{12}(3r_1c_1-c_1+8c_2) & -\frac{1}{12}(3r_1b_1-b_1+8b_2) \\
-\frac{8}{3}\delta_2 & +\frac{1}{6}(1-3r_1)c_1\delta_1-\frac{4}{3}c_2\delta_2 & -\frac{1}{6}(1-3r_1)b_1\delta_1+\frac{4}{3}b_2\delta_2 \\
\frac{1}{2}(r_1+r_2)-\left(\frac{1}{3}+r_1\right)\delta_1 & \frac{1}{12}(c_3-3r_1c_1+3r_2c_2) & -\frac{1}{12}(b_3-3r_1b_1+3r_2b_2) \\
+\left(\frac{1}{3}-r_2\right)\delta_2 & +\frac{1}{6}(1+3r_1)c_1\delta_1 & -\frac{1}{6}(1+3r_1)b_1\delta_1 \\
 & +\frac{1}{6}(1-3r_2)c_2\delta_2 & -\frac{1}{6}(1-3r_2)b_2\delta_2 \\
(r_2-r_1)+2(r_1\delta_1-r_2\delta_2) & \frac{1}{2}(r_1c_1+r_2c_2) & -\frac{1}{2}(r_1b_1+r_2b_2) \\
 & -r_1c_1\delta_1-r_2c_2\delta_2 & +r_1b_1\delta_1+r_2b_2\delta_2
\end{bmatrix}
$$

(11-153c)

in which b_i, c_i and $r_i\,(i=1,2,3)$ are given by Eq. (6-58); $\delta_i\,(i=1,2,3)$ are given by the first equation in (8-114).

Substitution of Eq. (11-151) into Eq. (11-148) yields

$$w=\boldsymbol{F}_\lambda'\boldsymbol{C}\overline{\boldsymbol{q}}^e=\boldsymbol{F}_\lambda'\boldsymbol{C}\boldsymbol{L}\boldsymbol{q}_p^e=\boldsymbol{N}^e\boldsymbol{q}_p^e,\quad \boldsymbol{N}^e=\boldsymbol{F}_\lambda'\boldsymbol{C}\boldsymbol{L} \tag{11-154}$$

where $\boldsymbol{N}^e$ is the shape function matrix of the deflection w. It can be verified that, this deflection field and the rotation fields given by Eq. (11-144) determined by this deflection field satisfy the following generalized conforming condition

$$\oint_{\partial A^e}[Q_n(w-\tilde{w})-M_n(\psi_n-\tilde{\psi}_n)-M_{ns}(\psi_s-\tilde{\psi}_s)]=0 \tag{11-155}$$

where Q_n, M_n and M_{ns} denote the shear force, normal bending moment and tangent bending moment along the element boundary ∂A^e. Hence, the element derived here is a generalized conforming element, and its convergence can be ensured.

The rotation field $\boldsymbol{\psi}$ in Eq. (11-144) can be rewritten as

$$\boldsymbol{\psi}=\begin{Bmatrix}\psi_x\\ \psi_y\end{Bmatrix}=\begin{Bmatrix}\dfrac{\partial w}{\partial x}-\gamma_{xz}\\ \dfrac{\partial w}{\partial y}-\gamma_{yz}\end{Bmatrix}=\left(\begin{bmatrix}\boldsymbol{F}'_{\lambda,x}\\ \boldsymbol{F}'_{\lambda,y}\end{bmatrix}\boldsymbol{C}-\boldsymbol{B}_{\mathrm{s}}\right)\boldsymbol{L}\boldsymbol{q}_{\mathrm{p}}^e \tag{11-156}$$

Then, the curvature field $\boldsymbol{\kappa}$ of the plate element is

$$\boldsymbol{\kappa}=\begin{Bmatrix}\kappa_x\\ \kappa_y\\ 2\kappa_{xy}\end{Bmatrix}=\begin{Bmatrix}-\dfrac{\partial\psi_x}{\partial x}\\ -\dfrac{\partial\psi_y}{\partial y}\\ -\dfrac{\partial\psi_x}{\partial y}-\dfrac{\partial\psi_y}{\partial x}\end{Bmatrix}=\left(-\begin{bmatrix}\boldsymbol{F}'_{\lambda,xx}\\ \boldsymbol{F}'_{\lambda,yy}\\ 2\boldsymbol{F}'_{\lambda,xy}\end{bmatrix}\boldsymbol{C}\boldsymbol{L}\right)\boldsymbol{q}_{\mathrm{p}}^e=\boldsymbol{B}_{\mathrm{b}}\boldsymbol{q}_{\mathrm{p}}^e \tag{11-157}$$

in which $\boldsymbol{B}_{\mathrm{b}}$ is the bending strain matrix.

Thus, the element stiffness matrix of the thick/thin bending element TSL-T9 can be obtained

$$\boldsymbol{K}_{\mathrm{p}}^{\ e}=\iint_{A^e}\boldsymbol{B}_{\mathrm{b}}^{\ \mathrm{T}}\boldsymbol{D}_{\mathrm{b}}\boldsymbol{B}_{\mathrm{b}}\,\mathrm{d}A+\iint_{A^e}\boldsymbol{B}_{\mathrm{s}}^{\ \mathrm{T}}\boldsymbol{D}_{\mathrm{s}}\boldsymbol{B}_{\mathrm{s}}\mathrm{d}A \tag{11-158}$$

Numerical results show that the element TSL-T9 possesses excellent performance for both thin and thick plate bending problems. And, its stress solutions are also improved by the hybrid-enhanced post-processing procedure in reference [9]. Here we will not expand this in detail. Readers who are interested in it can refer to reference [9].

11.5.4 Stiffness Matrix of the Flat-Shell Element GMST18

Assembling Eqs.(11-137) and (11-158) according to the DOF's sequence given by Eq. (11-133), we obtain the element stiffness matrix $\boldsymbol{K}^e$ of the flat-shell element GMST18 in the local co-ordinates. And, after transforming $\boldsymbol{K}^e$ to the global

coordinates by standard procedure, the element can be used to calculate shell structures.

11.5.5 Numerical Examples

Here, the numerical results of the flat-shell element are given. For comparison, the results by other elements are also listed. All element models used are listed in Table 11.8.

Table 11.8 Shell elements for comparison (17 elements)

Element symbol	Element types	References
1. GMST18	3-node triangular generalized conforming thick/thin flat-shell element	[9]
2. GST18	3-node triangular generalized conforming thin flat-shell element	[4]
3. GST18M	3-node triangular generalized conforming thin flat-shell element	[8]
4. RTS18	3-node triangular thin flat-shell element	[29]
5. PROVIDAS	3-node triangular thin flat-shell element	[30]
6. DKT-CST-15RB	3-node triangular thin flat-shell element	[31]
7. OLSON	triangular thin flat-shell element	[22]
8. STRI3	3-node triangular thin flat-shell element in ABAQUS	[32]
9. S3R	3-node triangular 3D degenerated shell element in ABAQUS	[32]
10. GCR24	4-node rectangular generalized conforming thin flat-shell element	[5]
11. QUAD4	4-node quadrilateral 3D degenerated shell element	[33]
12. AQR8	8-node quadrilateral hybrid stress shell element	[34]
13. GUAN	9-node quadrilateral quasi-conforming 3D degenerated shell element	[35]
14. DKQ	4-node quadrilateral plate element based on discrete Kirchhoff assumption	[36]
15. MITC4	4-node quadrilateral plate element based on the mixed interpolation technique	[37]
16. T15-R	Reduced or selected reduced integration triangular degenerated shell element	[38]
17. RDTS15	Discrete refined 3-node triangular degenerated shell element	[38]

Example 11.8 Test of applicability for both thick and thin plates—a clamped square plate under uniform load.

A clamped square plate is subjected to a uniform load q. The side length $L = 100$, the thickness-span ratio varies from 10^{-15} to 0.6, and the material

constants are: $E = 10^6$ and $\mu = 0.3$. The whole plate is analyzed using the irregular mesh shown in Fig. 11.17. In Fig. 11.18, the deflection coefficients $w_C / (qL^4 / D)$ obtained by the several shell elements under different thickness-span ratios are given. It can be seen that, the element GMST18 can produce satisfactory results for both thin and thick plates, only the element RDTS15 is close to this element.

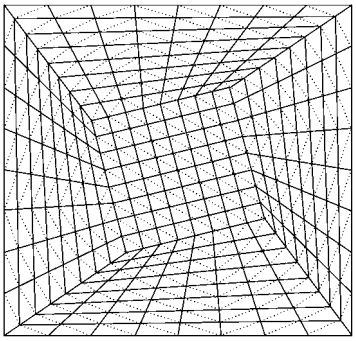

Figure 11.17 Irregular mesh for a square plate

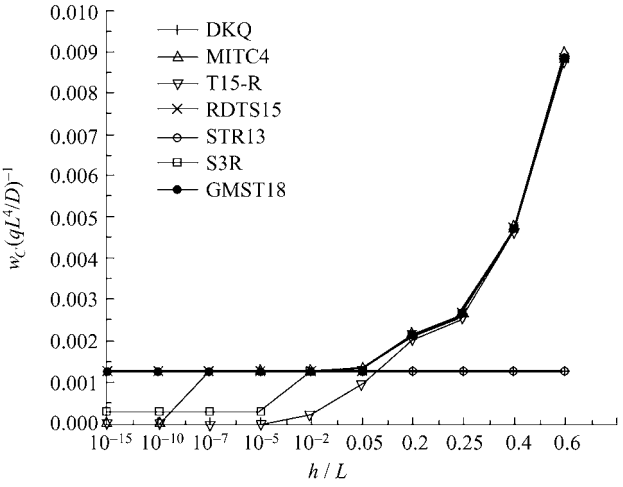

Figure 11.18 The variation of deflection coefficient with thickness-span ratio

Example 11.9 Scordelis-Lo Roof.

The cylindrical shell in Fig. 11.19 is supported by a rigid diaphragm at two ends and loaded vertically by its uniform dead weight. The theoretical solution from the deep shell theory for the vertical displacement at the midpoint of the free edge is 0.3008[39]. Because the shell is symmetric, only a quarter is taken for calculation.

Nondimensional results by different shell elements are listed in Tables 11.9

and 11.10. It can be seen that all the generalized conforming elements have good accuracy.

Example 11.10 Twisted Cantilever Beam.

A twisted cantilever beam is shown in Fig. 11.20. The free end is twisted 90° from the clamped end. Two types of load are applied to the free end of the beam: $P = 1.0$, $Q = 0.0$ and $P = 0.0$, $Q = 1.0$. The displacements in the direction of the load are reported in Table 11.11.

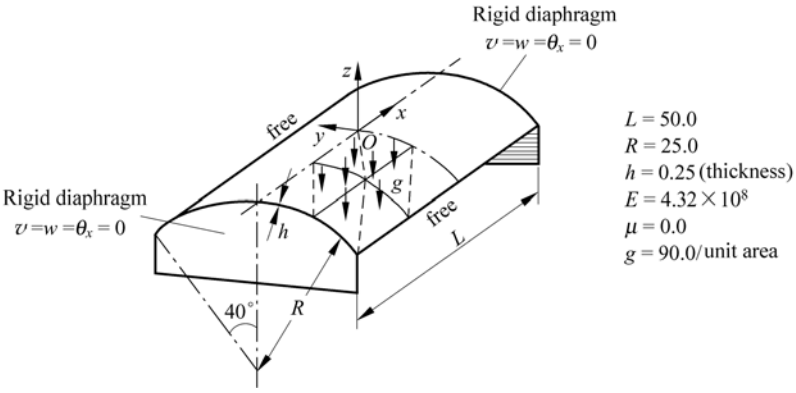

Figure 11.19 Scordelis-Lo roof

Table 11.9 Vertical displacement at the midpoint of free edge for Scordelis-Lo roof (rectangular and quadrilateral elements)

Mesh (1/4 shell)	QUAD4	AQR8	GUAN	GCR24
2 × 2	0.4161	0.3683	0.3078	0.3533
4 × 4	0.3175	0.3088	0.3033	0.3037
6 × 6	0.3078	0.3042		0.3011
8 × 8	0.3048	0.3033		0.3007
10 × 10	0.3036	0.3027		0.3006

Table 11.10 Vertical displacement at the midpoint of free edge for Scordelis-Lo roof (triangular elements)

Mesh (1/4 shell)	DKT-CST-15RB	OLSON	S3R	STRI3	GST18	GST18M	GMST18
2 × 2	0.2976	0.3809	0.2390	0.3310	0.3361	0.3525	0.3349
3 × 3		0.3024	0.2150	0.2221	0.2968	0.3027	0.2943
4 × 4	0.2144	0.2942			0.2921	0.2950	
5 × 5		0.2939			0.2931	0.2947	
6 × 6	0.2428		0.2438	0.2464	0.2947	0.2957	0.2946
8 × 8	0.2622		0.2627	0.2642	0.2969	0.2974	0.2965
10 × 10	0.2737	0.2970	0.2742	0.2751	0.2981	0.2984	0.2978

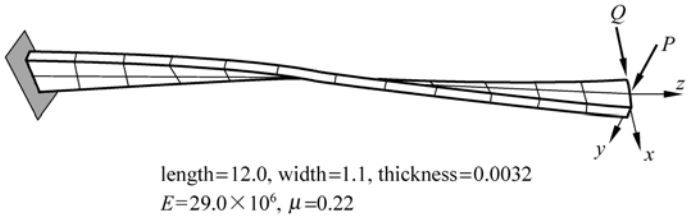

Figure 11.20 Twisted beam divided into 2 × 12 mesh

Table 11.11 Normalized deflection at the free edge of a cantilever twisted beam

Mesh	QUAD4	S3R	STRI3	RTS18	GST18	GST18M	GMST18
$P=1.0, Q=0.0$							
2 × 4		0.513	0.046	0.658			0.676
2 × 8		0.920	0.352	0.957			0.991
2 × 12	0.985	0.970	0.709	0.989	0.994	0.994	0.999
2 × 16		0.985	0.885	0.997			1.001
Theory	1294						
$P=0.0, Q=1.0$							
2 × 4		0.472	0.035	0.709			0.688
2 × 8		0.931	0.331	0.974			0.994
2 × 12	0.993	0.969	0.700	0.997	0.993	1.000	1.002
2 × 16		0.980	0.883	1.002			1.004
Theory	5256						

Example 11.11 Hemispherical shell.

As shown in Fig. 11.21, a hemispherical shell with a hole at the top is under two pairs of opposite radial concentrated loads at points *A* and *B*. Due to symmetry, only 1/4 of the hemispherical shell is analyzed. Results of the radial deflection at load points *A* and *B* are given in Table 11.12.

Table 11.12 Radial deflection at point *A* of the spherical under concentrated loads at *A* and *B*

Mesh	STRI3	S3R	RTS18	Providas	GST18	GST18M	GMST18
4 × 4	0.094	0.055	0.091	0.095	0.072	0.082	0.082
8 × 8	0.094	0.084	0.096	0.093	0.092	0.092	0.092
16 × 16	0.093	0.092	0.094 (14 × 14)		0.093	0.093	0.093
64 × 64	0.093	0.093					0.094
Comparison solution[29]						0.094	

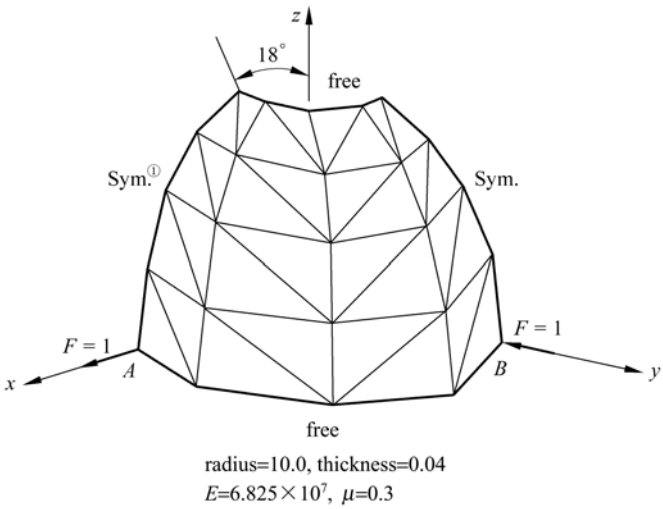

Figure 11.21 Hemispherical shell with hole at the top, mesh 8×8

11.6 Shallow Shell Element—Variational Principle and Membrane Locking Problem

Shell elements mainly have four discrete forms in geometry. Besides the flat-shell elements described above, there still are curved shell elements, degenerated shell elements derived from three-dimensional elements, and axisymmetric shell elements for the analysis of the shells of revolution. This section will introduce the construction procedure of the generalized conforming curved shell elements for shallow shells.

Reference [40] firstly takes the modified Hu-Washizu principle as the starting point, then, by introducing two types of the generalized conforming conditions and using the degenerated potential energy principle, it establishes a thick shallow shell element GC-S20 with 20 DOFs. For the bending part of the shell, the scheme proposed in reference [41] is adopted to eliminate the shear locking phenomenon; and for the membrane strain part of the shell, both displacement fields and membrane strain fields are assumed independently, and then by using the related generalized conforming conditions, membrane locking phenomenon can be eliminated. Reference [42] extends the generalized conforming rectangular thin plate elements RGC-12[14], LGC-R12[43] and triangular element TGC-9[14] to various shallow shell elements for the first time, but only the rectangular elements can pass the membrane locking test. Thereupon reference [42] continues the study on the membrane locking problem, and successfully constructs the generalized conforming rectangular and triangular shallow shell elements with mid-side nodes, which can completely avoid the membrane locking phenomenon.

① Sym. is the abbreviation for symmetrical.

11.6.1 Variational Principle for Shallow Shells and Its Degenerate Form

Let the base plane of the shallow shell be the *xOy* plane, and the *z*-axis be normal to the base plane. Then, the mid-surface equation of the shallow shell is

$$z = z(x, y) \tag{11-159}$$

The initial curvatures of the mid-surface are

$$\kappa_x^0 = -\frac{\partial^2 z}{\partial x^2} = \frac{1}{R_x}, \quad \kappa_y^0 = -\frac{\partial^2 z}{\partial y^2} = \frac{1}{R_y}, \quad \kappa_{xy}^0 = -\frac{\partial^2 z}{\partial x \partial y} = \frac{1}{R_{xy}} \tag{11-160}$$

where R_x, R_y and R_{xy} are the reciprocal values of the corresponding curvatures, respectively.

In shallow shell elements, the following quantities need to be assumed:

Displacements of mid-surface u, v, w

Membrane strains $\boldsymbol{\varepsilon} = [\varepsilon_x \quad \varepsilon_y \quad \gamma_{xy}]^{\mathrm{T}}$

The curvatures derived from the displacements are

$$\boldsymbol{\kappa} = [\kappa_x \quad \kappa_y \quad 2\kappa_{xy}]^{\mathrm{T}} = \left[-\frac{\partial^2 w}{\partial x^2} \quad -\frac{\partial^2 w}{\partial y^2} \quad -2\frac{\partial^2 w}{\partial x \partial y} \right]^{\mathrm{T}} \tag{11-161}$$

And, the membrane strains derived from the displacements are

$$\hat{\boldsymbol{\varepsilon}} = [\hat{\varepsilon}_x \quad \hat{\varepsilon}_y \quad \hat{\gamma}_{xy}]^{\mathrm{T}} = \left[\frac{\partial u}{\partial x} + \frac{w}{R_x} \quad \frac{\partial v}{\partial y} + \frac{w}{R_y} \quad \frac{\partial v}{\partial x} + \frac{\partial u}{\partial y} + 2\frac{w}{R_{xy}} \right]^{\mathrm{T}} \tag{11-162}$$

For thin shallow shell, the modified Hu-Washizu functional can be written as

$$\Pi^e = \Pi_1^e + \Pi_2^e \tag{11-163}$$

where Π_1^e is the energy due to the bending deformation of the shallow shell element,

$$\Pi_1^e = \iint_{A^e} \frac{1}{2} \boldsymbol{\kappa}^{\mathrm{T}} \boldsymbol{D}_{\mathrm{b}} \boldsymbol{\kappa} \mathrm{d}A + \oint_{\partial A^e} \left[M_n \left(\frac{\partial w}{\partial n} - \frac{\partial \tilde{w}}{\partial n} \right) + M_{ns} \left(\frac{\partial w}{\partial s} - \frac{\partial \tilde{w}}{\partial s} \right) - Q_n (w - \tilde{w}) \right] \mathrm{d}s \tag{11-164}$$

in which A^e is the projection area of the element; ∂A^e is the element boundary ; M_n, M_{ns} and Q_n are the bending moment, twisting moment and transverse shear force on the element boundary; w, $\frac{\partial w}{\partial n}$ and $\frac{\partial w}{\partial s}$ are the displacements on the

element boundary determined by the element deflection field; $\tilde{w}$, $\dfrac{\partial \tilde{w}}{\partial n}$ and $\dfrac{\partial \tilde{w}}{\partial s}$ are the given displacements on the element boundary; $\boldsymbol{D}_{\mathrm{b}}$ is the elastic matrix for thin plate bending,

$$\boldsymbol{D}_{\mathrm{b}} = \frac{Eh^3}{12(1-\mu^2)}\begin{bmatrix} 1 & \mu & 0 \\ \mu & 1 & 0 \\ 0 & 0 & \dfrac{1-\mu}{2} \end{bmatrix}$$

where h is the thickness of the shell ; E is the Young's modulus; μ is the Poisson's ratio.

Π_2^e is the energy due to the membrane deformation of the shallow shell element,

$$\Pi_2^e = \iint_{A^e}\left[\frac{1}{2}\boldsymbol{\varepsilon}^{\mathrm{T}}\boldsymbol{D}_{\mathrm{m}}\boldsymbol{\varepsilon} - \boldsymbol{N}^{\mathrm{T}}(\boldsymbol{\varepsilon}-\hat{\boldsymbol{\varepsilon}})\right]\mathrm{d}A \tag{11-165}$$

in which $\boldsymbol{\varepsilon}$ is the assumed element membrane strain vector; $\boldsymbol{N}$ is the element membrane stress vector; $\boldsymbol{D}_{\mathrm{m}}$ is the elastic matrix for thin membrane deformation (i.e., the elastic matrix for plane stress problem),

$$\boldsymbol{D}_{\mathrm{m}} = \frac{Eh}{1-\mu^2}\begin{bmatrix} 1 & \mu & 0 \\ \mu & 1 & 0 \\ 0 & 0 & \dfrac{1-\mu}{2} \end{bmatrix}$$

The displacement mode of the generalized conforming thin plate element is taken as the interpolation function for the normal displacement of the shallow shell element, when the mesh is refined by infinite elements, it satisfies

$$\oint_{\partial A^e}\left[M_n\left(\frac{\partial w}{\partial n}-\frac{\partial \tilde{w}}{\partial n}\right)+M_{ns}\left(\frac{\partial w}{\partial s}-\frac{\partial \tilde{w}}{\partial s}\right)-Q_n(w-\tilde{w})\right]\mathrm{d}s = 0 \tag{11-166}$$

When the mesh is refined by infinite elements, i.e., the element is under the limit state of constant internal forces, the second term in Eq. (11-165) should satisfy the following generalized conforming conditions

$$\iint_{A^e}\boldsymbol{N}^{\mathrm{T}}(\boldsymbol{\varepsilon}-\hat{\boldsymbol{\varepsilon}})\mathrm{d}A = 0 \tag{11-167}$$

Here, the energy functional degenerates to the following simplified form

$$\Pi^e = \iint_{A^e}\left[\frac{1}{2}\boldsymbol{\kappa}^{\mathrm{T}}\boldsymbol{D}_{\mathrm{b}}\boldsymbol{\kappa}+\frac{1}{2}\boldsymbol{\varepsilon}^{\mathrm{T}}\boldsymbol{D}_{\mathrm{m}}\boldsymbol{\varepsilon}\right]\mathrm{d}A \tag{11-168}$$

Then, according to Eq. (1-168), the stiffness matrix for the shallow shell element can be derived conveniently.

11.6.2 Notes on the Membrane Locking Problem

From Eq. (11-162), it can be seen that, the membrane strains are not only related to the tangential displacements u and v, but also related to the normal displacement w. The reason leading to membrane locking comes from the mismatching between the tangential displacements u, v and the normal displacement w in the assumed displacement mode for the shallow shell element, so that the displacement state of the rigid-body motion of the element cannot be presented. In order that the rigid-body motion of the element can be presented, the following zero strain state must come into existence

$$\kappa_x = -\frac{\partial^2 w}{\partial x^2} = 0, \quad \kappa_y = -\frac{\partial^2 w}{\partial y^2} = 0, \quad \kappa_{xy} = -2\frac{\partial^2 w}{\partial x \partial y} = 0 \tag{11-169}$$

$$\varepsilon_x = \frac{\partial u}{\partial x} + \frac{w}{R_x} = 0, \quad \varepsilon_y = \frac{\partial v}{\partial y} + \frac{w}{R_y} = 0, \quad \gamma_{xy} = \frac{\partial v}{\partial x} + \frac{\partial u}{\partial y} + \frac{2w}{R_{xy}} = 0 \tag{11-170}$$

From the first expression of Eq. (11-169), we obtain

$$w = xf_1(y) + f_2(y) \tag{11-171}$$

Substitution of the above equation into the last two expressions of Eq. (11-169) yields

$$f_1(y) = C_1, \quad f_2(y) = C_2 y + C_3 \tag{11-172}$$

where C_1, C_2 and C_3 are constants. Thereby, the normal displacement should be the following linear function

$$w = C_1 x + C_2 y + C_3 \tag{11-173}$$

Substituting Eq. (11-173) into the first two expressions of Eq. (11-170), and assume that R_x, R_y and R_{xy} are constants, we can obtain

$$\left.\begin{aligned} u &= -\frac{1}{R_x}\left[\frac{C_1}{2}x^2 + C_2 xy + C_3 x + g_1(y)\right] \\ v &= -\frac{1}{R_y}\left[C_1 xy + \frac{C_2}{2}y^2 + C_3 y + g_2(x)\right] \end{aligned}\right\} \tag{11-174}$$

Substitution of u and v into the third expression of Eq. (11-170) yields

$$-\frac{1}{R_y}g_2'(x)-\frac{C_2}{R_x}x+\frac{2C_1}{R_{xy}}x+\frac{2C_3}{R_{xy}}=\frac{1}{R_x}g_1'(y)+\frac{C_1}{R_y}y-\frac{2C_2}{R_{xy}}y \tag{11-175}$$

The above equation exists for arbitrary x and y, then we have

$$\left.\begin{aligned} g_2'(x)&=-\frac{R_y}{R_x}C_2x+\frac{2R_y}{R_{xy}}C_1x+\frac{2R_y}{R_{xy}}C_3-C_4R_y \\ g_1'(y)&=-\frac{R_x}{R_y}C_1y+\frac{2R_x}{R_{xy}}C_2y+C_4R_x \end{aligned}\right\} \tag{11-176}$$

Thereupon, it can be easily obtained that

$$\left.\begin{aligned} g_2(x)&=-\frac{R_y}{2R_x}C_2x^2+\frac{R_y}{R_{xy}}C_1x^2+\frac{2R_y}{R_{xy}}C_3x-C_4R_yx+C_5 \\ g_1(y)&=-\frac{R_x}{2R_y}C_1y^2+\frac{R_x}{R_{xy}}C_2y^2+C_4R_xy+C_6 \end{aligned}\right\} \tag{11-177}$$

in which C_4, C_5 and C_6 are all constants. Substitution of Eq. (11-177) into Eq. (11-174) yields

$$\left.\begin{aligned} u&=-\frac{1}{2R_x}C_1x^2-\frac{1}{R_x}C_2xy+\left(\frac{1}{2R_y}C_1-\frac{1}{R_{xy}}C_2\right)y^2-\frac{1}{R_x}C_3x-C_4y-\frac{1}{R_x}C_6 \\ v&=\left(\frac{1}{2R_x}C_2-\frac{1}{R_{xy}}C_1\right)x^2-\frac{1}{R_y}C_1xy-\frac{1}{2R_y}C_2y^2-\left(\frac{2}{R_{xy}}C_3-C_4\right)x-\frac{1}{R_y}C_3y-\frac{1}{R_y}C_5 \end{aligned}\right\} \tag{11-178}$$

Let

$$\theta_0=C_4-\frac{C_3}{R_{xy}},\quad u_0=-\frac{C_6}{R_x},\quad v_0=-\frac{C_5}{R_y} \tag{11-179}$$

Then, Eq. (11-178) can be rewritten as

$$\left.\begin{aligned} u&=-\frac{1}{2R_x}C_1x^2-\frac{1}{R_x}C_2xy+\left(\frac{1}{2R_y}C_1-\frac{1}{R_{xy}}C_2\right)y^2-\frac{1}{R_x}C_3x-\frac{1}{R_{xy}}C_3y-\theta_0y+u_0 \\ v&=\left(\frac{1}{2R_x}C_2-\frac{1}{R_{xy}}C_1\right)x^2-\frac{1}{R_y}C_1xy-\frac{1}{2R_y}C_2y^2-\frac{1}{R_{xy}}C_3x-\frac{1}{R_y}C_3y+\theta_0x+v_0 \end{aligned}\right\} \tag{11-180}$$

Equations (11-173) and (11-180) can be written together in the following form

$$\begin{Bmatrix} w \\ u \\ v \end{Bmatrix} = \begin{bmatrix} x & y & 1 \\ -\dfrac{x^2}{2R_x}+\dfrac{y^2}{2R_y} & -\dfrac{xy}{R_x}-\dfrac{y^2}{R_{xy}} & -\dfrac{x}{R_x}-\dfrac{y}{R_{xy}} \\ -\dfrac{x^2}{R_{xy}}-\dfrac{xy}{R_y} & \dfrac{x^2}{2R_x}-\dfrac{y^2}{2R_y} & -\dfrac{x}{R_{xy}}-\dfrac{y}{R_y} \end{bmatrix} \begin{Bmatrix} C_1 \\ C_2 \\ C_3 \end{Bmatrix} + \begin{Bmatrix} 0 \\ u_0-\theta_0 y \\ v_0+\theta_0 x \end{Bmatrix} \quad (11\text{-}181)$$

The second term on the right-side of the above equation denotes the displacement of the rigid-body motion when there is no normal displacement, and the first term denotes the displacement of the rigid-body motion when the normal displacement exists.

According to the above demonstration, the following deduction can be obtained.

Deduction If the shallow shell element can embody the displacement state of the rigid-body motion, the interpolation formulas for tangential displacements u, v should at least include the complete quadric polynomial.

From this conclusion, it follows that, the appearance of the membrane locking phenomena of some curved shell elements is just because the assumed tangential displacement trial functions cannot satisfy the above requirement.

11.7 Shallow Shell Element—Triangular Element SST21 with Mid-Side Nodes

Triangular shallow shell elements often suffer from the membrane locking phenomenon. In order to overcome this difficulty, some successful displacement-based triangular shallow shell elements are almost the high-order elements using high-order interpolation functions for tangential displacements. For example, in reference [44], tangential and normal displacements all adopt the cubic interpolation functions, and the triangular shallow shell elements with 36 and 27 DOFs are then constructed, respectively; in reference [45], the interpolation functions for the tangential and normal displacements are assumed to be complete cubic and incomplete quintic polynomials, respectively, and a triangular shallow shell element with 2 internal DOFs and 36 external DOFs is then constructed. In order to increase the order of the tangential displacement functions to quadric, the tangential freedoms at the mid-side nodes are considered. This is the scheme for the generalized conforming shallow shell element SST21. Here, we will introduce the construction procedure of this model.

11.7.1 The Local Coordinate System and the Geometric Description of the Element Surface

A triangular shallow shell element is shown in Fig. 11.22. The base plane of the element is formed by linking three corner nodes; let node 1 be the origin of the local coordinate system O*xyz*, the linking line of nodes 1 and 2 be the *x*-axis, and *xy* plane be within the base plane of the element.

Assume that the element surface is a quadric surface in the local coordinate system, and can be expressed in terms of the area coordinates as

$$z = h_1 L_1 + h_2 L_2 + h_3 L_3 + h_4 L_1 L_2 + h_5 L_2 L_3 + h_6 L_3 L_1 \tag{11-182}$$

Substituting the coordinates of the three corner nodes and three mid-side nodes into the above equation in turn, the coefficients h_i can be obtained:

$$\boldsymbol{h} = \begin{Bmatrix} h_1 \\ h_2 \\ h_3 \\ h_4 \\ h_5 \\ h_6 \end{Bmatrix} = \begin{bmatrix} 1 & 0 & 0 & 0 & 0 & 0 \\ 0 & 1 & 0 & 0 & 0 & 0 \\ 0 & 0 & 1 & 0 & 0 & 0 \\ -2 & -2 & 0 & 4 & 0 & 0 \\ 0 & -2 & -2 & 0 & 4 & 0 \\ -2 & 0 & -2 & 0 & 0 & 4 \end{bmatrix} \begin{Bmatrix} z_1 \\ z_2 \\ z_3 \\ z_4 \\ z_5 \\ z_6 \end{Bmatrix} \tag{11-183}$$

Substituting Eq. (11-183) into Eq. (11-182) (note that the local *z*-coordinates of the 3 corner nodes in Fig. 11.22 are all zero), we can obtain

$$z = 4(z_4 L_1 L_2 + z_5 L_2 L_3 + z_6 L_3 L_1) \tag{11-184}$$

From the above equation, the initial curvatures of the element, and the transformations between local and global coordinates can be derived.

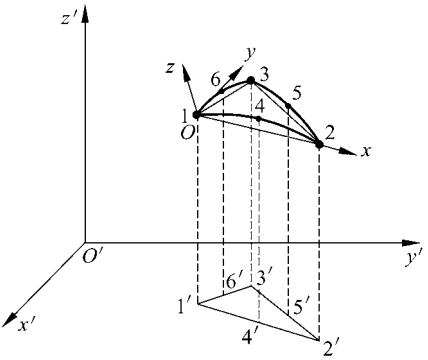

Figure 11.22 Triangular shallow shell element

11.7.2 Selection of DOFs and Determination of Displacement Functions

A triangular shallow shell element with mid-side nodes is shown in Fig. 11.23(a), it is composed of the 3-node bending element in Fig. 11.23(b) and 6-node membrane element in Fig. 11.23(c).

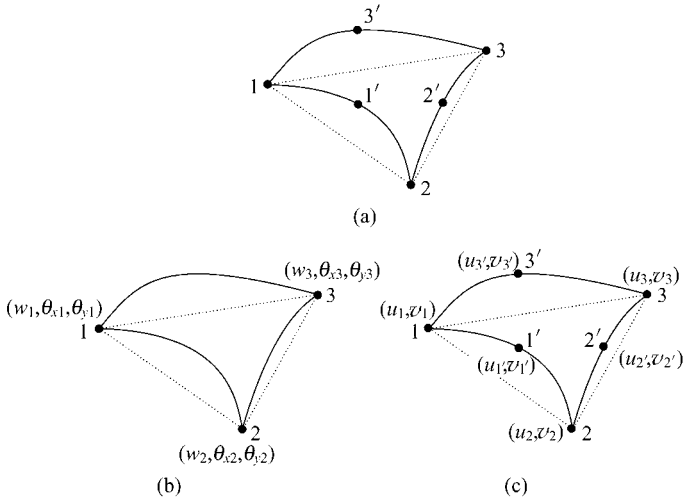

Figure 11.23 Triangular shallow shell element SST21

(a) Triangular shallow shell element with mid-side nodes;

(b) 3-node bending element; (c) 6-node membrane element

The element nodal displacement vector in local coordinate system is

$$\overline{\boldsymbol{q}}^{e}=[\boldsymbol{q}_1^{\mathrm{T}}\quad \boldsymbol{q}_{1'}^{\mathrm{T}}\quad \boldsymbol{q}_2^{\mathrm{T}}\quad \boldsymbol{q}_{2'}^{\mathrm{T}}\quad \boldsymbol{q}_3^{\mathrm{T}}\quad \boldsymbol{q}_{3'}^{\mathrm{T}}]^{\mathrm{T}} \tag{11-185}$$

where

$$\boldsymbol{q}_i=[u_i\quad v_i\quad w_i\quad \theta_{xi}\quad \theta_{yi}]^{\mathrm{T}},\quad \boldsymbol{q}_{i'}=[u_{i'}\quad v_{i'}]^{\mathrm{T}},\quad \theta_{xi}=\left(\frac{\partial w}{\partial y}\right)_i,\quad \theta_{yi}=-\left(\frac{\partial w}{\partial x}\right)_i \tag{11-186}$$

For convenience, the bending displacements and membrane displacements are separated as

$$\boldsymbol{q}^{\mathrm{me}}=[u_1\quad v_1\quad u_{1'}\quad v_{1'}\quad u_2\quad v_2\quad u_{2'}\quad v_{2'}\quad u_3\quad v_3\quad u_{3'}\quad v_{3'}]^{\mathrm{T}} \tag{11-187}$$

$$\boldsymbol{q}^{be}=[w_1\quad \theta_{x1}\quad \theta_{y1}\quad w_2\quad \theta_{x2}\quad \theta_{y2}\quad w_3\quad \theta_{x3}\quad \theta_{y3}]^{\mathrm{T}} \tag{11-188}$$

The tangential displacements of the shell element are assumed to be the displacement fields of the 6-node quadric triangular membrane element, which are the compatible displacement modes:

$$\boldsymbol{u}=\begin{Bmatrix}u\\v\end{Bmatrix}=\sum_{i=1}^{3}\boldsymbol{N}_i\boldsymbol{q}_i^{\mathrm{m}} \tag{11-189}$$

in which

$$\boldsymbol{N}_i=\begin{bmatrix}(2L_i-1)L_i & 0 & 4L_jL_m & 0\\ 0 & (2L_i-1)L_i & 0 & 4L_jL_m\end{bmatrix}\quad (i,j,m=1,2,3) \tag{11-190}$$

$$\boldsymbol{q}_i^{\mathrm{m}}=[u_i \quad v_i \quad u_{i'} \quad v_{i'}]^{\mathrm{T}} \tag{11-191}$$

And, the normal displacements of the shell element are assumed to be displacement fields of the generalized conforming 3-node triangular plate element TGC-9 introduced in Sect. 6.1.1.

11.7.3 Element Stiffness Matrix

The element membrane strains are

$$\boldsymbol{\varepsilon}=[\varepsilon_x \quad \varepsilon_y \quad \gamma_{xy}]^{\mathrm{T}}=\left[\frac{\partial u}{\partial x}+\frac{w}{R_x} \quad \frac{\partial v}{\partial y}+\frac{w}{R_y} \quad \frac{\partial v}{\partial x}+\frac{\partial u}{\partial y}+2\frac{w}{R_{xy}}\right]^{\mathrm{T}}=\boldsymbol{B}_{\mathrm{m}}\boldsymbol{q}^{\mathrm{m}e}+\boldsymbol{B}_{\mathrm{mw}}\boldsymbol{q}^{\mathrm{b}e} \tag{11-192}$$

where

$$\boldsymbol{B}_{\mathrm{m}}=[\boldsymbol{B}_{\mathrm{m1}} \quad \boldsymbol{B}_{\mathrm{m2}} \quad \boldsymbol{B}_{\mathrm{m3}}] \tag{11-193}$$

$$\boldsymbol{B}_{\mathrm{m}i}=\frac{1}{2A}\begin{bmatrix}b_i(2L_i-1) & 0 & 4(b_jL_m+b_mL_j) & 0\\ 0 & c_i(2L_i-1) & 0 & 4(c_jL_m+c_mL_j)\\ c_i(2L_i-1) & b_i(2L_i-1) & 4(c_jL_m+c_mL_j) & 4(b_jL_m+b_mL_j)\end{bmatrix} \tag{11-194}$$

$$(i,j,m=1,2,3)$$

$$b_i=y_j-y_m,\quad c_i=-(x_j-x_m) \tag{11-195}$$

A is the area of the base plane of the element; and

$$\boldsymbol{B}_{\mathrm{m}w}=\begin{bmatrix}\dfrac{1}{R_x}\boldsymbol{F}_\lambda\hat{\boldsymbol{C}}^{-1}\hat{\boldsymbol{G}}\\ \dfrac{1}{R_y}\boldsymbol{F}_\lambda\hat{\boldsymbol{C}}^{-1}\hat{\boldsymbol{G}}\\ \dfrac{2}{R_{xy}}\boldsymbol{F}_\lambda\hat{\boldsymbol{C}}^{-1}\hat{\boldsymbol{G}}\end{bmatrix} \tag{11-196}$$

where $\boldsymbol{F}_\lambda$ is given by Eq. (6-3), $\hat{\boldsymbol{G}}$ and $\hat{\boldsymbol{C}}$ can be expressed as follows:

$$\hat{\boldsymbol{G}}=\begin{bmatrix}0&0&0&-1&0&0&1&0&0\\1&0&0&0&0&0&-1&0&0\\0&-b_1&-c_1&0&-b_2&-c_2&0&-b_3&-c_3\\0&0&0&6&-b_1&-c_1&6&b_1&c_1\\6&b_2&c_2&0&0&0&6&-b_2&-c_2\\6&-b_3&-c_3&6&b_3&c_3&0&0&0\\0&0&0&0&c_1&-b_1&0&c_1&-b_1\\0&c_2&-b_2&0&0&0&0&c_2&-b_2\\0&c_3&-b_3&0&c_3&-b_3&0&0&0\end{bmatrix} \tag{11-197}$$

$$\hat{\boldsymbol{C}}=\begin{bmatrix}0&-1&1&0&0&0&0&0&0\\1&0&-1&0&0&0&0&0&0\\0&0&0&-1&-1&-1&1&1&1\\0&6&6&0&1&0&0&0&1\\6&0&6&0&0&1&1&0&0\\6&6&0&1&0&0&0&1&0\\\dfrac{f_2+f_3}{A}&\dfrac{-f_3}{A}&\dfrac{-f_2}{A}&F_2&-3F_2&5F_2&F_2&5F_2&-3F_2\\\dfrac{-f_3}{A}&\dfrac{f_3+f_1}{A}&\dfrac{-f_1}{A}&5F_3&F_3&-3F_3&-3F_3&F_3&5F_3\\\dfrac{-f_2}{A}&\dfrac{-f_1}{A}&\dfrac{f_1+f_2}{A}&-3F_1&5F_1&F_1&5F_1&-3F_1&F_1\end{bmatrix} \tag{11-198}$$

$$\left.\begin{aligned}f_i&=-(b_jb_m+c_jc_m)\\F_i&=\frac{f_i+f_j}{12A}\end{aligned}\right\}\quad(i,j,m=1,2,3) \tag{11-199}$$

The element bending strain matrix $\boldsymbol{B}_{\mathrm{b}}$ can be obtained by the conventional procedure. According to the sequence of DOFs given in Eq. (11-185), $\boldsymbol{B}_{\mathrm{m}}$, $\boldsymbol{B}_{\mathrm{m}w}$ and $\boldsymbol{B}_{\mathrm{b}}$ can be expanded to 3×21 matrices, and then, can be assembled to form the total strain matrix $\boldsymbol{B}$. Thus, the element stiffness matrix in the element local coordinate system can be written as

$$\overline{\boldsymbol{K}}^{e}=\iint_{A^{e}}\boldsymbol{B}^{\mathrm{T}}\boldsymbol{D}\boldsymbol{B}\mathrm{d}A \tag{11-200}$$

with

$$\boldsymbol{D}=\begin{bmatrix}\boldsymbol{D}_{\mathrm{m}} & 0\\ 0 & \boldsymbol{D}_{\mathrm{b}}\end{bmatrix} \tag{11-201}$$

Then, it can be transformed to the global coordinate system for the finite element solution.

11.7.4 Numerical Examples

Example 11.12 Scordelis-Lo roof problem.

As shown in Fig. 11.24, this problem is the same as the Example 11.9. The analytical solution of the shallow shell is used for comparison. The results are listed in Tables 11.13 and 11.14, in which Table 11.13 gives the vertical displacements of the center point of the roof and the mid-side point of the free edge obtained by different meshes; Table 11.14 gives the displacement results of the different points using 8×12 mesh. It can be seen that the element SST21 can successfully pass the membrane locking test, and converge to the analytical solution of the shallow shell.

Table 11.13 The vertical displacements of the center point of the cylindrical shell and the mid-side point of the free edge (membrane locking test)

Mesh	SST21 (21 DOFs)		Reference [44] (27 DOFs)		Reference [44] (36 DOFs)	
	w_B	w_C	w_B	w_C	w_B	w_C
2×3	0.171	−0.0068	0.211		0.323	−0.044
4×5	0.287	−0.0416	0.297	−0.0400	0.315	−0.0448
8×12	0.307	−0.0433	0.309	−0.0436		
Analytical solution of shallow shell[46]	0.308	−0.046	0.308	−0.046	0.308	−0.046

Table 11.14 The displacements of different points on the cylindrical shell (8 × 12 mesh)

Point		*A*	*B*	2	3	4	*C*
u	SST21	0.0126	0	0	0	0	0
	Analytical[46]	0.0126	0	0	0	0	0
v	SST21	0	−0.164	−0.0836	−0.0294	−0.0046	0
	Analytical[46]	0	−0.164	−0.082	−0.028	−0.004	0
w	SST21	0	0.307	0.192	0.0774	−0.0104	−0.0433
	Analytical[46]	0	0.308	0.190	0.076	−0.012	−0.046

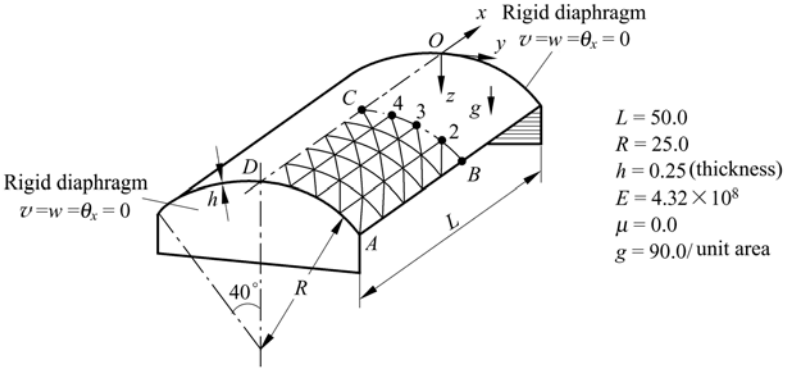

Figure 11.24 Scordelis-Lo roof. Mesh by shallow shell element 4 × 5

Example 11.13 Doubly curved shallow shell.

A simply-supported doubly curved shallow shell subjected to uniform vertical load q is shown in Fig. 11.25. Equation of its mid-surface is $z = 0.5k(x^2 + y^2)$. Due to symmetry, only 1/4 of the shell is analyzed. The results are listed in Table 11.15.

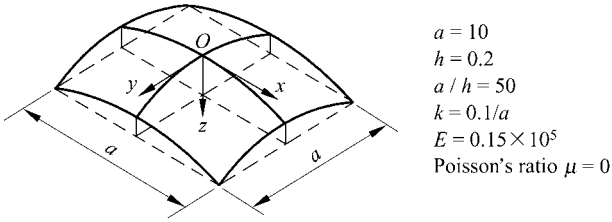

Figure 11.25 A doubly curved shallow shell

Table 11.15 The central vertical displacement of the doubly curved shallow shell $w/(10^{-3}qaD^{-1})$

Mesh for 1/4 shell	1 × 1	2 × 2	4 × 4	6 × 6
SST21	4.29	4.01	3.99	3.99
Analytical solution	3.99			

Example 11.14 Hyperbolic paraboloid shell.

A clamped hyperbolic paraboloid shell subjected to uniformly distributed normal load q is shown in Fig. 11.26. The results are listed in Table 11.16.

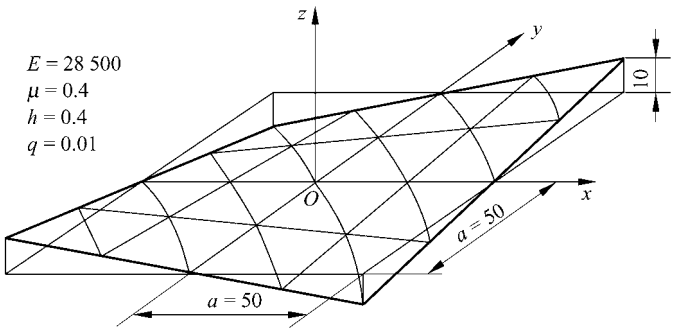

Figure 11.26 Hyperbolic paraboloid shell

Table 11.16 The central vertical displacement of the hyperbolic paraboloid shell

Element \ Mesh	2 × 2	4 × 4	8 × 8	12 × 12
SST21 (21 DOFs)	−0.0326	−0.0315	−0.0250	−0.0248
Reference [44] (27 DOFs)		−0.0345	−0.0283	
Reference [44] (36 DOFs)	−0.044	−0.0275	−0.0263	
Finite difference solution	−0.024 59			

11.8 Shell Element for Geometrically Nonlinear Analysis —Triangular Flat-Shell Element GMST18

On the basis of the generalized conforming thick/thin triangular flat-shell element GMST18 (refer to Sect. 11.4), reference [9] derives the UL (Updated Lagrangian) formulations of the element for the analysis of geometrically nonlinear problems, which exhibit good performance for numerical examples.

In the incremental method, all the physical components of a structure from time 0 to time t are assumed to have been obtained. What we are interested in is the increment that occurs from time t to time $t+\Delta t$. The reference configuration is the configuration at time t. The principle of virtual displacement expressed by the UL method can be written as

$$\iiint_V \left({}^{t+\Delta t}\sigma_{ij} \right) \delta \left({}^{t+\Delta t}\varepsilon_{ij} \right) \mathrm{d}V = {}^{t+\Delta t}W \tag{11-202}$$

where ${}^{t+\Delta t}\sigma_{ij}$ and ${}^{t+\Delta t}\varepsilon_{ij}$ are the modified Kirchhoff stress tensor and the modified Green strain tensor, respectively; ${}^{t+\Delta t}W$ is the virtual work done by external loadings at the time $t+\Delta t$.

$$ {}^{t+\Delta t}\sigma_{ij} = \sigma_{ij}^{E} + \Delta\sigma_{ij} \tag{11-203} $$

where σ_{ij}^{E} is the Cauchy stress tensor at the time t, and $\Delta\sigma_{ij}$ is the Kirchhoff stress tensor increment from time t to time $t+\Delta t$.

$$ \left.\begin{aligned} {}^{t+\Delta t}\varepsilon_{ij} &= \Delta\varepsilon_{ij} = \Delta e_{ij} + \Delta\eta_{ij} \\ \Delta e_{ij} &= \frac{1}{2}(\Delta u_{i,j} + \Delta u_{j,i}), \quad \Delta\eta_{ij} = \frac{1}{2}\Delta u_{k,i}\Delta u_{k,j} \end{aligned}\right\} \tag{11-204} $$

where Δe_{ij} and $\Delta\eta_{ij}$ are the linear and non-linear Green strain tensor increment from time t to time $t+\Delta t$, respectively. And, Δu_i is the displacement increment from time t to time $t+\Delta t$.

If Δt is small enough, the following relationship can be established

$$ \Delta\sigma_{ij} = D_{ijkl}\Delta\varepsilon_{kl} \tag{11-205} $$

where D_{ijkl} is the elastic tensor.

Substitution of Eqs. (11-203), (11-204) and (11-205) into Eq. (11-202) yields (the higher-order terms have been neglected)

$$ I_1 + I_2 = ({}^{t+\Delta t}W) - I_3 \tag{11-206} $$

with

$$ I_1 = \int_V D_{ijkl}\Delta e_{kl}\,\delta\Delta e_{ij}\mathrm{d}V, \quad I_2 = \int_V \sigma_{ij}^{E}\,\delta\Delta\eta_{ij}\mathrm{d}V, \quad I_3 = \int_V \sigma_{ij}^{E}\,\delta\Delta e_{ij}\mathrm{d}V \tag{11-207} $$

where I_1 is the linear increment of virtual work; I_2 is the incremental virtual work relevant to the initial stresses; I_3 is the incremental virtual work done by the internal forces.

For the flat-shell element in the local co-ordinates, I_1, I_2 and I_3 in Eq. (11-207) can be rewritten in the following discrete form

$$ \left.\begin{aligned} I_1 &= \iint_{A^e}(\delta\Delta\boldsymbol{\varepsilon}_{\mathrm{m}}{}^{\mathrm{T}}\boldsymbol{D}_{\mathrm{m}}\Delta\boldsymbol{\varepsilon}_{\mathrm{m}} + \delta\Delta\boldsymbol{\kappa}^{\mathrm{T}}\boldsymbol{D}_{\mathrm{b}}\Delta\boldsymbol{\kappa} + \delta\Delta\boldsymbol{\gamma}^{\mathrm{T}}\boldsymbol{D}_{\mathrm{s}}\Delta\boldsymbol{\gamma})\mathrm{d}A \\ I_2 &= \iint_{A^e}\delta\Delta\boldsymbol{w}'^{\mathrm{T}}\bar{\boldsymbol{N}}^{E}\Delta\boldsymbol{w}'\mathrm{d}A \\ I_3 &= \iint_{A^e}(\delta\Delta\boldsymbol{\varepsilon}_{\mathrm{m}}{}^{\mathrm{T}}\boldsymbol{N}_{\mathrm{m}}^{E} + \delta\Delta\boldsymbol{\kappa}^{\mathrm{T}}\boldsymbol{M}^{E} + \delta\Delta\boldsymbol{\gamma}^{\mathrm{T}}\boldsymbol{Q}^{E})\mathrm{d}A \end{aligned}\right\} \tag{11-208} $$

where Δ means the increment of relevant variables; $\Delta\boldsymbol{\varepsilon}_{\mathrm{m}}$ is the linear increment

of the membrane strain and given by

$$\Delta\boldsymbol{\varepsilon}_{\mathrm{m}}=\left[\begin{array}{ccc}\dfrac{\partial\Delta u}{\partial x} & \dfrac{\partial\Delta v}{\partial y} & \dfrac{\partial\Delta u}{\partial y}+\dfrac{\partial\Delta v}{\partial x}\end{array}\right]^{\mathrm{T}}=\boldsymbol{B}_{\mathrm{m}}\Delta\boldsymbol{q}_{\mathrm{m}}{}^{e} \tag{11-209}$$

$\Delta\boldsymbol{\kappa}$ is the linear increment of the curvature vector given in Eq. (11-157); $\Delta\boldsymbol{\gamma}$ is the increment of the transverse shear strain vector given in Eq. (11-140);

$$\Delta\boldsymbol{w}'=\left\{\begin{array}{c}\dfrac{\partial\Delta w}{\partial x}\\ \dfrac{\partial\Delta w}{\partial y}\end{array}\right\}=\left[\begin{array}{c}\boldsymbol{F}'_{\lambda,x}\\ \boldsymbol{F}'_{\lambda,y}\end{array}\right]\boldsymbol{CL}\Delta\boldsymbol{q}_{\mathrm{p}}{}^{e}=\boldsymbol{B}_{G}\Delta\boldsymbol{q}_{\mathrm{p}}{}^{e},\quad \boldsymbol{B}_{G}=\left[\begin{array}{c}\boldsymbol{F}'_{\lambda,x}\\ \boldsymbol{F}'_{\lambda,y}\end{array}\right]\boldsymbol{CL} \tag{11-210}$$

$$\bar{\boldsymbol{N}}^{E}=\left[\begin{array}{cc}\displaystyle\int_{-h/2}^{h/2}\sigma_{x}^{E}\mathrm{d}z & \displaystyle\int_{-h/2}^{h/2}\tau_{xy}^{E}\mathrm{d}z\\ \displaystyle\int_{-h/2}^{h/2}\tau_{xy}^{E}\mathrm{d}z & \displaystyle\int_{-h/2}^{h/2}\sigma_{y}^{E}\mathrm{d}z\end{array}\right]=\left[\begin{array}{cc}N_{x}^{E} & N_{xy}^{E}\\ N_{xy}^{E} & N_{y}^{E}\end{array}\right] \tag{11-211}$$

$\boldsymbol{N}_{\mathrm{m}}^{E}$, $\boldsymbol{M}^{E}$ and $\boldsymbol{Q}^{E}$ are the membrane force, bending moment and shear force vectors at the time t, respectively,

$$\boldsymbol{N}_{\mathrm{m}}^{E}=[N_{x}^{E}\quad N_{y}^{E}\quad N_{xy}^{E}]^{\mathrm{T}},\quad \boldsymbol{M}^{E}=[M_{x}^{E}\quad M_{y}^{E}\quad M_{xy}^{E}]^{\mathrm{T}},\quad \boldsymbol{Q}^{E}=[Q_{x}^{E}\quad Q_{y}^{E}]^{\mathrm{T}} \tag{11-212}$$

Substitution of the geometric relation Eqs. (11-140), (11-157) and (11-209) into Eq. (11-208) yields

$$\left.\begin{aligned}I_{1}&=\delta\Delta\boldsymbol{q}_{\mathrm{m}}{}^{e\mathrm{T}}\left(\iint_{A^{e}}\boldsymbol{B}_{\mathrm{m}}{}^{\mathrm{T}}\boldsymbol{D}_{\mathrm{m}}\boldsymbol{B}_{\mathrm{m}}\mathrm{d}A\right)\Delta\boldsymbol{q}_{\mathrm{m}}{}^{e}\\ &\quad+\delta\Delta\boldsymbol{q}_{\mathrm{p}}{}^{e\mathrm{T}}\left(\iint_{A^{e}}(\boldsymbol{B}_{\mathrm{b}}{}^{\mathrm{T}}\boldsymbol{D}_{\mathrm{b}}\boldsymbol{B}_{\mathrm{b}}+\boldsymbol{B}_{\mathrm{s}}{}^{\mathrm{T}}\boldsymbol{D}_{\mathrm{s}}\boldsymbol{B}_{\mathrm{s}})\mathrm{d}A\right)\Delta\boldsymbol{q}_{\mathrm{p}}{}^{e}\\ I_{2}&=\delta\Delta\boldsymbol{q}_{\mathrm{p}}{}^{e\mathrm{T}}\left(\iint_{A^{e}}\boldsymbol{B}_{G}{}^{\mathrm{T}}\bar{\boldsymbol{N}}^{E}\boldsymbol{B}_{G}\mathrm{d}A\right)\Delta\boldsymbol{q}_{\mathrm{p}}{}^{e}\\ I_{3}&=\delta\Delta\boldsymbol{q}_{\mathrm{m}}{}^{e\mathrm{T}}\left(\iint_{A^{e}}\boldsymbol{B}_{\mathrm{m}}{}^{\mathrm{T}}\boldsymbol{N}_{\mathrm{m}}^{E}\mathrm{d}A\right)\Delta\boldsymbol{q}_{\mathrm{m}}{}^{e}\\ &\quad+\delta\Delta\boldsymbol{q}_{\mathrm{p}}{}^{e\mathrm{T}}\left(\iint_{A^{e}}(\boldsymbol{B}_{\mathrm{b}}{}^{\mathrm{T}}\boldsymbol{M}^{E}+\boldsymbol{B}_{\mathrm{s}}{}^{\mathrm{T}}\boldsymbol{Q}^{E})\mathrm{d}A\right)\Delta\boldsymbol{q}_{\mathrm{p}}{}^{e}\end{aligned}\right\} \tag{11-213}$$

And, ${}^{t+\Delta t}W$ can be rewritten as

$${}^{t+\Delta t}W=\delta\Delta\boldsymbol{q}_{\mathrm{m}}{}^{e\mathrm{T}}\,{}^{t+\Delta t}\boldsymbol{R}_{\mathrm{m}}{}^{e}+\delta\Delta\boldsymbol{q}_{\mathrm{p}}{}^{e\mathrm{T}}\,{}^{t+\Delta t}\boldsymbol{R}_{\mathrm{p}}{}^{e} \tag{11-214}$$

where ${}^{t+\Delta t}\boldsymbol{R}_{\mathrm{m}}{}^{e}$ and ${}^{t+\Delta t}\boldsymbol{R}_{\mathrm{p}}{}^{e}$ are the equivalent nodal force vectors at the time $t+\Delta t$ of the membrane element and plate bending element, respectively.

Since $\delta\Delta\boldsymbol{q}_{\mathrm{m}}{}^{e}$ and $\delta\Delta\boldsymbol{q}_{\mathrm{p}}{}^{e}$ are arbitrary, thus, according to the variational principle and Eqs. (11-206), (11-213) and (11-214), we can obtain the element incremental equations in the local co-ordinates:

$$\begin{bmatrix} \boldsymbol{K}_{\mathrm{m}}{}^{e} & \boldsymbol{0} \\ \boldsymbol{0} & \boldsymbol{K}_{\mathrm{p}}{}^{e}+\boldsymbol{K}_{\sigma}{}^{e} \end{bmatrix} \begin{Bmatrix} \Delta\boldsymbol{q}_{\mathrm{m}}{}^{e} \\ \Delta\boldsymbol{q}_{\mathrm{p}}{}^{e} \end{Bmatrix} = \begin{Bmatrix} {}^{t+\Delta t}\boldsymbol{R}_{\mathrm{m}}{}^{e} \\ {}^{t+\Delta t}\boldsymbol{R}_{\mathrm{p}}{}^{e} \end{Bmatrix} - \begin{Bmatrix} \boldsymbol{\Psi}_{\mathrm{m}}{}^{e} \\ \boldsymbol{\Psi}_{\mathrm{p}}{}^{e} \end{Bmatrix} \tag{11-215}$$

where $\boldsymbol{K}_{\mathrm{m}}^{e}$ is the linear stiffness matrix of the membrane element and given by Eq. (11-97); $\boldsymbol{K}_{\mathrm{p}}^{e}$ is the linear stiffness matrix of the plate bending element and given by Eq. (11-158); $\boldsymbol{K}_{\sigma}^{e}$ is the geometric stiffness matrix,

$$\boldsymbol{K}_{\sigma}{}^{e} = \iint_{A^e} \boldsymbol{B}_{G}{}^{\mathrm{T}} \bar{\boldsymbol{N}}^{E} \boldsymbol{B}_{G} \mathrm{d}A \tag{11-216}$$

$\boldsymbol{\Psi}_{\mathrm{m}}^{e}$ is the equivalent nodal internal force vector of the membrane element; $\boldsymbol{\Psi}_{\mathrm{p}}^{e}$ is the equivalent nodal internal force vector of the plate bending element,

$$\boldsymbol{\Psi}_{\mathrm{m}}{}^{e} = \iint_{A^e} \boldsymbol{B}_{\mathrm{m}}{}^{\mathrm{T}} \boldsymbol{N}_{\mathrm{m}}^{E} \mathrm{d}A, \quad \boldsymbol{\Psi}_{\mathrm{p}}{}^{e} = \iint_{A^e} (\boldsymbol{B}_{\mathrm{b}}{}^{\mathrm{T}} \boldsymbol{M}^{E} + \boldsymbol{B}_{\mathrm{s}}{}^{\mathrm{T}} \boldsymbol{Q}^{E}) \mathrm{d}A \tag{11-217}$$

Rewriting (11-215) according to the DOF's sequence yields

$$(\boldsymbol{K}^{e} + \boldsymbol{K}_{\sigma}{}^{e}) \Delta\boldsymbol{q}^{e} = {}^{t+\Delta t}\boldsymbol{R}^{e} - \boldsymbol{\Psi}^{e} \tag{11-218}$$

After transforming (11-218) to the global co-ordinates by standard procedure, the element GMST18 can be used to analyze the geometrically nonlinear problem of shells.

Example 11.15 Post-buckling analysis of a square plate.

As shown in Fig. 11.27, a square plate is controlled by four clamps along each edge. Thus, the displacements in the controlled directions are uniform. This plate is subjected to a pair of concentrated loads on two opposite sides. Only a quarter of the plate using 4×4 mesh division is analyzed because of symmetry.

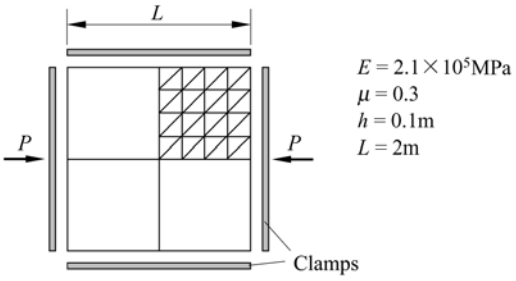

Figure 11.27 Post-buckling problem for a square plate

According to the series method presented by Budiansky[47], the critical load and post-buckling path are given by

$$P_{\mathrm{cr}} = \frac{4\pi^2 D}{L} \qquad \text{and} \qquad \frac{P}{P_{\mathrm{cr}}} = 1 + \frac{3}{8}(1-\mu^2)\left(\frac{w_{\max}}{h}\right)^2$$

where $w_{\max}$ is the central deflection of the square plate. The post-buckling paths obtained by presented element GMST18 and element STRI3 in ABAQUS are plotted in Fig. 11.28. It can be seen that the results of GMST18 are more consistent with Budiansky's solutions than those of STRI3.

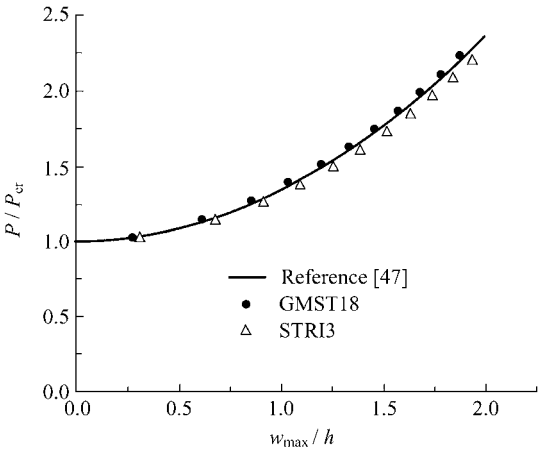

Figure 11.28 Post-buckling path for a square plate, mesh 4×4

11.9 Shell Element for Geometrically Nonlinear Analysis —Rectangular Shallow Shell Element SSR28

11.9.1 Nonlinear Strains and TL (Total Lagrangian) Formulations

The simplified nonlinear strain components of the shallow shell element given by reference [48] have already been successfully applied in the nonlinear analysis of the shell structures. Here, these nonlinear strain components will be adopted to construct the generalized conforming rectangular shallow shell element for geometrically nonlinear analysis. The expressions of these strains are as follows:

$$\varepsilon_{11} = \frac{\partial u}{\partial x} + \frac{w}{R_1} + \frac{1}{2}\left(\frac{\partial w}{\partial x} - \frac{u}{R_1}\right)^2 + z\left(-\frac{\partial^2 w}{\partial x^2} + \frac{1}{R_1}\frac{\partial u}{\partial x}\right) \qquad (11\text{-}219a)$$

$$\varepsilon_{22}=\frac{\partial v}{\partial y}+\frac{w}{R_2}+\frac{1}{2}\left(\frac{\partial w}{\partial y}-\frac{v}{R_2}\right)^2+z\left(-\frac{\partial^2 w}{\partial y^2}+\frac{1}{R_2}\frac{\partial v}{\partial y}\right) \tag{11-219b}$$

$$\varepsilon_{12}=\frac{\partial u}{\partial y}+\frac{\partial v}{\partial x}+\left(\frac{\partial w}{\partial x}-\frac{u}{R_1}\right)\left(\frac{\partial w}{\partial y}-\frac{v}{R_2}\right)+z\left(-2\frac{\partial^2 w}{\partial x\partial y}+\frac{1}{R_1}\frac{\partial u}{\partial y}+\frac{1}{R_2}\frac{\partial v}{\partial x}\right) \tag{11-219c}$$

where $\varepsilon_{11}=\varepsilon_x$, $\varepsilon_{22}=\varepsilon_y$, $\varepsilon_{12}=\varepsilon_{xy}$, $R_1=R_x$, $R_2=R_y$.

The above strain components can be decomposed as follows:

$$\boldsymbol{\varepsilon}^{\mathrm{m}}=[e_{11}\quad e_{22}\quad e_{12}+e_{21}]^{\mathrm{T}}=\left[\frac{\partial u}{\partial x}+\frac{w}{R_1}\quad \frac{\partial v}{\partial y}+\frac{w}{R_2}\quad \frac{\partial u}{\partial y}+\frac{\partial v}{\partial x}\right]^{\mathrm{T}} \tag{11-220a}$$

$$\begin{aligned}\boldsymbol{\varepsilon}^{\mathrm{b}}&=[\kappa_{11}\quad \kappa_{22}\quad \kappa_{12}+\kappa_{21}]^{\mathrm{T}}\\&=\left[-\frac{\partial^2 w}{\partial x^2}+\frac{1}{R_1}\frac{\partial u}{\partial x}\quad -\frac{\partial^2 w}{\partial y^2}+\frac{1}{R_2}\frac{\partial v}{\partial y}\quad -2\frac{\partial^2 w}{\partial x\partial y}+\frac{1}{R_1}\frac{\partial u}{\partial y}+\frac{1}{R_2}\frac{\partial v}{\partial x}\right]^{\mathrm{T}}\end{aligned} \tag{11-220b}$$

$$\boldsymbol{\varepsilon}^{\mathrm{g}}=[e_{13}\quad e_{23}]^{\mathrm{T}}=\left[\frac{\partial w}{\partial x}-\frac{u}{R_1}\quad \frac{\partial w}{\partial y}-\frac{v}{R_2}\right]^{\mathrm{T}} \tag{11-220c}$$

Compared with von Kármán nonlinear strain components, it can be seen that in the above expressions, $\frac{\partial w}{\partial x}$ and $\frac{\partial w}{\partial y}$ are replaced by $\frac{\partial w}{\partial x}-\frac{u}{R_1}$ and $\frac{\partial w}{\partial y}-\frac{v}{R_2}$, respectively; $-\frac{\partial^2 w}{\partial x^2}$ and $-\frac{\partial^2 w}{\partial y^2}$ are replaced by $-\frac{\partial^2 w}{\partial x^2}+\frac{1}{R_1}\frac{\partial u}{\partial x}$ and $-\frac{\partial^2 w}{\partial y^2}+\frac{1}{R_2}\frac{\partial v}{\partial y}$, respectively; and $-2\frac{\partial^2 w}{\partial x\partial y}$ is replaced by $-2\frac{\partial^2 w}{\partial x\partial y}+\frac{1}{R_1}\frac{\partial u}{\partial y}+\frac{1}{R_2}\frac{\partial v}{\partial x}$. In total Lagrangian coordinates, the increments of strain components are

$$\Delta\varepsilon_{11}=\Delta e_{11}+e_{13}\Delta e_{13}+\frac{1}{2}\Delta e_{13}{}^2+z\Delta\kappa_{11} \tag{11-221a}$$

$$\Delta\varepsilon_{22}=\Delta e_{22}+e_{23}\Delta e_{23}+\frac{1}{2}\Delta e_{23}{}^2+z\Delta\kappa_{22} \tag{11-221b}$$

$$\Delta\varepsilon_{12}=\Delta e_{12}+\Delta e_{21}+e_{13}\Delta e_{23}+e_{23}\Delta e_{13}+\Delta e_{13}\Delta e_{23}+z(\Delta\kappa_{12}+\Delta\kappa_{21}) \tag{11-221c}$$

where Δe_{11} and Δe_{22} are the strains caused by displacement increments; e_{13} and e_{23} are the strains caused by total displacements corresponding to original coordinate system. After the determination of the normal and tangential displacement functions, the linear strains in Eq. (11-221) can be written as

$$\Delta\bar{\boldsymbol{\varepsilon}}^{\mathrm{m}} = \begin{Bmatrix} \Delta\bar{e}_{11} \\ \Delta\bar{e}_{22} \\ \Delta\bar{e}_{12} + \Delta\bar{e}_{21} \end{Bmatrix} = \begin{Bmatrix} \Delta e_{11} + e_{13}\Delta e_{13} \\ \Delta e_{22} + e_{23}\Delta e_{23} \\ \Delta e_{12} + \Delta e_{21} + e_{13}\Delta e_{23} + e_{23}\Delta e_{13} \end{Bmatrix}$$
$$= \Delta\boldsymbol{\varepsilon}^{\mathrm{m}} + \Delta\boldsymbol{\varepsilon}^{\mathrm{m}\theta} = (\boldsymbol{B}^{\mathrm{m}p} + \boldsymbol{B}^{\mathrm{m}\theta})\Delta\bar{\boldsymbol{q}}^{e} \tag{11-222}$$

where

$$\Delta\boldsymbol{\varepsilon}^{\mathrm{m}} = \begin{Bmatrix} \Delta e_{11} \\ \Delta e_{22} \\ \Delta e_{12} + \Delta e_{21} \end{Bmatrix} = \boldsymbol{B}^{\mathrm{m}p}\Delta\bar{\boldsymbol{q}}^{e} \tag{11-223}$$

$$\Delta\boldsymbol{\varepsilon}^{\mathrm{m}\theta} = \begin{Bmatrix} e_{13}\Delta e_{13} \\ e_{23}\Delta e_{23} \\ e_{13}\Delta e_{23} + e_{23}\Delta e_{13} \end{Bmatrix} = \begin{Bmatrix} e_{13}\boldsymbol{B}_{13}^{\mathrm{g}} \\ e_{23}\boldsymbol{B}_{23}^{\mathrm{g}} \\ e_{13}\boldsymbol{B}_{23}^{\mathrm{g}} + e_{23}\boldsymbol{B}_{13}^{\mathrm{g}} \end{Bmatrix}\Delta\bar{\boldsymbol{q}}^{e} = \boldsymbol{B}^{\mathrm{m}\theta}\Delta\bar{\boldsymbol{q}}^{e} \tag{11-224}$$

From Eqs. (11-220b) and (11-220c), the following incremental strains can be obtained:

$$\Delta\boldsymbol{\varepsilon}^{\mathrm{g}} = \begin{Bmatrix} \Delta e_{13} \\ \Delta e_{23} \end{Bmatrix} = \begin{Bmatrix} \boldsymbol{B}_{13}^{\mathrm{g}} \\ \boldsymbol{B}_{23}^{\mathrm{g}} \end{Bmatrix}\Delta\bar{\boldsymbol{q}}^{e} = \boldsymbol{B}^{\mathrm{g}}\Delta\bar{\boldsymbol{q}}^{e} \tag{11-225}$$

$$\Delta\boldsymbol{\varepsilon}^{\mathrm{b}} = \begin{Bmatrix} \Delta\kappa_{11} \\ \Delta\kappa_{22} \\ \Delta\kappa_{12} + \Delta\kappa_{21} \end{Bmatrix} = \boldsymbol{B}^{\mathrm{b}p}\Delta\bar{\boldsymbol{q}}^{e} \tag{11-226}$$

Then, the TL formulations for nonlinear tangential stiffness matrix of the shallow shell element can be written as

$$\bar{\boldsymbol{K}}_{T}^{\ e} = \bar{\boldsymbol{K}}^{\mathrm{m}e} + \bar{\boldsymbol{K}}^{\mathrm{m}\theta e} + \bar{\boldsymbol{K}}^{\mathrm{b}e} + \bar{\boldsymbol{K}}^{\mathrm{g}e} + \Delta\bar{\boldsymbol{K}}^{e} \tag{11-227}$$

where

$$\bar{\boldsymbol{K}}^{\mathrm{m}e} = \iint_{A^e} \boldsymbol{B}^{\mathrm{m}p\mathrm{T}}\boldsymbol{D}_{\mathrm{m}}\boldsymbol{B}^{\mathrm{m}p}\mathrm{d}A$$

$$\bar{\boldsymbol{K}}^{\mathrm{m}\theta e} = \bar{\boldsymbol{K}}_{1}^{\mathrm{m}\theta e} + \bar{\boldsymbol{K}}_{2}^{\mathrm{m}\theta e} + \bar{\boldsymbol{K}}_{2}^{\mathrm{m}\theta e\mathrm{T}}$$

$$\bar{\boldsymbol{K}}_{1}^{\mathrm{m}\theta e} = \frac{Eh}{1-\mu^2}\iint_{A^e} \boldsymbol{B}^{\mathrm{g}\mathrm{T}} \begin{bmatrix} e_{13}^2 + \dfrac{1-\mu}{2}e_{23}^2 & \dfrac{1+\mu}{2}e_{13}e_{23} \\ \dfrac{1+\mu}{2}e_{13}e_{23} & e_{23}^2 + \dfrac{1-\mu}{2}e_{13}^2 \end{bmatrix} \boldsymbol{B}^{\mathrm{g}}\mathrm{d}A$$

$$\overline{\boldsymbol{K}}_2^{\mathrm{m}\theta e}=\frac{Eh}{1-\mu^2}\iint_{A^e}\boldsymbol{B}^{\mathrm{gT}}\begin{bmatrix} e_{13} & \mu e_{13} & \dfrac{1-\mu}{2}e_{23} \\ \mu e_{23} & e_{23} & \dfrac{1-\mu}{2}e_{13}\end{bmatrix}\boldsymbol{B}^{\mathrm{m}p}\mathrm{d}A$$

$$\overline{\boldsymbol{K}}^{\mathrm{b}e}=\iint_{A^e}\boldsymbol{B}^{\mathrm{b}p\mathrm{T}}\boldsymbol{D}_{\mathrm{b}}\boldsymbol{B}^{\mathrm{b}p}\mathrm{d}A$$

$$\overline{\boldsymbol{K}}^{\mathrm{g}e}=h\iint_{A^e}\boldsymbol{B}^{\mathrm{gT}}\begin{bmatrix}\sigma_{11} & \tau_{12}\\ \tau_{12} & \sigma_{22}\end{bmatrix}\boldsymbol{D}_{\mathrm{m}}\boldsymbol{B}^{\mathrm{g}}\mathrm{d}A$$

$$\Delta\overline{\boldsymbol{K}}^{e}=\Delta\overline{\boldsymbol{K}}_1^{\ e}+\Delta\overline{\boldsymbol{K}}_2^{\ e}+\Delta\overline{\boldsymbol{K}}_2^{\ e\mathrm{T}}+\Delta\overline{\boldsymbol{K}}_3^{\ e}$$

$$\Delta\overline{\boldsymbol{K}}_1^{\ e}=\frac{Eh}{1-\mu^2}\iint_{A^e}\boldsymbol{B}^{\mathrm{gT}}\begin{bmatrix}\dfrac{1}{2}(3\Delta e_{13}^2+\Delta e_{23}^2) & \Delta e_{13}\Delta e_{23}\\ \Delta e_{13}\Delta e_{23} & \dfrac{1}{2}(3\Delta e_{23}^2+\Delta e_{13}^2)\end{bmatrix}\boldsymbol{B}^{\mathrm{g}}\mathrm{d}A$$

$$\Delta\overline{\boldsymbol{K}}_2^{\ e}=\frac{Eh}{1-\mu^2}\iint_{A^e}\boldsymbol{B}^{\mathrm{gT}}\begin{bmatrix}\Delta e_{13} & \mu\Delta e_{13} & \dfrac{1}{2}(1-\mu)\Delta e_{23}\\ \mu\Delta e_{23} & \Delta e_{23} & \dfrac{1}{2}(1-\mu)\Delta e_{13}\end{bmatrix}(\boldsymbol{B}^{\mathrm{m}p}+\boldsymbol{B}^{\mathrm{m}\theta})\mathrm{d}A$$

$$\Delta\overline{\boldsymbol{K}}_3^{\ e}=\frac{Eh}{1-\mu^2}\iint_{A^e}\boldsymbol{B}^{\mathrm{gT}}\begin{bmatrix}\Delta\overline{e}_{11}+\mu\Delta\overline{e}_{22} & \dfrac{1}{2}(1-\mu)(\Delta\overline{e}_{12}+\Delta\overline{e}_{21})\\ \dfrac{1}{2}(1-\mu)(\Delta\overline{e}_{12}+\Delta\overline{e}_{21}) & \Delta\overline{e}_{22}+\mu\Delta\overline{e}_{11}\end{bmatrix}\boldsymbol{B}^{\mathrm{g}}\mathrm{d}A$$

where σ_{11}, σ_{22} and τ_{12} are the second Piola-Kirchhoff stresses.

11.9.2 The Formulations of the Rectangular Shallow Shell Element SSR28

A generalized conforming rectangular shallow shell element with tangential DOFs at the mid-side points is shown in Fig. 11.29. It is composed of two parts: 4-node bending element and 8-node membrane element.

The element nodal displacement vector is

$$\overline{\boldsymbol{q}}^{e}=[\boldsymbol{q}_1^{\mathrm{T}}\quad\boldsymbol{q}_{1'}^{\mathrm{T}}\quad\boldsymbol{q}_2^{\mathrm{T}}\quad\boldsymbol{q}_{2'}^{\mathrm{T}}\quad\boldsymbol{q}_3^{\mathrm{T}}\quad\boldsymbol{q}_{3'}^{\mathrm{T}}\quad\boldsymbol{q}_4^{\mathrm{T}}\quad\boldsymbol{q}_{4'}^{\mathrm{T}}]^{\mathrm{T}}\qquad(11\text{-}228)$$

where the definition of $\boldsymbol{q}_i$ and $\boldsymbol{q}_{i'}$ are given by Eq. (11-186).

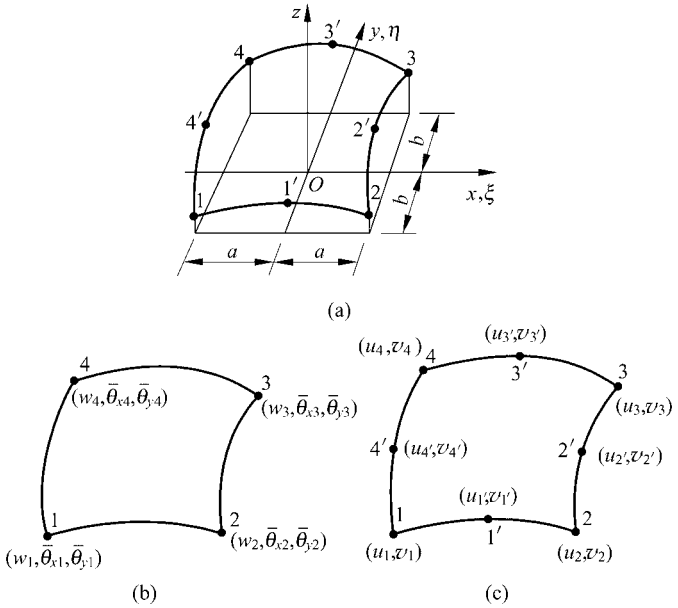

Figure 11.29 (a) = (b) + (c)

(a) nodes of rectangular shallow shell element; (b) nodes of bending element;
(c) nodes of membrane element

Similar to Eqs. (11-187) and (11-188), for convenience, the displacement vector (11-228) is decomposed into membrane displacement and bending displacement vectors:

$$\boldsymbol{q}^{\mathrm{me}} = [u_1 \quad v_1 \quad u_{1'} \quad v_{1'} \quad u_2 \quad v_2 \quad u_{2'} \quad v_{2'} \quad u_3 \quad v_3 \quad u_{3'} \quad v_{3'} \quad u_4 \quad v_4 \quad u_{4'} \quad v_{4'}]^{\mathrm{T}} \tag{11-229}$$

$$\boldsymbol{q}^{\mathrm{be}} = [w_1 \quad \theta_{x1} \quad \theta_{y1} \quad w_2 \quad \theta_{x2} \quad \theta_{y2} \quad w_3 \quad \theta_{x3} \quad \theta_{y3} \quad w_4 \quad \theta_{x4} \quad \theta_{y4}]^{\mathrm{T}} \tag{11-230}$$

Assume that the tangential displacement fields are cubic polynomials:

$$\overline{\boldsymbol{u}}^{e} = \begin{Bmatrix} u \\ v \end{Bmatrix} = \sum_{i=1}^{4} \boldsymbol{N}_i \boldsymbol{q}_i^{\mathrm{m}} \tag{11-231}$$

where

$$\boldsymbol{N}_i = \begin{bmatrix} N_i & 0 & N_{i'} & 0 \\ 0 & N_i & 0 & N_{i'} \end{bmatrix}, \quad \boldsymbol{q}_i^{\mathrm{m}} = [u_i \quad v_i \quad u_{i'} \quad v_{i'}]^{\mathrm{T}} \quad (i = 1,2,3,4) \tag{11-232}$$

$$\left.\begin{aligned}
&N_{1'}=\frac{1}{2}(1-\xi^2)(1-\eta), \qquad N_{2'}=\frac{1}{2}(1-\eta^2)(1+\xi)\\
&N_{3'}=\frac{1}{2}(1-\xi^2)(1+\eta), \qquad N_{4'}=\frac{1}{2}(1-\eta^2)(1-\xi)\\
&N_1=N_1^0-\frac{1}{2}N_{1'}-\frac{1}{2}N_{4'}, \quad N_2=N_2^0-\frac{1}{2}N_{1'}-\frac{1}{2}N_{2'}\\
&N_3=N_3^0-\frac{1}{2}N_{2'}-\frac{1}{2}N_{3'}, \quad N_4=N_4^0-\frac{1}{2}N_{3'}-\frac{1}{2}N_{4'}\\
&N_i^0=\frac{1}{4}(1+\xi_i\xi)(1+\eta_i\eta) \quad (i=1,2,3,4)
\end{aligned}\right\} \tag{11-233}$$

The above tangential displacement functions not only are complete quadric polynomials, but also include the cubic terms $\xi^2\eta$ and $\xi\eta^2$. The displacement functions of the generalized conforming rectangular plate element RGC-12[14] are adopted to form the normal displacement field of the shallow shell element:

$$w=\boldsymbol{F}_\lambda(\hat{\boldsymbol{C}}^{-1}\hat{\boldsymbol{G}})\boldsymbol{q}^{be} \tag{11-234}$$

where

$$\boldsymbol{F}_\lambda=[1 \;\; \xi \;\; \eta \;\vdots\; \xi^2 \;\; \xi\eta \;\; \eta^2 \;\vdots\; \xi^3 \;\; \xi^2\eta \;\; \xi\eta^2 \;\; \eta^3 \;\vdots\; \xi^3\eta \;\; \xi\eta^3]^{\mathrm{T}} \tag{11-235}$$

$$\hat{\boldsymbol{C}}=\left[\begin{array}{c:cc:ccc:cccc:cc}
0 & 0 & \frac{2}{b} & 0 & 0 & -\frac{4}{b} & 0 & \frac{2}{3b} & 0 & \frac{6}{b} & 0 & 0\\
0 & \frac{2}{a} & 0 & \frac{4}{a} & 0 & 0 & \frac{6}{a} & 0 & \frac{2}{3a} & 0 & 0 & 0\\
0 & 0 & \frac{2}{b} & 0 & 0 & \frac{4}{b} & 0 & \frac{2}{3b} & 0 & \frac{6}{b} & 0 & 0\\
0 & \frac{2}{a} & 0 & -\frac{4}{a} & 0 & 0 & \frac{6}{a} & 0 & \frac{2}{3a} & 0 & 0 & 0\\
\hdashline
0 & 2 & 0 & 0 & -2 & 0 & 2 & 0 & 2 & 0 & -2 & -2\\
0 & 0 & 2 & 0 & 2 & 0 & 0 & 2 & 0 & 2 & 2 & 2\\
0 & -2 & 0 & 0 & -2 & 0 & -2 & 0 & -2 & 0 & -2 & -2\\
\hdashline
2 & 0 & -2 & \frac{2}{3} & 0 & 2 & 0 & -\frac{2}{3} & 0 & -2 & 0 & 0\\
2 & 2 & 0 & 2 & 0 & \frac{2}{3} & 2 & 0 & \frac{2}{3} & 0 & 0 & 0\\
2 & 0 & 2 & \frac{2}{3} & 0 & 2 & 0 & \frac{2}{3} & 0 & 2 & 0 & 0\\
\hdashline
0 & \frac{1}{a} & 0 & -\frac{2}{a} & -\frac{1}{a} & 0 & \frac{3}{a} & \frac{2}{a} & \frac{1}{a} & 0 & -\frac{3}{a} & -\frac{1}{a}\\
0 & 0 & \frac{1}{b} & 0 & -\frac{1}{b} & -\frac{2}{b} & 0 & \frac{1}{b} & \frac{2}{b} & \frac{3}{b} & -\frac{1}{b} & -\frac{3}{b}
\end{array}\right] \tag{11-236}$$

$$\hat{\boldsymbol{G}}=\left[\begin{array}{ccc:ccc:ccc:ccc}
0 & 1 & 0 & 0 & 1 & 0 & 0 & 0 & 0 & 0 & 0 & 0 \\
0 & 0 & 0 & 0 & 0 & -1 & 0 & 0 & -1 & 0 & 0 & 0 \\
0 & 0 & 0 & 0 & 0 & 0 & 0 & 1 & 0 & 0 & 1 & 0 \\
0 & 0 & -1 & 0 & 0 & 0 & 0 & 0 & 0 & 0 & 0 & -1 \\
\hdashline
-1 & 0 & 0 & 1 & 0 & 0 & 0 & 0 & 0 & 0 & 0 & 0 \\
0 & 0 & 0 & -1 & 0 & 0 & 1 & 0 & 0 & 0 & 0 & 0 \\
0 & 0 & 0 & 0 & 0 & 0 & -1 & 0 & 0 & 1 & 0 & 0 \\
\hdashline
1 & 0 & -\frac{a}{3} & 1 & 0 & \frac{a}{3} & 0 & 0 & 0 & 0 & 0 & 0 \\
0 & 0 & 0 & 1 & \frac{b}{3} & 0 & 1 & -\frac{3}{b} & 0 & 0 & 0 & 0 \\
0 & 0 & 0 & 0 & 0 & 0 & 1 & 0 & \frac{a}{3} & 1 & 0 & -\frac{a}{3} \\
\hdashline
0 & 0 & -1 & 0 & 0 & 0 & 0 & 0 & 0 & 0 & 0 & 0 \\
0 & 1 & 0 & 0 & 0 & 0 & 0 & 0 & 0 & 0 & 0 & 0
\end{array}\right] \tag{11-237}$$

The incremental displacement vector of the element is

$$\Delta\overline{\boldsymbol{q}}^{e}=[\Delta\boldsymbol{q}_1^{\mathrm{T}}\quad\Delta\boldsymbol{q}_{1'}^{\mathrm{T}}\quad\Delta\boldsymbol{q}_2^{\mathrm{T}}\quad\Delta\boldsymbol{q}_{2'}^{\mathrm{T}}\quad\Delta\boldsymbol{q}_3^{\mathrm{T}}\quad\Delta\boldsymbol{q}_{3'}^{\mathrm{T}}\quad\Delta\boldsymbol{q}_4^{\mathrm{T}}\quad\Delta\boldsymbol{q}_{4'}^{\mathrm{T}}]^{\mathrm{T}} \tag{11-238}$$

where

$$\Delta\boldsymbol{q}_i=[\Delta u_i\quad\Delta v_i\quad\Delta w_i\quad\Delta\theta_{xi}\quad\Delta\theta_{yi}]^{\mathrm{T}},\quad\Delta\boldsymbol{q}_{i'}=[\Delta u_{i'}\quad\Delta v_{i'}]^{\mathrm{T}} \tag{11-239}$$

The incremental displacements corresponding to Eqs. (11-229) and (11-230) are

$$\begin{aligned}\Delta\boldsymbol{q}^{\mathrm{m}e}=[&\Delta u_1\quad\Delta v_1\quad\Delta u_{1'}\quad\Delta v_{1'}\quad\Delta u_2\quad\Delta v_2\quad\Delta u_{2'}\quad\Delta v_{2'}\quad\Delta u_3\quad\Delta v_3\quad\Delta u_{3'}\quad\Delta v_{3'}\\&\Delta u_4\quad\Delta v_4\quad\Delta u_{4'}\quad\Delta v_{4'}]^{\mathrm{T}}\end{aligned} \tag{11-240}$$

$$\Delta\boldsymbol{q}^{\mathrm{b}e}=[\Delta w_1\quad\Delta\theta_{x1}\quad\Delta\theta_{y1}\quad\Delta w_2\quad\Delta\theta_{x2}\quad\Delta\theta_{y2}\quad\Delta w_3\quad\Delta\theta_{x3}\quad\Delta\theta_{y3}\quad\Delta w_4\quad\Delta\theta_{x4}\quad\Delta\theta_{y4}]^{\mathrm{T}} \tag{11-241}$$

According to Eqs. (11-220a) and (11-222), matrix $\boldsymbol{B}^{\mathrm{m}p}$ can be written as

$$\begin{aligned}\boldsymbol{B}^{\mathrm{m}p}\Delta\overline{\boldsymbol{q}}^{e}&=\left[\frac{\partial\Delta u}{\partial x}+\frac{\Delta w}{R_1}\quad\frac{\partial\Delta v}{\partial y}+\frac{\Delta w}{R_2}\quad\frac{\partial\Delta u}{\partial y}+\frac{\partial\Delta v}{\partial x}\right]^{\mathrm{T}}\\&=\boldsymbol{B}^{\mathrm{m}}\Delta\boldsymbol{q}^{\mathrm{m}e}+\boldsymbol{B}^{\mathrm{m}w}\Delta\boldsymbol{q}^{\mathrm{b}e}\end{aligned} \tag{11-242}$$

where

$$\boldsymbol{B}^{\mathrm{m}}=[\boldsymbol{B}_1^{\mathrm{m}}\quad\boldsymbol{B}_{1'}^{\mathrm{m}}\quad\boldsymbol{B}_2^{\mathrm{m}}\quad\boldsymbol{B}_{2'}^{\mathrm{m}}\quad\boldsymbol{B}_3^{\mathrm{m}}\quad\boldsymbol{B}_{3'}^{\mathrm{m}}\quad\boldsymbol{B}_4^{\mathrm{m}}\quad\boldsymbol{B}_{4'}^{\mathrm{m}}]$$

$$\boldsymbol{B}_{i'}^{\mathrm{m}}=\frac{1}{4ab}\begin{bmatrix} b(1+\eta_0)(2\xi+\xi_i\eta_0) & 0 \\ 0 & a(1-\xi_0)(2\eta+\eta_i\xi_0) \\ a(1-\xi_0)(2\eta+\eta_i\xi_0) & b(1+\eta_0)(2\xi+\xi_i\eta_0) \end{bmatrix},\quad \xi_0=\xi_i\xi,\quad \eta_0=\eta_i\eta$$

$$\boldsymbol{B}_{i}^{\mathrm{m}}=\frac{1}{ab}\begin{bmatrix} b_{1i'} & 0 \\ 0 & b_{2i'} \\ b_{2i'} & b_{1i'} \end{bmatrix}$$

$$b_{11'}=-b\xi(1-\eta),\quad b_{12'}=\frac{b}{2}(1-\eta^2),\quad b_{13'}=-b\xi(1+\eta),\quad b_{14'}=-\frac{b}{2}(1-\eta^2)$$

$$b_{21'}=-\frac{a}{2}(1-\xi^2),\quad b_{22'}=-a\eta(1+\xi),\quad b_{23'}=\frac{a}{2}(1-\xi^2),\quad b_{24'}=-a\eta(1-\xi)$$

$$\boldsymbol{B}^{\mathrm{m}w}=\begin{bmatrix} \dfrac{1}{R_1}\boldsymbol{F}_\lambda(\hat{\boldsymbol{C}}^{-1}\hat{\boldsymbol{G}}) \\ \dfrac{1}{R_2}\boldsymbol{F}_\lambda(\hat{\boldsymbol{C}}^{-1}\hat{\boldsymbol{G}}) \\ 0 \end{bmatrix}$$

The element bending strain matrix is

$$\begin{aligned}\boldsymbol{B}^{\mathrm{b}p}\Delta\overline{\boldsymbol{q}}^{e}&=\left[-\frac{\partial^2\Delta w}{\partial x^2}+\frac{1}{R_1}\frac{\partial\Delta u}{\partial x}\quad -\frac{\partial^2\Delta w}{\partial y^2}+\frac{1}{R_2}\frac{\partial\Delta v}{\partial y}\quad -2\frac{\partial^2\Delta w}{\partial x\partial y}+\frac{1}{R_1}\frac{\partial\Delta u}{\partial y}+\frac{1}{R_2}\frac{\partial\Delta v}{\partial x}\right]^{\mathrm{T}}\\&=\boldsymbol{B}^{\mathrm{b}}\Delta\boldsymbol{q}^{\mathrm{b}e}+\boldsymbol{B}^{\mathrm{b}m}\Delta\boldsymbol{q}^{\mathrm{m}e}\end{aligned}\tag{11-240}$$

where

$$\boldsymbol{B}^{\mathrm{b}}=\overline{\boldsymbol{B}}^{\mathrm{b}}(\hat{\boldsymbol{C}}^{-1}\hat{\boldsymbol{G}})$$

$$\overline{\boldsymbol{B}}^{\mathrm{b}}=\frac{-1}{a^2b^2}\begin{bmatrix} 0&0&0&2b^2&0&0&6b^2\xi&2b^2\eta&0&0&6b^2\xi\eta&0 \\ 0&0&0&0&0&2a^2&0&0&2a^2\xi&6a^2\eta&0&6a^2\xi\eta \\ 0&0&0&0&2ab&0&0&4ab\xi&4ab\eta&0&6ab\xi^2&6ab\eta^2 \end{bmatrix}$$

$$\boldsymbol{B}^{\mathrm{b}m}=[\boldsymbol{B}_1^{\mathrm{b}m}\quad \boldsymbol{B}_{1'}^{\mathrm{b}m}\quad \boldsymbol{B}_2^{\mathrm{b}m}\quad \boldsymbol{B}_{2'}^{\mathrm{b}m}\quad \boldsymbol{B}_3^{\mathrm{b}m}\quad \boldsymbol{B}_{3'}^{\mathrm{b}m}\quad \boldsymbol{B}_4^{\mathrm{b}m}\quad \boldsymbol{B}_{4'}^{\mathrm{b}m}]$$

$$\boldsymbol{B}_{i}^{\mathrm{b}m}=\frac{1}{ab}\begin{bmatrix} \dfrac{1}{R_1}b_{1i'} & 0 \\ 0 & \dfrac{1}{R_2}b_{2i'} \\ \dfrac{1}{R_1}b_{2i'} & \dfrac{1}{R_2}b_{1i'} \end{bmatrix}$$

$$\boldsymbol{B}_{i'}^{\mathrm{bm}}=\frac{1}{4ab}\begin{bmatrix}\dfrac{b}{R_1}(1+\eta_0)(2\xi+\xi_i\eta_0) & 0\\ 0 & \dfrac{a}{R_2}(1-\xi_0)(2\eta+\eta_i\xi_0)\\ \dfrac{a}{R_1}(1-\xi_0)(2\eta+\eta_i\xi_0) & \dfrac{b}{R_2}(1+\eta_0)(2\xi+\xi_i\eta_0)\end{bmatrix}$$

Matrix $\boldsymbol{B}^{\mathrm{g}}$ can be expressed by

$$\begin{aligned}\boldsymbol{B}^{\mathrm{g}}\Delta\bar{\boldsymbol{q}}^{e}&=\begin{bmatrix}\dfrac{\partial\Delta w}{\partial x}-\dfrac{\Delta u}{R_1} & \dfrac{\partial\Delta w}{\partial y}-\dfrac{\Delta v}{R_2}\end{bmatrix}^{\mathrm{T}}\\&=\bar{\boldsymbol{G}}\Delta\boldsymbol{q}^{\mathrm{b}e}-\sum_{i=1}^{4}\begin{bmatrix}\dfrac{1}{R_1} & 0\\ 0 & \dfrac{1}{R_2}\end{bmatrix}\boldsymbol{N}_i\Delta\boldsymbol{q}_i^{\mathrm{m}e}\end{aligned}\tag{11-244}$$

where

$$\bar{\boldsymbol{G}}=\frac{1}{ab}\begin{bmatrix}0 & b & 0 & 2b\xi & b\eta & 0 & 3b\xi^2 & 2b\xi\eta & b\eta^2 & 0 & 3b\xi^2\eta & b\eta^3\\ 0 & 0 & a & a & a\xi & 2a\eta & 0 & a\xi^2 & 2a\xi\eta & 3a\eta^2 & a\xi^3 & 3a\xi\eta^2\end{bmatrix}(\hat{\boldsymbol{C}}^{-1}\hat{\boldsymbol{G}})$$

$$\Delta\boldsymbol{q}_i^{\mathrm{m}e}=[\Delta u_i \quad \Delta v_i \quad \Delta u_{i'} \quad \Delta v_{i'}]^{\mathrm{T}}$$

Then, from the above equations, the nonlinear tangential stiffness matrix of the shallow shell element can be obtained according to Eq. (11-227).

11.9.3 Numerical Examples

In the following nonlinear numerical examples, the variable arc length iteration method[42], in which the current stiffness parameter is taken as the control variable, is used, and the materials are all assumed to be linear elastic.

Example 11.16 The nonlinear analysis of a clamped square plate subjected to uniform load.

A clamped square plate subjected to uniform load q is shown in Fig. 11.30, its Poisson's ratio $\mu=0.316$. Due to the symmetry, only 1/4 of the plate is analyzed by using two meshes 2×2 and 4×4. The results are listed in Table 11.17, in which $\bar{W}=w/h$ and $\bar{Q}=qa^4/Eh^4$. It can be seen that the element SSR28 can provide higher precision with less DOFs.

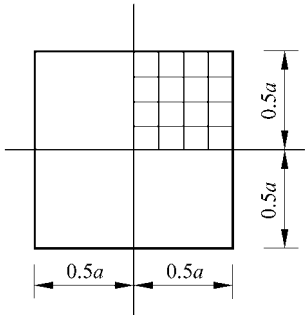

Figure 11.30 A clamped square plate

Table 11.17 The central deflection parameter $\bar{W}$ in nonlinear analysis of a clamped square plate subjected to uniform load

Load parameter $\bar{Q}$	Analytical[49]	QH[49]	SSR28 2 × 2	SSR28 4 × 4
17.79	0.237	0.2361	0.2254	0.2333
30.8	0.471	0.4687	0.4509	0.4621
63.4	0.695	0.6902	0.6694	0.6815
95	0.912	0.9015	0.8804	0.8909
134.9	1.121	1.1050	1.0848	1.0936
184	1.323	1.2997	1.2807	1.2942
245	1.521	1.4916	1.4739	1.4900
318	1.714	1.6775	1.6607	1.6834
402	1.902	1.8545	1.8382	1.8643
DOFs		405	69	205

Example 11.17 Post-buckling analysis of a thin cylindrical shell subjected to concentrated load.

A cylindrical shell is shown in Fig. 11.31. Its longitudinal straight edges are hinged while curved edges are free. A concentrated load acts on the center of the

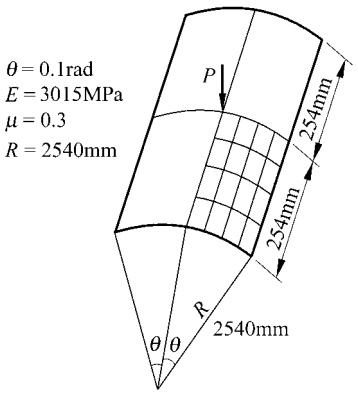

Figure 11.31 Cylindrical shell

shell. Two different thickness cases are considered: $h = 12.7$mm and $h = 6.35$mm. The critical load of this structures obtained by computations are listed in Tables 11.18 and 11.19, and also plotted in Figs. 11.32 and 11.33. It can be seen that the results by the element SSR28 agree with those obtained by the cylindrical shell element[50], the flat-shell element[51] and the quasi-conforming rectangular shallow shell element[52].

Table 11.18 The critical load P_{cr} of a cylindrical shell ($h = 12.7$mm) subjected to concentrated load

Mesh / Model	2 × 2		4 × 4		16 × 16	
	Up limit	Low limit	Up limit	Low limit	Up limit	Low limit
SSR28	2.223	0.6066	2.200	0.5169		
Reference [52]					2.222 86	0.546 40
Reference [51]			2.27			
Reference [50]			2.22			

Table 11.19 The critical load P_{cr} of a cylindrical shell ($h = 6.35$mm) subjected to concentrated load

Mesh / Model	2 × 2		4 × 4		16 × 16	
	Up limit	Low limit	Up limit	Low limit	Up limit	Low limit
SSR28	0.5956	– 0.3324	0.5837	– 0.3739		
Reference [52]					0.5907	– 0.3794

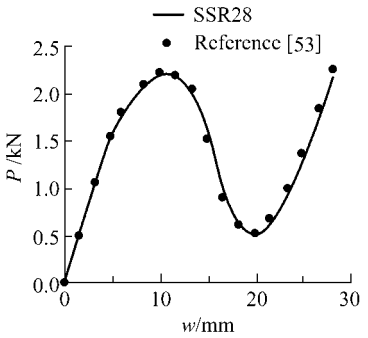

Figure 11.32 Load-central deflection relation curve of a cylindrical shell ($h = 12.7$mm)

Example 11.18 Post-buckling analysis of a thin cylindrical shell subjected to uniform load.

The dimensions and material properties of a cylindrical shell structure are shown in Fig. 11.31. This cylindrical shell is clamped and subjected to vertical

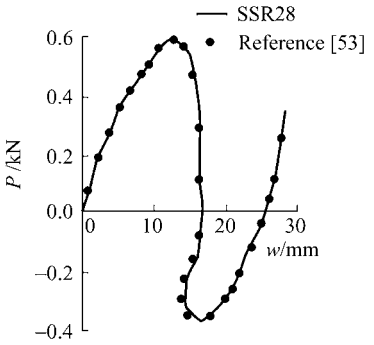

Figure 11.33 Load-central deflection relation curve of a cylindrical shell ($h = 6.35$mm)

uniformly distributed load q, and its thickness $h = 3.175$mm. The results of the post-buckling analysis by 4×4 mesh are plotted in Fig. 11.34, in which w is the vertical deflection at central point.

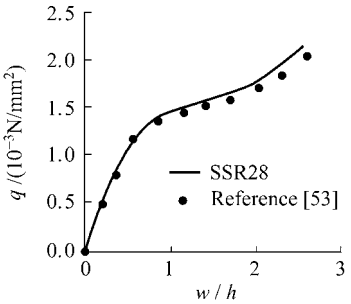

Figure 11.34 Post-buckling analysis of a clamped cylindrical shell ($h = 3.175$mm)

Example 11.19 Post-buckling analysis of a shallow spheric shell.

A simply-supported shallow spheric shell subjected to a central concentrated load P is shown in Fig. 11.35. Its stability problem has already been analyzed by

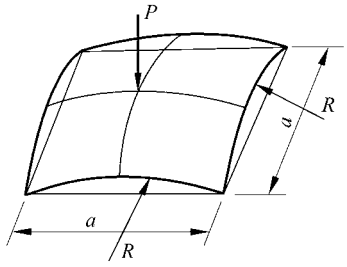

$R = 2540$mm, $a = 1569.8$mm, $h = 99.45$mm
$E = 68.95$MPa, $\mu = 0.3$

Figure 11.35 A shallow spheric shell

many element models[51,52,54]. The results of the critical load obtained by the element SSR28 using 2×2 and 4×4 meshes are listed in Table 11.20. A comparison between the results by the element SSR28 using 4×4 mesh and those in reference [51] is given in Fig. 11.36.

Table 11.20 The critical load P_{cr} (kN) of a shallow spheric shell subjected to concentrated load

Model \ Mesh	2×2		4×4		5×5		16×16	
	Up	Low limit	Up limit	Low limit	Up limit	Low limit	Up limit	Low limit
SSR28	48.991	37.360	49.874	36.562				
Reference							48.172	36.951
Reference			52.000					
Reference					51.400			

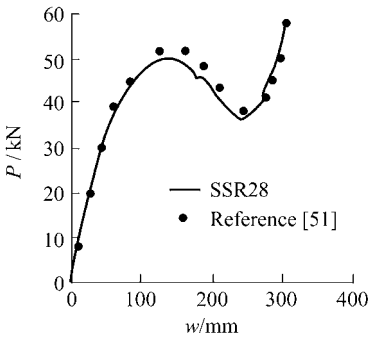

Figure 11.36 Post-buckling analysis of a shallow spheric shell

References

[1] Long YQ, Huang MF (1988) A generalized conforming isoparametric element. Applied mathematics and Mechanics (English Edition) 9(10): 929 – 936

[2] Long YQ, Xu Y (1994) Generalized conforming quadrilateral membrane element with vertex rigid rotational freedom. Computers & Structures 52(4): 749 – 755

[3] Long YQ, Xu Y (1994) Generalized conforming triangular membrane element with vertex rigid rotational freedom. Finite Elements in Analysis and Design 17: 259 – 271

[4] Long YQ, Xu Y (1993) Generalized conforming triangular flat shell element. Gong Cheng Li Xue/Engineering Mechanics 10(4): 1 – 7 (in Chinese)

[5] Long YQ, Xu Y (1994) Generalized conforming flat rectangular thin shell element. Computational Structural Mechanics and Applications 11(2): 154 – 160 (in Chinese)

[6] Xu Y, Long YQ, Long ZF (1994) A triangular shell element with drilling freedoms based on generalized compatibility conditions. In: Proc. WCCMⅢ. Japan, pp1234 – 1235

[7] Xu Y, Long ZF (1996) Advances of membrane and thin shell elements with the generalized conforming approach. In: Yuan Si, Ma Zhiliang (eds) New Developments in Structural Engineering, pp218 – 223
[8] Xu Y, Long YQ, Long ZF (1999) A generalized conforming triangular flat shell element with high accuracy. In: Long YQ (ed) The Proceedings of the First International Conference on Structural Engineering. China, KunMing, pp700 – 706
[9] Chen YL, Cen S, Yao ZH, Long YQ, Long ZF (2003) Development of triangular flat-shell element using a new thin-thick plate bending element based on SemiLoof constraints. Structural Engineering and Mechanics 15(1): 83 – 114
[10] Sun JH, Xia HX, Long YQ (1999) A generalized conforming rectangular shallow shell element. In: Long YQ (ed) The Proceedings of the First International Conference on Structural Engineering. China, KunMing, pp803 – 810
[11] Sun JH, Long ZF, Long YQ (1999) A generalized conforming element with vertex rotational freedoms for thin shell analysis. In: Long YQ (ed) The Proceedings of the First International Conference on Structural Engineering. China, KunMing, pp811 – 818
[12] Sun JH, Long ZF, Long YQ, Zhang CS (2001) Geometrically nonlinear stability analysis of shells using generalized conforming shallow shell element. International Journal of Structural Stability and Dynamics 1(3): 313 – 332
[13] Wilson EL, Taylor RL, Doherty WP, Ghabussi T (1973) Incompatible displacement models. In: Fenven ST et al (eds) Numerical and Computer Methods in Structural Mechanics. Academic Press, New York, pp43 – 57
[14] Long YQ, Xin KG (1989) Generalized conforming element for bending and buckling analysis of plates. Finite Elements in Analysis and Design 5:15 – 30
[15] Taylor RL, Beresford PJ, Wilson EL (1976) A non-conforming element for stress analysis. International Journal for Numerical Methods in Engineering 10: 1211 – 1219
[16] Wachspress EL (1978) Incomptiable quadrilateral basis functions. International Journal for Numerical Methods in Engineering 12: 589 – 595
[17] Pian THH, Wu CC (1986) General formulation of incompatible shape function and an incompatible isoparametric element. In: Proc of the Invitational China-American Workshop on FEM. Chengde, pp159 – 165
[18] Chen WJ, Tang LM (1981) Isoparametric quasi-conforming element. Journal of Dalian Institute of Technology 20(1): 63 – 74 (in Chinese)
[19] Cook RD (1974) Improved two-dimensional finite element. Journal of the Structural Division ASCE, 100, ST9: 1851 – 1863
[20] Zienkiewicz OC, Taylor RL (1991) The finite element method, 4th edn. Volume 2—Solid and Fluid Mechanics & Dynamics and Non-linearity. McGRAW-HILL Book Company, London
[21] Clough RW, Johnson CP (1968) A finite element approximation for the analysis of thin shells. International Journal of Solids and Structures 4: 43 – 60
[22] Olsen MD, Bearden TW (1979) A simple flat shell element revisited. International Journal for Numerical Methods in Engineering 14: 51 – 68
[23] Allman DJ (1988) A quadrilateral finite element including vertex rotation for plane elasticity analysis. International Journal for Numerical Methods in Engineering 26: 717 – 730
[24] Felippa CA, Alexander S (1992) Membrane triangles with corner drilling freedom—III. Implementations and performane evolution. Finite Element in Analysis and Design 12: 203 – 249

[25] Bergan PG, Felippa CA (1985) A triangular membrane element with rotational degrees of freedom. Computer Methods in Applied Mechanics and Engineering 50: 25 – 69
[26] Long ZF, Cen S (1992) New monograph of finite element method: principle, programming, developments. Hydraulic and Water-power Press, China, Beijing (in Chinese)
[27] Long YQ, Bu XM, Long ZF, Xu Y (1995) Generalized conforming plate bending elements using point and line compatibility conditions. Computers & Structures 54(4): 717 – 723
[28] Fish J, Belytshko T (1992) Stabilized rapidly convergent 18-degree-of-freedom flat shell triangular element. International Journal for Numerical Methods in Engineering 33: 149 – 162
[29] Chen WJ, Cheung YK (1999) Refined non-conforming triangular elements for analysis of shell structures. International Journal for Numerical Methods in Engineering 46: 433 – 455
[30] Providas E, Kattis MA (2000) An assessment of two fundamental flat triangular shell elements with drilling rotations. Computers & Structure 77(2): 129 – 139
[31] Carpenter N, Stolarski H, Belyschko T (1986) Improvements in 3-node triangular shell elements. International Journal for Numerical Methods in Engineering 23: 1643 – 1667
[32] ABAQUS/Standard User's Manual, Version 5.8 (1998) Hibbitt, Karlsson & Sorensen, Inc.: Rawtucket, Rhode Island
[33] MacNeal RH, Harder RL (1985) A proposed standard set of problems to test finite element accuracy. Finite Element in Analysis and Design 1: 3 – 20
[34] Aminpour MA (1992) An assumed-stress hybrid 4-node shell element with drilling degrees of freedom. International Journal for Numerical Methods in Engineering 33: 19 – 38
[35] Guan Y, Tang L (1992) A quasi-conforming nine-node degenerated shell finite element. Finite Elements in Analysis and Design 11: 165 – 176
[36] Batoz JL, Tahar MB (1982) Evaluation of a new quadrilateral thin plate bending element. International Journal for Numerical Methods in Engineering 18: 1655 – 1677
[37] Bathe KJ, Dvorkin EN (1985) Short communication: a four-node plate bending element based on Mindlin/Ressiner plate theory and mixed interpolation. International Journal for Numerical Methods in Engineering 21: 367 – 383
[38] Chen WJ (2001) Advances in finite element with high performances. In: Yuan MW, Sun SL (eds) Computational Mechanics in Engineering and Science (Proceedings of the Chinese Conference on Computational Mechanics'2001). Peking Univerisuty Press, China, Guangzhou, pp136 – 151 (in Chinese)
[39] Parish HA (1979) Critical survey of the 9-node degenerated shell element with special emphasis on thin shell application and reduced integration. Computer Methods in Applied Mechanics and Engineering 20: 323 – 350
[40] Long YQ, Zhao JQ (1992) Generalized conforming curved rectangular element for shallow shells. Gong Cheng Li Xue/Engineering Mechanics, 9(1): 3 – 10 (in Chinese)
[41] Long YQ, Xi F (1992) A universal method for including shear deformation in thin plate elements. International Journal for Numerical Methods in Engineering 34: 171 – 177
[42] Sun JH (1998) Research on generalized conforming shallow shell element and nonlinear analysis of plate and shell structures [Doctoral Dissertation]. Tsinghua University, Beijing (in Chinese)
[43] Bu XM, Long YQ (1991) A high-precise rectangular element for thin plate bending analysis. Tumu Gongcheng Xuebao/China Civil Engineering Journal 24(1): 17 – 22 (in Chinese)

[44] Bonnes G, Dhatt G, Giroux Y, Robichaud (1968) Curved triangular elements for analysis of shell. In: Proceedings of Conference on Matrix Method in Structural Mechanics. A. F. Base, Ohio: Wright Patterson pp617 – 640
[45] Cowper G, Lindberg GM, Olson MD (1970) A shallow shell finite element of triangular shape. International Journal of Solids and Structures 6: 1133 – 1156
[46] Cook RD (1974) Concept and Applications of Finite Element Analysis. John Wiley & Sons, Inc, New York
[47] Badiansky B (1974) Theory of buckling and post-buckling behavior of elastic structure. In: Yih Chia-Shun (eds) Advances in Applied Mechanics (Vol. 14), Academic Press, New York, pp2 – 63
[48] Jiang HY (1984) Nonlinear finite element method of quasi-conforming technique model. Computational Structural Mechanics and Applications 1(2): 49 – 59 (in Chinese)
[49] Pica A, Wood RD, Hinton E (1980) Finite element analysis of geometrically nonlinear plate behaviour using a Mindlin formulation. Computers & Structures 11: 203 – 215
[50] Sabir AB, Lock AC (1972) The application of finite element to the large deflection geometrically nonlinear behavior of cylindrical shells. In: Brebbia CA (ed) Variational Methods in Engineering, Southampton University Press, Southampton pp54 – 65
[51] Ramesh G, Krishnamoorthy CS (1993) Post-buckling analysis of structures by dynamic relaxation. International Journal for Numerical Methods in Engineering 36: 1339 – 1364
[52] Wei G, Zhao CX (1990) A large deflection quasi-conforming rectangular shallow shell element and applications. Computational Structural Mechanics and Applications 7(1): 15 – 43 (in Chinese)
[53] Crisfield MA (1981) A fast incremental / iterative solution procedure that handles "snap-through". Computers & Structures 13: 55 – 62
[54] Horrigmoe G, Bergan PG (1978) Nonlinear analysis of free-form shells by flat finite elements. Computer Methods in Applied Mechanics and Engineering 16: 11 – 35